DEVELOPMENT OF REASONABLE WORST-CASE VALUES OF OVERWATER HORIZONTAL TURBULENCE INTENSITIES (IYW)

1. Introduction

The main purpose of this analysis is to assess the overwater dispersion parameters in the OCDCPM model and to document the development of the reasonable worst-case turbulence intensities used to simulate plume dimensions observed offshore Santa Barbara County. The development of the reasonable worst-case turbulence intensity values used in the Santa Barbara County APCD OCDCPM modeling protocol was based on several basic premises. These premises are summarized as follows:

a. Plume dimensions calculated by OCD (both horizontal and vertical) should reflect actual worst-case plume dimensions observed offshore. Hourly averaged plume concentrations indicative of P-G stability class F or more stable (G) were measured during the 1980 SANBOX study in the Santa Barbara Channel. OCD-calculated plume dimensions should emulate these observed values. A discussion of the observed plume dimensions during the SANBOX study is contained in the analysis section (Section 2) of this document. Also, the Santa Barbara County APCD comments to OAQPS regarding the proposed revisions to the air quality modeling guidelines discuss this subject in greater detail.

b. Plumes observed offshore should reflect less dispersion than dispersion calculated by the EPA-preferred onshore model, MPTER (comparing non-complex terrain models). The 1980 SANBOX study observed plume dimensions smaller than those calculated by MPTER σ_y and σ_z values for P-G stability class F. The OCD model using default dispersion parameters results in much greater dispersion than that calculated by the MPTER model.

c. It is the product of turbulence intensity, distance from source to receptor and the non-dimensional function relating turbulence intensities to plume dimensions which must be considered, not just the value of the turbulence intensity itself. The argument that certain values of turbulence intensities are too conservative is not valid without appropriate consideration of the other terms contributing to the plume dimension calculation. The "bottom line" is what should be considered, not an individual component which contributes to the "bottom line."

The analysis section of this document presents a comparison of MPTER and OCD dispersion calculations. The dispersion calculations are used to match $\sigma_y\sigma_z$ products between OCD and MPTER for P-G stability class F. From the matching of $\sigma_y\sigma_z$ products between the two models, a value of OCD σ_y is calculated. A value of overwater horizontal turbulence intensity is then calculated based on the OCDCPM formulation which relates turbulence intensity to σ_y. Also, a comparison of modeled results between OCDCPM and CPX2APCD (COMPLEX-II with overwater dispersion corrections) is discussed in the analysis section.

2. Analysis

a. Rationale for Developing Turbulence Intensity Values Which Result in Plume Dimensions Equivalent to P-G Stability Class F Dispersion

The OCD model contains many of the features of the EPA MPTER model, and was based in large part on the formulations contained in MPTER. MPTER is the EPA guideline model for assessing onshore impacts in areas of level terrain. The MPTER model uses algorithms to emulate P-G stability class dispersion, which ranges from "A" (unstable) to "F" (very stable). Using EPA-approved methods to calculate P-G stability classes for input into MPTER and other EPA models, it is generally observed that there is a large number of P-G stability class F conditions with low wind speeds included in any data set used for onshore modeling analyses. The percentage of P-G stability class F conditions generally averages about 30 percent of the total hours in an annual data set.

There is general agreement that offshore dispersion is more restrictive than onshore dispersion. Thus, it is reasonable to require that plume dimensions offshore should be less than or equal to those used in onshore modeling analyses. The OCD model in the default mode calculates much larger plume dimensions, and therefore smaller pollutant concentrations, than does MPTER. In order to be consistent with plume dimensions used in onshore modeling, turbulence intensity inputs into OCD and OCDCPM should be chosen to emulate P-G stability class F conditions. This would ensure that offshore modeling would use plume dimensions as restrictive, not more restrictive, than those commonly used onshore.

Further evidence that P-G stability class F conditions are a reasonable assumption for offshore dispersion in the Santa Barbara region can be found in the analysis of the 1980 Santa Barbara Oxidant (SANBOX) study (Smith et al., 1983). During the SANBOX study, tracer gas (SF_6) was released on six occasions to study plume transport and diffusion in the Santa Barbara Channel. During each of the six tracer release days, hourly values of tracer gas concentrations were collected at specific offshore and onshore locations and compared to Xu/Q values to estimate pollutant diffusion in terms of P-G stability categories.

The hourly averaged samples demonstrated that dispersion offshore Santa Barbara was consistent with the P–G stability class methodology. Hourly averaged samples revealed dispersion to range from P–G stability class C to G depending on whether the flow was categorized as organized or as light and meandering. The light and meandering winds produced hourly tracer sample concentrations corresponding to P–G stability classes C through E, while the more organized flows produced hourly tracer sample concentrations corresponding to P–G stability classes E through G. The computations used to obtain the Xu/Q values from which the the stability values were derived are the same as those included in MPTER. Refer to Figure 1 for a summary of Xu/Q values as they relate to distance and stability class for the 17 September 1980 SANBOX release. Similar figures for the five other tracer releases can be found in (Smith et al., 1983).

The SANBOX comparison of plume concentrations to P–G stability classes did not consider mixing depths (equation 3.5 Turner's Workbook (Turner, 1970). However, consideration of mixing depths in the estimates of hourly P–G stability classes still results in observed hourly concentrations which would correspond to P–G stability class F. Figure 2 illustrates the change in P–G stability class determination when mixing depth is considered. It is observed that for stable cases (P–G stability class F), mixing depth is not a factor in stability class determination until downwind travel distances exceed approximately 70 kilometers. Thus, the idea that P–G stability classes are appropriate for estimating hourly averaged offshore pollutant concentrations remains valid even if mixing depth is considered.

It should also be noted that the comparison of monitored tracer values to the Xu/Q curves is not a conservative method of estimating P–G stability class. The chance of an individual monitor in the network measuring the plume centerline concentration is very remote. The P–G stability class determinations were based on Xu/Q curves which assume the plume concentration (X) is at plume centerline. Therefore, it is probable that many of the P–G stability class determinations made as a result of the SANBOX study were in reality more stable (less dispersive) than could be determined by the SANBOX sampling network.

Based on the determination that P–G stability class F is a realistic measure of offshore plume dimensions, an exercise to match $\sigma_y \sigma_z$ products between OCD and MPTER was conducted to determine appropriate values of OCD turbulence parameters. The following section presents the algorithms used in OCD and MPTER to calculate plume dimensions. From this information, a value of overwater horizontal turbulence intensity is calculated which results in the matching of OCD and MPTER $\sigma_y \sigma_z$ values for P–G stability class F conditions.
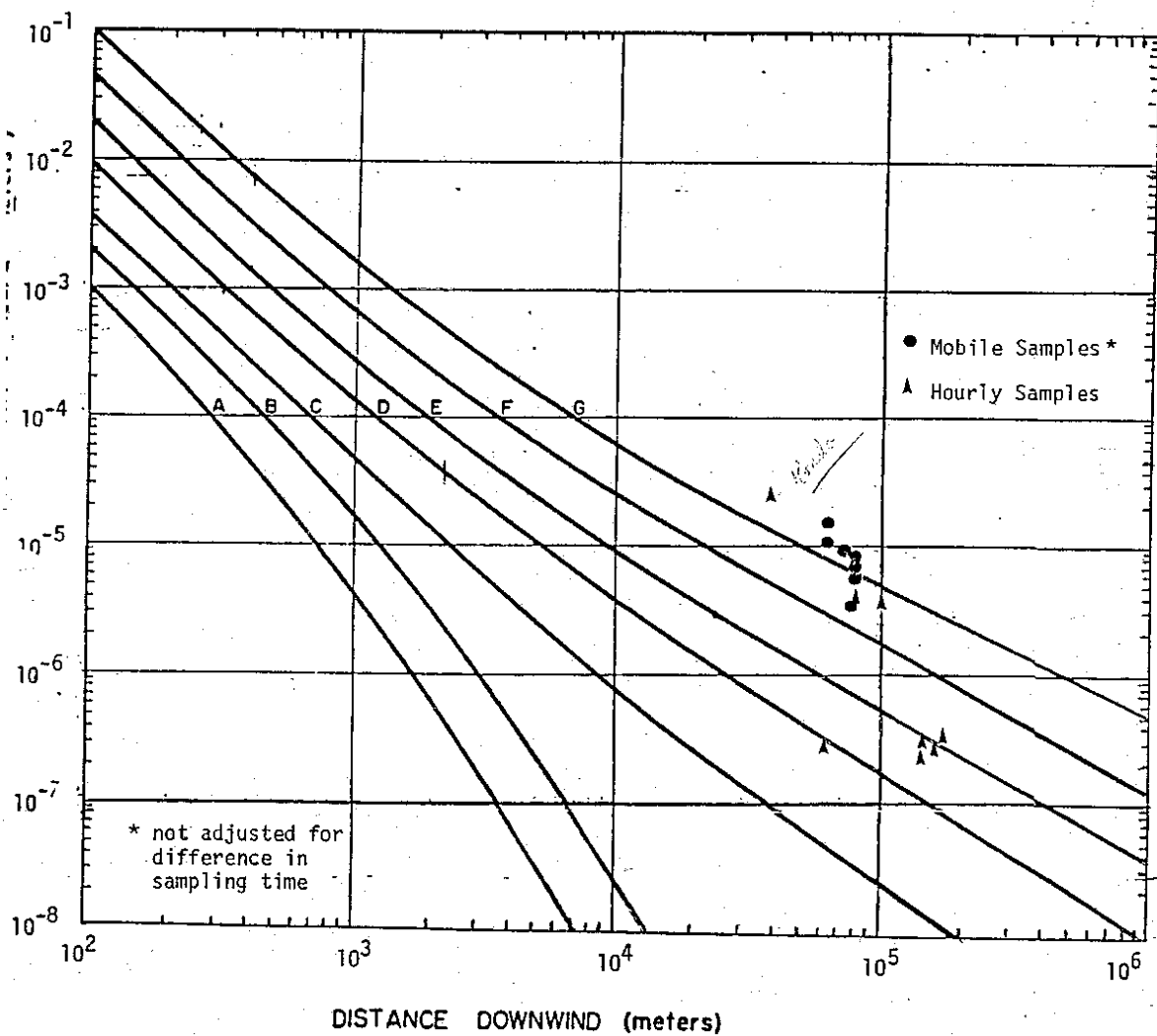
DISTANCE DOWNWIND (meters)

Fig. 4.2.15 XU/Q VALUES - Test 1
September 17,1980

Figure 1

10^{-1}

10^{-2}

10^{-3}

10^{-4}

10^{-5}

10^{-6}

10^{-7}

10^{-8}

A, B, C, D, E, F, G : Pasquill-Gifford
Turner Curves uncorrected for Mixing Depth.

A', D', E', F' : Pasquill-Gifford-Turner
Curves Corrected for 100m Mixing Depth.

● Mobile Samples*

▲ Hourly Samples

A   B   C   D   E   F   G

F'

F'

D'   E'

* not adjusted for
difference in
sampling time

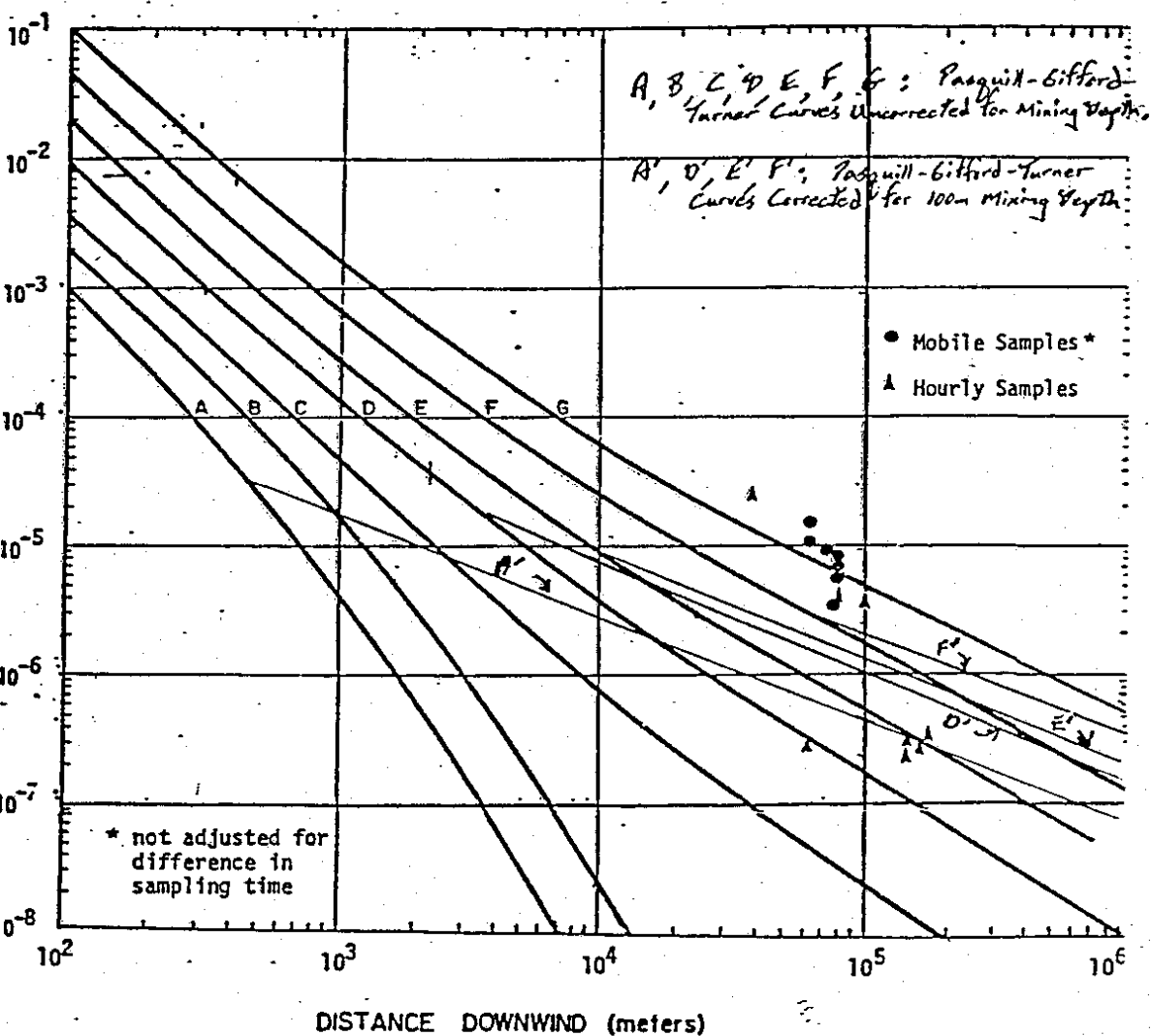10^2 10^3 10^4 10^5 10^6

DISTANCE   DOWNWIND   (meters)

Fig. 4.2.15   XU/Q VALUES   - Test 1
September 17, 1980

SANBOX Experiment (Smith et al., 1985)

Figure 1

In OCD and OCDCPM;

$$\sigma_y{}^2 = \sigma_{yt}{}^2 + \sigma_{yb}{}^2 + \sigma_{ys}{}^2 + \sigma_{yo}{}^2$$

$$\sigma_z{}^2 = \sigma_{zt}{}^2 + \sigma_{zb}{}^2 + \sigma_{zo}{}^2$$

where;

σ_{yt}, σ_{zt} represent components due to turbulence

σ_{yb}, σ_{zb} represent buoyant plume enhancement components

σ_{ys} represents wind direction shear component (no contribution to the vertical component).

σ_{yo}, σ_{zo} represent structure downwash components.

Further;

$$\sigma_{yt} = i_y * x * S_y(x)$$

where;

x = distance from source to receptor if receptor is located between shoreline and where the plume enters the TIBL, else x is the distance from source to where the plume enters the TIBL

$i_y = IYW$ = overwater horizontal turbulence intensity

$\quad = \sigma_v/UPL = \sigma_\theta \approx \tan \sigma_\theta$ (for small angles only)

UPL = wind speed at stack height

σ_v = standard deviation of horizontal wind speed fluctuations

σ_θ = standard deviation of horizontal wind direction fluctuations

$S_y(x)$ = non-dimensional function which relates overwater horizontal turbulence intensity to horizontal plume dimension

$\quad = (1 + 10^{-4}x)^{-.5}; \ x \leq 10^4 m$

for $x > 10^4 m$, assume $x = 10^4 m$ and $S_y(x)$ is equal to 0.707 for all distances greater than or equal to $10^4 m$.

$\sigma_{zt} = i_z \cdot x \cdot S_z(x)$

x = distance from source to receptor if receptor is located between shoreline and where the plume enters the TIBL, else x is the distance from source to where the plume enters the TIBL

i_z = overwater vertical turbulence intensity

$= \sigma_w/UPL = \sigma_t \approx \tan \sigma_t$ (for small angles only)

σ_w = standard deviation of vertical wind speed fluctuations

σ_t = standard deviation of vertical wind direction fluctuations

$S_z(x)$ is calculated as follows:

P-G KST	$S_z(x)$
A,B	1.0
C	$(1 + 0.0002X)^{-.5}$
D	$(1 + 0.0\ 15X)^{-.5}$
E,F	$(1 + 0.003X)^{-1.0}$
G	$(1 + S^{.5}X/(0.32 \cdot UPL))^{-.5}$

P-G stability class G is implemented when the value of the overwater vertical temperature gradient is greater than or equal to 0.05 °C/m.

$s = g\,\dfrac{\delta\Theta}{\Theta\ \delta z}$

g = acceleration due to gravity (9.81 ms^{-2})

Θ = potential temperature (°K); the temperature a parcel of air would have if it were brought <u>dry</u> adiabatically from its existing height (pressure) to a reference pressure of 1000 mb.

$\dfrac{\delta\Theta}{\delta z}$ = overwater vertical potential temperature gradient (WDTHDZ)

$\sigma_{yb}^2 = \sigma_{zb}^2 = \dfrac{(\delta h)^2}{10}$

δh = plume rise in meters

$= 2.6(F/us)^{1/3}$; usual calculation as buoyancy plume rise usually dominates

$F = gV_f/\Pi(1 - T_a/T_s)$

V_f = volumetric flow rate (m³s⁻¹)

$= \Pi r_s^2 V_s$

u = mean wind speed at anemometer height

V_s = stack exit velocity (ms⁻¹)

r_s = stack radius (m)

T_a = ambient air temperature (°K)

T_s = stack gas temperature (°K)

$\sigma_{ys}^2 = 0.03(\delta WD)^2 X^2$

δWD = wind direction shear in radians

σ_{yo} and σ_{zo} are calculated as follows:

HB = height of building or other source (in meters) to which the stack
    is attached (SOURCE(4,J))
COMPON = stack deviation angle from vertical
DELHM = momentum plume rise (m) (PTR01850)

EFFHT = THT + DELHM * COMPON
   THT = physical stack height (m) (SOURCE (5,J))
   COMPON = COS(SOURCE(9,J)/57.29578)
   57.2598 = 180./Π
A = AMAX1(1.0,ABS(EFFHT/HB))

With this background, the building downwash effects are calculated in
OCD and OCDCPM as follows:

IF(A.LT.1.2) both σ_y and σ_z are modified
IF(A.GE.1.2.AND.A.LT.3.0) only σ_z is modified
IF(A.GE.3.0) neither σ_y or σ_z are modified

IF(A.LT.1.2) THEN
   σ_{yo} = 0.79788 * HB/2.0 * (6.0 - 5.0*A)
   σ_{zo} = 0.79788 * HB/2.0 * (3.0 - A)
ELSEIF(A.GE.1.2.AND.A.LT.3.0) THEN
   σ_{zo} = 0.79788 * HB/2.0 * (3.0 - A)
ENDIF

3. MPTER

The following information applies only to P–G stability class F:

$$\sigma_y{}^2 = \sigma_{yt}{}^2 + \sigma_{yb}{}^2$$

$$\sigma_z{}^2 = \sigma_{zt}{}^2 + \sigma_{zb}{}^2$$

σ_{yt} is calculated in the following manner in MPTER:

$$TH = (4.1667 - 0.36191 \cdot ALOG(XY))/57.2958$$

XY = distance from source to receptor in km.
$ALOG$ = ln

$$\sigma_{yt} = 465.116 \cdot XY \cdot SIN(TH)/COS(TH)$$

$$465.116 = 1000.(m/km)/2.15$$

σ_{zt} is calculated in the following manner:

```
REAL XF(9),AF(10),BF(10)
DATA XF/60.,30.,15.,7.,3.,2.,1.,0.7,0.2/
DATA AF/34.219,27.074,22.651,17.386,16.187,14.283,13.953
*        13.953,14.457,15.209/
DATA BF/0.21716,0.27436,0.32681,0.41507,0.46490,.054503
*        0.63227,0.68465,0.78407,0.81558/

    DO ID = 1,9
        IF(X.GE.XF(ID)) GOTO 160
    ENDDO
    ID = 10
160    σzt = AF(ID) ' X**BF(ID)
    IF (σzt.GT.5000.) σzt = 5000.
```

X = distance from source to receptor in km

For example: P-G KST F; $x = 2000m = 2$ km

Per the above do loop, ID = 6
AF(6) = 14.823
BF(6) = 0.54503

$$\sigma_{zt} = 14.823 \cdot 2.^{**}0.54503 = 21.6m$$

$$\sigma_{zb}{}^2 = \sigma_{yb}{}^2 = \frac{(\delta h)^2}{(3.5)^2} = \frac{(\delta h)^2}{12.25}$$

The second step in the analysis was to match $\sigma_y\sigma_z$ products calculated by OCD and MPTER for reasonable worst-case conditions. The matching of $\sigma_y\sigma_z$ products is all that is necessary as the other terms in the Gaussian distribution equations for the two models are equivalent and drop out. Based on the above algorithms, $\sigma_y\sigma_z$ product calculations were made for source to receptor distances of 1000, 2000, 3000, 4000 and 5000 meters. From the matching of the $\sigma_y\sigma_z$ products, a value of IYW can be determined for each source to receptor distance analyzed. The average of the IYW value needed to result in a match of $\sigma_y\sigma_z$ values was then taken and used as the reasonable worst-case value of overwater horizontal turbulence intensity input into OCDCPM.

The analysis to match $\sigma_y\sigma_z$ products between OCD and MPTER contained several assumptions. The assumptions used are as follows:

1. Buoyancy-induced dispersion (IOPT(4).EQ.1) is employed in both MPTER and OCD.

2. The hypothetical source(s) considered in the analysis were assumed to have a 75m buoyancy plume rise (typical for a tanker at a marine terminal). The buoyancy plume rise is used to calculate buoyancy contributions to total σ_y and σ_z.

3. The overwater vertical potential temperature gradient (WDTHDZ) was assumed to be 0.05 °C/m. This forces the value of IZW to be 0.02 and the $S_z(x)$ term relating IZW to σ_{zt} to be calculated using P-G stability class G methodology.

4. Wind direction shear is not considered as this parameter is measured very infrequently (σ_{ys} in OCD is not contributing to total σ_y).

5. The height of the structure to which the stack is attached is assumed to be 15m. This parameter is necessary to calculate structure downwash (σ_{yo} and σ_{zo}) contributions to total σ_y and σ_z.

6. The value of A used in the OCD structure downwash algorithms was assumed to equal 2.0. This is based on an assumed height of the structure to which the stack is attached of 15m and an effective stack height of 30m (physical stack height plus momentum, not buoyancy plume rise). As A = 2.0, then only σ_z is modified for structure downwash effects.

The calculations involved in determining the reasonable worst-case overwater horizontal turbulence intensity value for OCD are presented below:

MPTER

$$\sigma_y{}^2 \;=\; \sigma_yt{}^2 \;+\; \sigma_yb{}^2$$

Distance (m)	σ_{yt}	σ_{yb}	σ_y
1000	33.23	21.43	39.54
2000	63.68	21.43	67.19
3000	91.92	21.43	94.39
4000	119.18	21.43	121.09
5000	145.67	21.43	147.24

$$\sigma_z{}^2 \;=\; \sigma_zt{}^2 \;+\; \sigma_zb{}^2$$

Distance (m)	σ_{zt}	σ_{zb}	σ_z	$\sigma_y\sigma_z$
1000	13.95	21.43	25.57	1011.04
2000	21.63	21.43	30.45	2045.94
3000	26.98	21.43	34.46	3252.68
4000	30.48	21.43	37.55	4546.93
5000	34.21	21.43	40.37	5944.08

OCD

$$\sigma_y{}^2 \;=\; \sigma_yt{}^2 \;+\; \sigma_yb{}^2 \;+\; \sigma_ys{}^2 \;+\; \sigma_yo{}^2$$

Distance (m)	σ_{yt}	σ_{yo}	σ_{ys}	σ_{yb}	σ_y
1000	**	0.	0.	23.72	**
2000	**	0.	0.	23.72	**
3000	**	0.	0.	23.72	**
4000	**	0.	0.	23.72	**
5000	**	0.	0.	23.72	**

** To be calculated later

$$\sigma_z{}^2 \;=\; \sigma_zt{}^2 \;+\; \sigma_zb{}^2 \;+\; \sigma_zo{}^2$$

Distance (m)	σ_{zt}	σ_{zo}	σ_{zb}	σ_z
1000	2.44	7.98	23.72	25.15
2000	3.47	7.98	23.72	25.27
3000	4.26	7.98	23.72	25.39
4000	4.93	7.98	23.72	25.51
5000	5.51	7.98	23.72	25.63

OCD σ_y and *IYW* calculations

Distance (m)	OCD $\sigma_y\sigma_z$		MPTER $\sigma_y\sigma_z$
1000	$25.15\,\sigma_y$	=	1011.04
2000	$25.27\,\sigma_y$	=	2045.94
3000	$25.39\,\sigma_y$	=	3252.68
4000	$25.51\,\sigma_y$	=	4546.93
5000	$25.63\,\sigma_y$	=	5944.08

Distance (m)	OCD σ_y		$(\sigma_{yt}^2 + \sigma_{yb}^2)^{1/2}$
1000	40.20	=	$(\sigma_{yt}^2 + 562.5)^{1/2}$
2000	80.96	=	$(\sigma_{yt}^2 + 562.5)^{1/2}$
3000	128.11	=	$(\sigma_{yt}^2 + 562.5)^{1/2}$
4000	178.24	=	$(\sigma_{yt}^2 + 562.5)^{1/2}$
5000	231.92	=	$(\sigma_{yt}^2 + 562.5)^{1/2}$

Distance (m)	σ_{yt}^2		σ_{yb}^2		σ_y^2	σ_{yt}
1000	σ_{yt}^2	+	562.5	=	1616.04	32.46
2000	σ_{yt}^2	+	562.5	=	6554.42	77.41
3000	σ_{yt}^2	+	562.5	=	16412.17	125.90
4000	σ_{yt}^2	+	562.5	=	31769.50	176.66
5000	σ_{yt}^2	+	562.5	=	53786.88	230.70

$$\sigma_{yt} = \ 32.46 = IYW \cdot 1000 \cdot S_y(x) \ ; \quad S_y(x) = 0.9535$$
$$\sigma_{yt} = \ 77.41 = IYW \cdot 2000 \cdot S_y(x) \ ; \quad S_y(x) = 0.9129$$
$$\sigma_{yt} = 125.90 = IYW \cdot 3000 \cdot S_y(x) \ ; \quad S_y(x) = 0.8771$$
$$\sigma_{yt} = 176.66 = IYW \cdot 4000 \cdot S_y(x) \ ; \quad S_y(x) = 0.8452$$
$$\sigma_{yt} = 230.70 = IYW \cdot 5000 \cdot S_y(x) \ ; \quad S_y(x) = 0.8165$$

$$IYW = \ 32.46/(1000 \cdot 0.9535) = \ 0.034$$
$$IYW = \ 77.41/(2000 \cdot 0.9129) = \ 0.042$$
$$IYW = 125.90/(3000 \cdot 0.8771) = \ 0.048$$
$$IYW = 176.66/(4000 \cdot 0.8452) = \ 0.052$$
$$IYW = 230.70/(5000 \cdot 0.8165) = \ \underline{0.056}$$

mean: **0.046**

The mean value of *IYW* was calculated to be 0.046 for the five distances analyzed. The mean value of *IYW* was then "rounded" to 0.045 for implementation into the reasonable worst-case data set.

A few observations can be made on the matching of $\sigma_y\sigma_z$ products between MPTER and OCD:

1. As the source (virtual source) to receptor distance decreases, the value of IYW necessary to match $\sigma_y\sigma_z$ products decreases. This is due to the insensitivity of OCD σ_z values to distance, while the MPTER values of σ_z decrease significantly with decreasing distance (x).

2. Buoyancy is the dominant factor in OCD σ_z values at all distances; buoyancy is the dominant factor in MPTER σ_z values at distances of less than one kilometer.

3. In these exercises, IYW is equal to 0.045 only at a 2500m distance from source (virtual source) to receptor.

4. Considerably smaller values of IYW would be necessary to match $\sigma_y\sigma_z$ products between OCD and COMPLEX-II corrected for overwater dispersion ($\sigma_z = 0.5\ \sigma_z$ as in CPX2APCD).

5. Considerably smaller values of IYW would be necessary to match $\sigma_y\sigma_z$ products between OCD and MPTER if OCD σ_z calculations were based on P-G stability class F calculations.

6. Buoyancy contributions to total σ_y and σ_z are greater in OCD than MPTER.

7. For all distances analyzed, σ_y values calculated by OCD are greater than those calculated by MPTER; σ_z values calculated by OCD are less than those calculated by MPTER at all distances analyzed.

8. Matching $\sigma_y\sigma_z$ products between OCD and MPTER (or COMPLEX-II) does not mean a matching of calculated concentrations. For example, terrain interactions, inversion height plume penetration and plume rise are not handled identically between the two models.

The matching of $\sigma_y\sigma_z$ products was performed between MPTER (COMPLEX-II without overwater dispersion corrections) and OCD. In order to review the relative concentrations calculated by OCDCPM and CPX2APCD (COMPLEX-II with overwater dispersion corrections ($\sigma_z = 0.5\ \sigma_z$)), modeling analyses were performed for eight emissions scenarios (four different source configurations and two pollutants for each configuration). For each of the following four scenarios, SO_x and NO_x emissions were analyzed:

a. Exxon NMT at SALM approximately 11,500 feet from shore
b. Exxon NMT at SALM approximately 5,500 feet from shore
c. Platform Harmony in normal position
d. Platform Harmony 5 km closer to shore than normal position.

These emissions scenarios are representative of typical project configurations offshore Santa Barbara County.

The current APCD reasonable worst-case meteorological data set was utilized as input to OCDCPM, with the exception that IYW values of 0.035, 0.040, 0.050 and 0.060 were considered as a sensitivity analysis. Extensive onshore receptor grids used in the Exxon ATC modeling were employed.

CPX2APCD was run with reasonable worst-case meteorology per the current APCD protocol and with actual pre-construction meteorological data collected by Exxon in Las Flores Canyon. For CPX2APCD, the largest modeled concentrations resulted from the use of the actual meteorology data set. The results of the 8 scenarios modeled are summarized below.

OCDCPM/CPX2APCD MODELING RESULT RATIOS

IYW	MIN	MEAN	MAX
0.035	0.66	0.91	1.25
0.040	0.62	0.81	1.11
0.050	0.50	0.66	0.91
0.060	0.41	0.57	0.77

These figures indicate that an IYW value of 0.045 would probably result in a mean ratio of OCDCPM/CPX2APCD modeled concentrations of approximately 0.73. An IYW value of 0.045 was not specifically modeled in these analyses.

3. Conclusions

An IYW value of approximately 0.045 was determined to result in a matching of $\sigma_y\sigma_z$ products between OCD and MPTER. The IYW value of 0.045 provided a match of $\sigma_y\sigma_z$ products for OCD P-G stability class G σ_z values and no overwater dispersion corrections to the MPTER dispersion values. The value of IYW would have been considerably smaller had the MPTER dispersion values been modified to account for overwater dispersion ($\sigma_z = 0.5\ \sigma_z$) or had OCD σ_z values been based on P-G stability class F calculations.

The mean ratio of OCDCPM/CPX2APCD modeled concentrations was approximately 0.73. The results of the OCDCPM and CPX2APCD modeling are consistent with the value of IYW necessary to match $\sigma_y\sigma_z$ products between OCD and MPTER. The mean ratio of 0.73 for OCDCPM/CPX2APCD modeled concentrations is likely due to the differences in terrain corrections between the two models, partial plume penetrations calculated by OCDCPM and somewhat different plume rise calculations between the two models.

The *IYW* value of 0.045 compares to P–G σ_y values as follows:

DISTANCE	OCD σ_y	P–G F σ_y	P–G E σ_y
1000	49.03	39.54	50.94
2000	85.52	67.19	95.70
3000	120.76	94.39	138.13
4000	153.97	121.09	179.06
5000	185.24	147.24	218.87
MEAN:	118.90	93.89	136.54

This indicates that the use of *IYW* = 0.045 is an emulation of P–G stability class E–F (somewhat closer to E).

The choice of *IYW* equal to 0.045 as a reasonable worst–case value must still include a safety factor to avoid model underprediction. Based on EPA concerns that the OCD model appears to underpredict by 10 to 20 percent and APCD concerns that OCD underpredicts by roughly 45 percent (different statistics were used to draw the separate conclusions), a multiplication factor of 1.2 was chosen to alleviate concerns that OCDCPM would significantly underpredict observed pollution concentrations. The use of a multiplier to alleviate APCD concerns was first suggested by the ARB.

4. References

Smith, T.B, W.D. Saunders and F.H. Shair (1983), "Analysis of Santa Barbara Oxidant Study," MRI FR–1900, Meteorological Research Inc., Altadena, CA 91001.

Turner, D.B. (1970), "Workbook on Atmospheric Dispersion Estimates," Environmental Protection Agency, Office of Air Programs, Publication No. AP–26.

Chapter 1

TRANSPORT AND DISPERSION OF AIRBORNE POLLUTANTS ASSOCIATED WITH THE LAND BREEZE-SEA BREEZE SYSTEM

by

F. H. Shair, E. J. Sasaki and D. E. Carland
Chemical Engineering

G. R. Cass and W. R. Goodin[*]
Environmental Quality Laboratory

California Institute of Technology
Pasadena, California 91125

J. G. Edinger
Department of Atmospheric Sciences
UCLA
Los Angeles, California 90024

and

G. E. Schacher
Department of Physics and Chemistry
Naval Postgraduate School
Monterey, California 93940

October 1981

[*]Present affiliation: Dames & Moore, 1100 Glendon Avenue
Los Angeles, California 90024

ABSTRACT

Two atmospheric tracer experiments were conducted in July 1977. SF_6 was released for a 5-hour period during each of two nights from a coastal power plant stack located at the El Segundo Generating Station in the Los Angeles Basin. The purpose of this study was to investigate the transport and dispersion of plumes released into the land breeze portion of a land breeze/sea breeze circulation system. Even though a portion of the plume was apparently injected above the base of the nighttime inversion, essentially all of the tracer was observed to return across a control surface (from sea level to the base of the inversion) along the coast throughout the sea breeze regime during the following day. The residence time distribution functions of tracer material over the sea were almost identical in both experiments. The average residence time for tracer material over the ocean was 10 hours in both cases; however, some of the tracer spent as much as 16 hours out over the sea. The horizontal dispersion of tracer was also greater than expected, with between 75 and 100 km of coastline impacted by the return of SF_6 from a single elevated source. Data from both shipborne and coastal monitoring stations indicated that the path followed by the tracer over the ocean could not have been tracked accurately using trajectories constructed from conventionally available meteorological data.

1. Introduction

Coastal emission sources present special difficulties for air quality control programs because of the complexities associated with coastal meteorological processes. Differential heating of land and sea surfaces often generates an inland flow of air during the daylight hours. However at night, the land cools faster than the sea, and the wind may reverse direction. The fate of pollutants emitted into the nighttime offshore breeze is difficult to evaluate using conventional air quality models because of the lack of meteorological data needed to describe the flow reversal and mixing processes over the water.

The objective of the present study was to explore the transport and dispersion of elevated plumes released into the land breeze portion of a land breeze/sea breeze circulation system. An inert gaseous tracer, SF_6, was used to determine the extent to which pollutants sent seaward at night from elevated coastal Los Angeles emission sources by a land breeze could return to the Los Angeles region at ground level during the next day's sea breeze. Multiple passes of the same air mass over coastal emission sources could lead to pollutant accumulation in the air basin of interest. In order to gauge the potential magnitude of this accumulation problem, the fraction of the emissions into the land breeze that returned the next day was determined, along with the degree of dilution observed and the retention time available for chemical reaction of pollutants while they resided in the marine environment.

2

2. Previous Studies of Land-Sea Breeze Transport Phenomena

Land-sea breeze circulation systems-- their extent, duration,
frequency and intensity have been studied for many years (see for
example Eatontown Signal Laboratory Group, 1945; Defant, 1951; Kraus,
1972; Scorer, 1978). It has been shown that sea breeze/land breeze
systems influence air pollutant transport over the Great Lakes and East
Coast regions of the United States (Lyons and Olsson, 1973; Lyons,
1975; Raynor et al. 1975; Lyons and Keen, 1976; SethuRaman and Raynor,
1980). But perhaps the most widely studied coastal breeze system is
that associated with the Los Angeles region. Beginning in the late
1940's it was realized that the sea breeze portion of this coastal
meteorological phenomenon dominates air pollution transport across the
Los Angeles Basin (Beer and Leopold, 1947; Kauper, 1960; Taylor, 1962;
DeMarrais, Holzworth and Hosler, 1965). In succeeding years, air
pollution aspects of the Los Angeles land-sea breeze system have been
explored by trajectory calculations, tetroon flights, fluorescent
particle releases and SF_6 tracer studies.

Early studies of air parcel transport in the Los Angeles Basin
were based on trajectories constructed from surface wind data (Edinger,
1948; Neiburger and Edinger, 1954; Neiburger, Renzetti and Tice, 1956;
Taylor, 1962). Emphasis was placed on inland sea breeze transport of
photochemically-reacting pollutants. Forward and backward trajectories
were calculated between major source areas and inland receptor points
such as downtown Los Angeles. In the absence of routine meteorological
measurements over the ocean, only a few studies paid attention to the

3

fate of materials transported seaward by the land breeze. Kauper

(1960) analyzed meteorological and air quality data from a day during

which the measured oxidant concentration exceeded 0.5 ppm in the

afternoon at the coast near El Segundo. His conclusion was that

transport of oxidant precursors offshore by the land breeze and

subsequent reaction and onshore transport of oxidant by the following

sea breeze caused the high concentration of pollutants observed at the

coast. Kauper and Niemann (1975, 1977) conducted two studies to

characterize interbasin pollutant transport. Their analyses utilized

extensive pibal, surface, aircraft, and ship data to calculate the path

of specific "parcels" of air as they moved from the Los Angeles Basin

over water to downwind receptors. They concluded that high ozone

levels measured at Oxnard during June and July, 1975, and at San Diego

during October, 1976, were the result of ozone transport aloft from the

Los Angeles Basin.

In order to study transport into zones of sparse meteorological

data, tracer techniques can be employed. Holzworth, Kauper and Smith

(1963) released three tetroons from downtown Los Angeles on a summer

day and tracked their movement visually along generally inland

trajectories. Pack and Angell (1963) released 88 tetroons from nine

Los Angeles area coastal sites into both land and sea breeze flows and

tracked their motion using radar mounted on Catalina Island. Of

special interest were 4 releases made from Long Beach during two

successive nights. One of the tetroons moved parallel to the coastline

before being transported inland at about 4 a.m.; a second one spent the

nighttime hours over water before recrossing the coastline at dawn,

4

while two of the four tetroons moved seaward and spent considerable time over water before recrossing the coastline the next day with the afternoon sea breeze. Angell et al. (1972) monitored the three-dimensional motion of tetroons over the Los Angeles Basin. Most of those releases were into the sea breeze although the balloons were tracked at all hours of the day and night. They concluded that during the day, trajectories computed from surface wind data provide a reasonably good estimate of the motion in the lowest few hundred meters of the atmosphere. However, at night the situation is much more complex due to the presence of substantial wind shear in the vertical direction. As a result, quantitative evaluation of pollutant transport and dispersion processes that occur at night over the ocean will have to proceed by means other than surface wind trajectory calculations.

Information on pollutant dispersion can be derived from tracer experiments that employ fluorescent particles or SF_6. Fluorescent particle studies attempted in the Los Angeles area have met with mixed results. The fraction of the fluorescent tracer material released which can be accounted for at monitoring sites is often quite low, as experienced by Kauper, Holmes and Street (1955). Neiburger (1955) designed an experiment in which fluorescent particles were released into the Los Angeles nighttime land breeze, but the fate of the particles released could not be determined. Vaughan and Stankunas (1974) released fluorescent particles during the morning of seven days between the summer of 1972 and the fall of 1973. They obtained no information concerning the fate of emissions transported seaward at night.

5

Sulfur hexafluoride gas (SF_6) is a much better tracer than fluorescent particles when attempting to characterize the transport and dispersion of gaseous pollutants. SF_6 is detectible at concentrations less than one part in 10^{12} parts air. Ground level dry deposition, which adversely affects recovery of fluorescent particles, is eliminated because SF_6 is an inert gas. Drivas and Shair (1974, 1975) and Lamb et al. (1977) have employed SF_6 to investigate transport and dispersion of gaseous pollutants during daytime sea breeze conditions in the Los Angeles area. The nighttime seaward transport and dispersion characteristics within land-sea breeze systems remain to be determined.

3. Experimental Design and Procedures

On two occasions during July 1977, SF_6 tracer was released late at night into the stack of Unit 4 at the Southern California Edison Company's El Segundo Generating Station. Pilot balloon observations made at Hermosa Beach prior to each release indicated that an offshore land breeze set up aloft above 300 meters around midnight on these occasions and propagated downward with time. Tracer releases were initiated after the offshore flow was confirmed to exist at and above about 200 m in elevation. During Test 1, SF_6 was released at a rate of 5.0 g s^{-1} from 0005 hours to 0500 hours PDT on July 22, 1977. Test 2 occurred at an SF_6 release rate of 13.6 g s^{-1} from 2303 hours PDT July 23, 1977 until 0400 hours PDT July 24, 1977.

6

Prior to each release, SF_6 sampling was initiated aboard the U.S. Navy Research Vessel Acania as it cruised in a zig-zag pattern across the Santa Monica Bay downwind of the tracer release point. Air samples of 10-second duration were taken at one to five minute intervals using 30 cm^3 plastic syringes. Portable electron capture gas chromatographs placed onboard the ship permitted rapid feedback of tracer concentration information during each test. A description of electron capture detection of SF_6 is provided elsewhere (Drivas, 1974; Lamb et al. 1977). Calibration results show that SF_6 concentrations down to 10^{-12} parts SF_6 per part air are readily detected. For comparison, if the total amount of tracer released during each test were uniformly distributed throughout an air volume of 40 km by 40 km by 300 m (i.e. the air volume over the entire Santa Monica Bay from the sea surface to above the effective stack height of the power plant), then the average tracer concentrations would have been about 29 and 78 ppt for Tests 1 and 2 respectively. Ability to detect the power plant plume if encountered at the sea surface thus was reasonably assured.

Tracer releases were halted when the land breeze subsided. In anticipation of a reversal in wind direction associated with the following sea breeze, SF_6 sampling then was initiated at a network of 29 fixed coastal monitoring sites located from Ventura to Corona del Mar (see Fig. 1). Hourly average samples were collected consecutively from 0500 to 1700 hours PDT at these coastal fixed sites during both

7

tests. SF_6 concentrations also were monitored hourly from July 19 through July 29 at Santa Catalina Island.

Automobile sampling traverses were conducted periodically along coastal highways between 1000-1427 hours PDT July 22 and between 0235-1540 hours PDT July 24. Grab samples were collected at 0.8 to 3.2 km intervals along coastal U.S. Highway 1 between Redondo Beach and Malibu, and along Interstate Highway 405 between the San Fernando Valley and either the Long Beach harbor area or northern Orange County. The purpose of the coastal fixed samplers and highway traverses was to assess the time and place at which pollutants sent seaward at night were returned back across the coastline.

Meteorological data were collected both at sea and on land during each test in order to assist explanation of the tracer concentrations observed. The depth of the mixed layer above the sea surface over Santa Monica Bay was established by continuous acoustic sounder recordings made aboard the R.V. Acania. Vertical temperature profiles up to 1000 m altitude were obtained by radiosondes released from the ship at 0200 hours, 0600 hours and 0900 hours PDT on both July 22 and July 24. In addition, the Acania was equipped with two masts instrumented to measure wind speed, temperature, dew point/humidity, temperature fluctuations and wind speed fluctuations at elevations of 4.2 m, 7.0 m, 14.7 m and 20.5 m above the sea surface. Sea surface temperature was monitored from a boom extending 3.1 m in front of the ship's bow. Meteorological data taken aboard the Acania are presented

8

by Schacher et al. (1978, 1980). The ship's instrumentation is
described in detail by Houlihan et al. (1978).

Data on winds aloft were gathered from a limited number of pibal
releases conducted at Hermosa Beach near the point of tracer injection.
Pilot balloons were launched at 5 times from 2100 hours PDT on July 21
through 0400 hours PDT on July 22, and at 9 times from 2100 hours PDT
on July 23 through 0540 hours PDT on July 24. Wind speed and direction
were recorded at 100 m intervals above sea level. Low strata
inhibited the use of pibals at altitudes greater than 400 to 600 m on
several occasions. Hourly observations of surface wind speed and
direction can be obtained in the Los Angeles area at more than 50
land-based meteorological stations operated by the National Weather
Service, local air pollution control districts, the California Air
Resources Board and the U.S. Navy.

4. Tracer Test Results

   Test 1   July 22, 1977

   Pibal observations taken at Hermosa Beach at 2100 hours PDT on
July 21 showed an onshore flow at the surface with an offshore flow
aloft above 500 m elevation. By 2200 hours on that day, the land
breeze had propagated downward to about 300 m elevation. Shortly
before midnight, the land breeze was observed at the ocean's surface
aboard the Acania as it cruised less than 10 km seaward from El
Segundo. Starting at 0005 hours PDT on July 22, the SF_6 tracer was
released into the offshore flow from the El Segundo power plant stack.

9

Radiosonde measurements taken at the ship at 0200 hours PDT showed that a strong temperature inversion based at between 200 and 240 m elevation existed over the Acania at that time. The acoustic sounder indicated the depth of the mixed layer to be about 200 m at 0000 PDT July 22. From that time until 0630 PDT the depth of the mixed layer above the ship remained at or below about 220 m (with the exception of a single value of 250 m recorded at 0220 hours PDT). At 0630 PDT, the top of the mixed layer rose above 220 m, and remained between 220 m and 280 m until noon (again with the exception of one measurement at about 200 m depth).

The trajectory of the SF_6 plume over the Santa Monica Bay was estimated from available meteorological data. Streaklines corresponding to plume centerlines were constructed from sparse upper level pibal data. Using Briggs' (1971) plume rise formula, the effective stack height of the power plant was estimated to be approximately 250 m. Plume rise calculations by the method of Schatzmann (1979) yield similar results (McRae et al, 1981). Thus during the SF_6 release, it appears that the plume would have risen at least to the base of the temperature inversion and possibly into the stable air mass within the inversion. Because of the uncertainties associated with plume rise calculations, possible plume trajectories in the horizontal plane were computed using pibal observations from two heights, 108 m and 315 m. Pibal measurements taken on the hour were assumed to apply to the following full hour. Surface wind data were used to compute horizontal transport for comparative purposes.

10

SF$_6$ tracer concentrations measured aboard the Acania and estimated plume locations are compared in Figure 2. On three occasions prior to 0530 PDT, the ship passed beneath the computed location of the plume: at about 0100 hours, between 0300 and 0330 hours, and again between 0430 and 0500 hours PDT. The mixing depth on all three occasions was below 200 m and no significant concentrations of SF$_6$ were detected, except that as the ship passed beneath the plume at 0325 and at 0437 PDT, very small amounts of SF$_6$ were detected (14 ppt and 11 ppt, respectively). At 0220 hours when the mixing depth above the ship briefly exceeded 220 m, the ship was located far to the south of the likely location of the plume.

Between 0530 and 0545 PDT, the first significant peak in SF$_6$ concentration (80 ppt) was recorded at the ship. At this time the top of the mixed layer was rising toward the 200 m level. The ship was well south of the plume centerline computed from 100 m wind data. Trajectories computed from 300 m winds would place the plume in the vicinity of the ship at that time.

At 0615 PDT the ship moved northward to recross the path of the plume. Between 0620 and 0640 PDT the depth of the mixed layer increased to 240 m. Shortly thereafter high concentrations of SF$_6$ were measured at sea level as the ship passed beneath the computed location of the plume. From 0830 until 1130 PDT the ship saw no less than 18 ppt of SF$_6$ at the sea surface as it cruised across the central portion of the Santa Monica Bay.

11

Between 0700 and 0800 hours PDT, net onshore sea breeze flow was established along the coastline from Ventura to northern Orange County. SF_6 concentrations greater than 10 ppt were first observed in air recrossing the coast between 0900 and 1000 PDT. For the next 8 hours, SF_6 continued to cross the coastline from north of Pt. Mugu to as far south as Long Beach, a distance of roughly 100 km, as shown in Figure 3.

SF_6 Mass Balance Calculations

In order to determine the residence time distribution of the stack gases within the marine environment, a mass balance was constructed for the flux of SF_6 tracer returning landward during the day following each tracer release. A control surface, generally paralleling the coastline, was constructed from seven straight line segments attached end to end such that each segment traversed a zone of common topographic conditions, as listed in Table 1. Surface wind stations lying along each stretch of coastline were reviewed. A station or pair of stations was chosen to represent air mass motion along each section of the control surface, as listed in Table 1. Whenever possible, the average of the wind speed and direction measured at two wind stations located as far apart as possible along each stretch of coastline was employed to estimate average air velocity along that entire coastal segment. This was done in order to reduce the effect of errors in a single wind station's record that could affect the large air fluxes calculated across coastal flatlands.

12

Wind vectors apparent at each hour along each segment of the control surface were resolved into their components normal to the coast. The distance that the wind penetrated across each stretch of coastline during each hour was defined in this manner. Using the length of each control surface segment as a crosswind dimension, and the mixing depth data from the Acania as a vertical dimension, the volume of air crossing the coast within the surface mixed layer was determined at each hour.

The control surface parallel to the coast was subdivided into short intervals approximately centered on each SF_6 monitoring site. This subdivision was accomplished by bisecting the distance between each adjacent pair of SF_6 sampling stations and then drawing a line perpendicular to the control surface from the midpoint between each pair of monitoring sites. In that manner, the volume of air crossing the coast during each hour was apportioned between SF_6 monitoring sites.

The SF_6 concentration averaged over each hour at each sampling station was assumed to represent the average concentration of SF_6 in the air flow assigned to the coastline interval surrounding it. SF_6 concentrations shown in Figure 3 were then converted to SF_6 mass fluxes within the surface mixed layer of the atmosphere crossing each coastal interval at each hour. By summing these SF_6 fluxes, a mass balance for SF_6 released and recovered was constructed, and the residence time distribution of the tracer and associated emissions over the ocean was determined.

13

The results of the SF_6 mass balance from Test 1 are shown in Figure 4a. These calculations indicate that essentially all of the SF_6 released into the land breeze at night was observed to recross the coastline of the air basin within the surface mixed layer during the following day's sea breeze regime. Sixty-nine percent of the tracer material recrossed the Los Angeles County coastline along the Santa Monica Bay (near the release point), while thirty-one percent of the SF_6 returned across the Ventura County coastline near Oxnard to the north. Transport of such a large fraction of the tracer material northward into Ventura County would not have been predicted from trajectories drawn from available surface wind data.

Test 2   July 24, 1977

At 2200 hours PDT July 23, pilot balloons released from Hermosa Beach showed an onshore flow at 108 m elevation with offshore flow aloft at and above 216 m elevation. One half hour later, pibal observations indicated that the land breeze existed at 108 m elevation and above. At 2303 hours PDT the second release of tracer was begun from the power plant stack.

The first acoustic sounder measurements made following the start of this experiment place the base of the sub-tropical inversion at about 500 m above the Acania. A strong temperature inversion at that elevation persisted throughout the night as shown by both the acoustic sounder and the radiosondes taken at 0200 plus 0600 PDT. Between 1000 and 1100 hours PDT, the inversion base dropped from around 500 m to about 300 m elevation, then returned to 500 m briefly before

14

stabilizing at a height between 260-350 m during the rest of the experiment.

Possible plume trajectories in the horizontal plane were computed using pibal observations at 108 m and 315 m elevations plus surface wind data. In Figure 5, SF_6 concentration measurements obtained aboard the Acania are co-ordinated with the ship's position and possible plume centerline locations. SF_6 was first observed at the sea surface aboard the Acania at 0144 hours, reaching a short term peak of 59 ppt at 0152 hours while the ship was very close to the coast at Santa Monica. Low levels of tracer were measured at the ship almost continuously thereafter. SF_6 was first observed at the surface at the coast from Santa Monica to Carbon Canyon Road (near Malibu) between 0250 and 0330 PDT during two automobile traverses along Highway 1. Concentrations up to 64 ppt SF_6 were found ashore at a point closely corresponding to the end point of the plume trajectory computed from 100 m winds shown in Figure 5.

At 0400 hours, the plume trajectories computed from Hermosa Beach pibal data and surface winds would suggest that the plume was confined to an area over Santa Monica Bay within 15 km of the coastline to the north and west of the release point. SF_6 measurements obtained aboard the Acania, however, show a quite different picture. The Acania first encountered high SF_6 concentrations (up to 461 ppt) shortly after 0400 hours PDT at a location well west of the plume trajectory computed from 300 m winds. After apparently crossing through the plume at about 0415 PDT, SF_6 concentrations dropped to a low of 34 ppt. The ship then

15

executed a series of turns and eventually headed in a southeast

direction parallel to the El Segundo coastline at a distance of about

20 km offshore. SF_6 concentrations at the ship were observed to

increase continuously from 0600 hours to 0800 hours to levels above 250

ppt, although the ship was west or south of the computed position of

the plume at most times. Southward motion of a portion of the plume

over the ocean also is confirmed by the SF_6 monitoring station at Santa

Catalina Island which recorded SF_6 concentrations up to 36 ppt briefly

during the period 1200-1500 hours PDT.

Onshore flow was already apparent at the coast from Malibu

southward when sampling commenced at 0500 hours at the coastal fixed

monitoring stations. As in Test 1, the tracer material was observed to

be transported over long distances within the marine environment before

recrossing the coast the next day. In this case, the predominant

direction of flow was more northerly (toward the south) than

encountered during Test 1. Tracer material was measured recrossing

both the Santa Monica Bay and Long Beach portions of the Los Angeles

County coast, as well as along the Los Alamitos to Newport Beach

stretch of the coast of Orange County to the south of Los Angeles (see

Figure 6).

A mass balance for SF_6 released versus that returned inland by

the sea breeze was constructed by methods previously described. The

acoustic sounder showed a weak intermittent return during Test 2 at an

elevation below the location of the sub-tropical inversion base. Mass

balance calculations using that return height as a mixing depth would

16

indicate a 49% recovery of the tracer released. Careful reexamination of the acoustic sounder records indicates that the sub-tropical inversion base was the true limit to vertical dispersion in this case. Using the base of the sub-tropical inversion as as estimate of the mixing depth during Test 2, 244 kg of SF_6 (essentially all of the SF_6 released) would have recrossed the coastal monitoring network (as shown in Figure 4b).

It is clear that selection of wind stations and mixing depths influences mass balance results. A sensitivity analysis of mass balance results was conducted independently by Sackinger et al. (1981). Their calculations also indicate that the great majority of the tracer material sent seaward at night during both Tests 1 and 2 returned inland the next day with the sea breeze.

5. Summary and Discussion

Results from both Tests 1 and 2 show that a major portion of the tracer material released into a land breeze at night from an elevated coastal emission source was advected back over the coast during the following day's sea breeze. Multiple passes of the same air mass over coastal point sources thus leads to pollutant accumulation within the Los Angeles basin.

The retention time for pollutants within the marine environment during these tests can be estimated from Figures 4a and 4b, and is shown in Figure 7. When normalized on the basis cf the total amount of SF_6 returned to land, the residence time distributions for SF_6 over the

ocean during Tests 1 and 2 are remarkably similar. The median age of the material returned to land was about 10 hours in both tests. On a first in/last out basis, some of the emissions could have been retained over the ocean for up to 16 hours. Even relatively slow chemical reactions involving pollutants trapped in such a land/sea breeze circulation system would have considerable time to proceed toward completion before emissions returned to encounter receptor populations.

Dispersion of tracer material during these tests was much greater than expected. The tracer dosage accumulated along the coastal monitoring sites is given in Figure 8, and shows that SF_6 released into the land breeze from a single source crossed between 75 and 125 km of coastline during the following day's sea breeze. During both tests, at least some tracer material was found in the vicinity of trajectories drawn from surface or upper level wind data. But in both cases, the northward or southward edge of the returning tracer cloud was much farther from the release point than would be indicated by trajectories drawn from pibal releases made near the source. During Test 1, two pronounced peaks in SF_6 mass were observed to be crossing the coast simultaneously (see Figure 3), one near the SF_6 release point and another far to the northwest near the Ventura/Los Angeles County line. This plume apparently was dispersed by wind shear over the Santa Monica Bay.

In the case of Test 1, a description of transport and dispersion processes can be provided which is compatible with shipboard observations of SF_6 concentrations, mixing heights, inversion height,

18

and data on winds aloft. The essential features are:

(a)   The heated plume from the stack rises to the base of the inversion where it arrives still a little warmer than the ambient air but not as warm as the air a short distance above. The plume levels out at this height and partially penetrates the base of the inversion. The coolest plume material is below the inversion base and the warmest just above. Stronger winds aloft carry the upper parts of the plume farther out to sea than the lower portion which moves more nearly with the surface wind field.

(b)   A mixed layer begins forming at the sea surface as air, previously cooled by contact with the nocturnally cooled land surface, crosses the coastline on the land-breeze and encounters the warmer ocean surface. The convectively mixed layer which develops grows in thickness as the heating from below continues, and in time the top of this mixed layer approaches the base of the inversion.

(c)   Upon reaching the lower edge of the plume, the convective mixing motions fumigate SF_6 down to the sea surface. This fumigation process accounts for the observation that the SF_6 suddenly appeared at the sea surface after 0500 PDT but was not observed during three prior ship passages beneath the plume earlier in the experiment. Fumigation continues as long as plume material remains near the base of the inversion, in time distributing it almost uniformly from sea surface to inversion base. A detailed quantitative treatment of the convective downmixing processes

19

which act on the plume during this experiment is provided by
McRae et al. (1981), and shows that the time scales for
convective mixing during this experiment are consistent with the
above fumigation hypothesis.

(d)   The plume material begins moving back toward land when the
        seaward limit of the land breeze begins to move toward land as
        the morning sea breeze develops. This zone of convergence
        between the land- and sea-breeze produces a swelling of the sub-
        inversion layer and can propagate through the atmosphere at
        speeds exceeding the sea breeze. The ship passed through this
        zone at 0735 PDT at which time the maximum mixing height, 280 m,
        was observed at the ship.

Results obtained during Test 2 would not have been explained by
an air quality model using commonly available meteorological
measurements. In particular, transport of material southward to Santa
Catalina Island, Newport Beach and Corona Del Mar would not have been
predicted from pibals launched near the SF_6 release point or from
trajectories drawn from surface wind data. Uncertainties in the mixing
depth estimates would have further complicated pollutant concentration
calculations. Under these circumstances, a tracer like SF_6 is
essential to an assessment of pollutant transport and dispersion.

20

Acknowledgement

REFERENCES

Angell J.K., Pack D.H., Machta L., Dickson C.R. and Hoecker W.H.(1972)
    Three-dimensional air trajectories determined from tetroon
    flights in the planetary boundary layer of the Los Angeles basin.
    J. Appl. Met. 11, 451-471.

Beer C.G.P. and Leopold L.B. (1947) Meteorological factors influencing
    air pollution in the Los Angeles area. Trans. Amer. Geophysical
    Union 28, 173-192.

Briggs G.A. (1971) Plume rise: a recent critical review, Nuclear
    Safety 12, 15-24.

Defant F. (1951) Local winds, in Compendium of Meteorology, Amer. Met.
    Soc., Boston, Mass., 655-662.

DeMarrais G.A., Holzworth G.C. and Hosler C.R. (1965) Meteorological
    summaries pertinent to atmospheric transport and dispersion over
    southern California, Report No. 54, U.S. Weather Bureau,
    Washington, D.C., 90 pp.

Drivas P.J. (1974) Investigation of atmospheric dispersion problems by
    means of a tracer technique, Ph.D. Thesis, California Institute
    of Technology, Pasadena, California, 91125.

Drivas P.J. and Shair F.H. (1975) The chemistry, dispersion and transport
    of air pollutants emitted from fossil fuel power plants in California-
    Transport of plumes associated with the complex coastal meteorology,
    Division of Chemistry and Chemical Engineering, California Institute
    of Technology, performed under California Air Resources Board
    Contract No. ARB-915.

Drivas P.G. and Shair F.H. (1974) A tracer study of pollutant transport
    and dispersion in the Los Angeles area. Atmospheric Environment
    8, 1155-1163.

Eatontown Signal Laboratory Group (1945) Local Winds — mountain and
    valley winds, land and sea breezes, Report No. 982, U.S. Army
    Signal Corps, Dugway Proving Grounds, Tooele, Utah, 50 pp.

Edinger J.G. (1948) A study of air flow in the Los Angeles basin,
    Meteorology Department, UCLA, June, 106 pp.

Holzworth G.C., Kauper E.K. and Smith T.B. (1963) Some observed low-
    level air trajectories over Los Angeles, California. Mon. Wea.
    Rev. 91, 387-392.

Houlihan T.M., Davidson K.L. Fairall C.W. and Schacher G.E. (1978)
Experimental aspects of a shipboard system used in investigation
of overwater turbulence and profile relationships, Naval Post
Graduate School Report No. NPS 61-78-001, Monterey, California.

Kauper E.K., Holmes R.G. and Street A.B. (1955) The verification of
surface trajectories in the Los Angeles basin by means of upper
air observations and tracer techniques, Tech. Paper No. 14, Air
Pollution Control District, Los Angeles, California, 19 pp.

Kauper E.K. and Niemann B.L. (1975) Los Angeles to Ventura over water
ozone transport study, Metro Monitoring Services, Covina,
California, 51 pp.

Kauper E.K. (1960) The zone of discontinuity between the land and sea
breeze and its importance to southern California air pollution
studies, Bull. Amer. Met. Soc. 41 410-422.

Kauper E.K. and Niemann B.L. (1977) Los Angeles to San Diego three
dimensional ozone transport study, Metro Monitoring Services,
Covina, California, 43 pp.

Kraus, E.B. (1972), Atmosphere-Ocean Interaction, Clarendon Press,
Oxford, 275 pp.

Lamb B.K., Lorenzen A. and Shair F.H. (1977) Atmospheric dispersion
and transport within coastal regions -- Part I., Tracer study of
power plant emissions from the Oxnard Plain. Atmospheric
Environment 12, 2089-2100.

Lyons W.A. (1975) Turbulent diffusion and pollutant transport in
shoreline environments, Lectures on Air Pollution and
Environmental Impact Analyses, ed: D.A. Haugen, Amer. Met. Soc.,
Boston, Mass., 136-208.

Lyons W.A. and Olsson L.E. (1973) Detailed mesometeorological studies
of air pollution dispersion in the Chicago lake breeze. Mon.
Wea. Rev. 101, 387-403.

Lyons W.A. and Keen C.S. (1976)) Computed 24-hour trajectories for
aerosols and gases in a lake/land breeze circulation cell on the
western shore of Lake Michigan, Proc. Sixth Conf. on Weather
Forecasting and Analysis, Amer. Met. Soc., Albany, New York, May
10-14, 78-83.

McRae G.J., Shair F.H. and Seinfeld J.H. (1981) Convective downmixing
of plumes in a coastal environment, J. Applied Meteorology, (in
press).

Neiburger M. (1955) Tracer tests of trajectories computed from
observed winds, Tech. Report No. 7, Air Pollution Foundation, Los
Angeles, California, 59 pp.

Neiburger M. and Edinger J.G. (1954) Summary report on meteorology of the Los Angeles basin with particular respect to the "smog" problem, Report No. 1, Southern California Air Pollution Foundation, Los Angeles, California, 97 pp.

Neiburger M., Renzetti N.A. and Tice R. (1956) Wind trajectory studies of the movement of polluted air in the Los Angeles basin, Report No. 13, Air Pollution Foundation, Los Angeles, California, 74 pp.

Pack D.H. and Angell J.K. (1963) A preliminary study of air trajectories in the Los Angeles Basin as derived from tetroon flights. Mon. Wea. Rev. 91, 583-604.

Raynor G.S., Michael P., Brown R.M. and SethuRaman S. (1975) Studies of atmospheric diffusion from a nearshore oceanic site. J. Appl. Met. 14, 1080-1094.

Sackinger, P., Reible, D.D., Shair F.H. (1981) Uncertainty Propagation for Mass Balances Associated with Transport of Atmospheric Pollutants, submitted for publication in J Air Pollut. Control Assoc.

Schacher G.E., Davidson K.L. and Fairall C.W. (1980) Atmospheric marine boundary layer mixing rates in the California coastal region, Naval Post Graduate School Report No. NPS61-80-003, Monterey, California, 115 pp.

Schacher G.E., Fairall C.W., Davidson K.L. and Houlihan T.M. (1978) Experimental investigation of the marine boundary layer in support of air pollution studies in the Los Angeles Air Basin, Naval Post Graduate School Report No. NPS61-78-002. Monterey, California, 257 pp.

Schatzmann M. (1979) An integral model of plume rise. Atmospheric Environment 13 721-731.

Scorer R.S. (1978) Environmental Aerodynamics, Ellis Horwood Ltd., Chichester, U.K., 488 pp.

SethuRaman S. and Raynor G.S. (1980) Comparison of mean wind speeds and turbulence at a coastal site and an offshore location. J. Appl. Met. 19, 15-21.

Taylor J.R. (1962) Normalized air trajectories and associated pollution levels in the Los Angeles basin, Air Quality Report No. 45, Air Pollution Control District, Los Angeles, California, 135 pp.

Vaughan L.M. and Stankunas A.R. (1974) Field study of air pollution transport in the South Coast Air Basin. Tech. Report No. 197. Metronics Associates, Inc., Palo Alto, California, 135 pp.

TABLE 1

Description of the Coastline Segments that form
the Control Surface for SF$_6$ Mass Balance Calculations

COASTLINE SEGMENT	TOPOGRAPHIC FEATURES	WIND STATION(S) USED TO CALCULATE AIR FLOW ACROSS COAST	SF$_6$ MONITORING SITES ALONG THAT SEGMENT OF COASTLINE
1. Ventura to Pt. Mugu	Coastal Plain	Average of Ventura and Pt. Mugu	Stations 1 through 5
2. Pt. Mugu to Pt. Dume	Coastal Mountains	Zuma Beach	Stations 6 and 7
3. Pt. Dume to Pacific Palasades	Coastal Mountains	Malibu	Stations 8 through 10
4. Pacific Palasades to Redondo Beach	Coastal Plain	Average of Venice and Redondo Beach	Stations 11 through 16
5. Redondo Beach to Long Beach	Coastal Mountains	Average of Redondo Beach and Long Beach (APCD Station)	Stations 17 through 19
6. Long Beach to Los Alamitos	Coastal Plain	Average of Long Beach (APCD Station) and Long Beach Airport	Stations 20 through 22
7. Los Alamitos to Newport Beach	Coastal Plain	Average of Los Alamitos and Newport Beach	Stations 24 through 29

Figure Captions

Figure 1   Southern California showing the monitoring sites used
            during the tracer experiment.

Figure 2 SF_6 concentrations observed aboard the Acania, coordinated
            with the ship's position and possible plume centerline
            locations: Test 1.

Figure 3   Hourly average SF_6 concentrations measured at
            the coastline during Test 1.

Figure 4a   Material balance on SF_6 release and return: Test 1.

Figure 4b   Material balance on SF_6 release and return during Test 2,
            computed using mixing depths implied by the location of the
            sub-tropical inversion base.

Figure 5 SF_6 concentrations observed aboard the Acania, coordinated
            with the ship's position and possible plume centerline
            locations: Test 2.

Figure 6   Hourly average SF_6 concentrations measured at the
            coastline during Test 2.

Figure 7   Retention time distribution for tracer material within the
            marine environment. Symbols indicate time measured from the
            midpoint of the tracer release. Error bounds indicate the
            5 hour span during which the returning tracer might have
            been released.

Figure 8 SF_6 dosage (ppt-hr) observed along the coastline
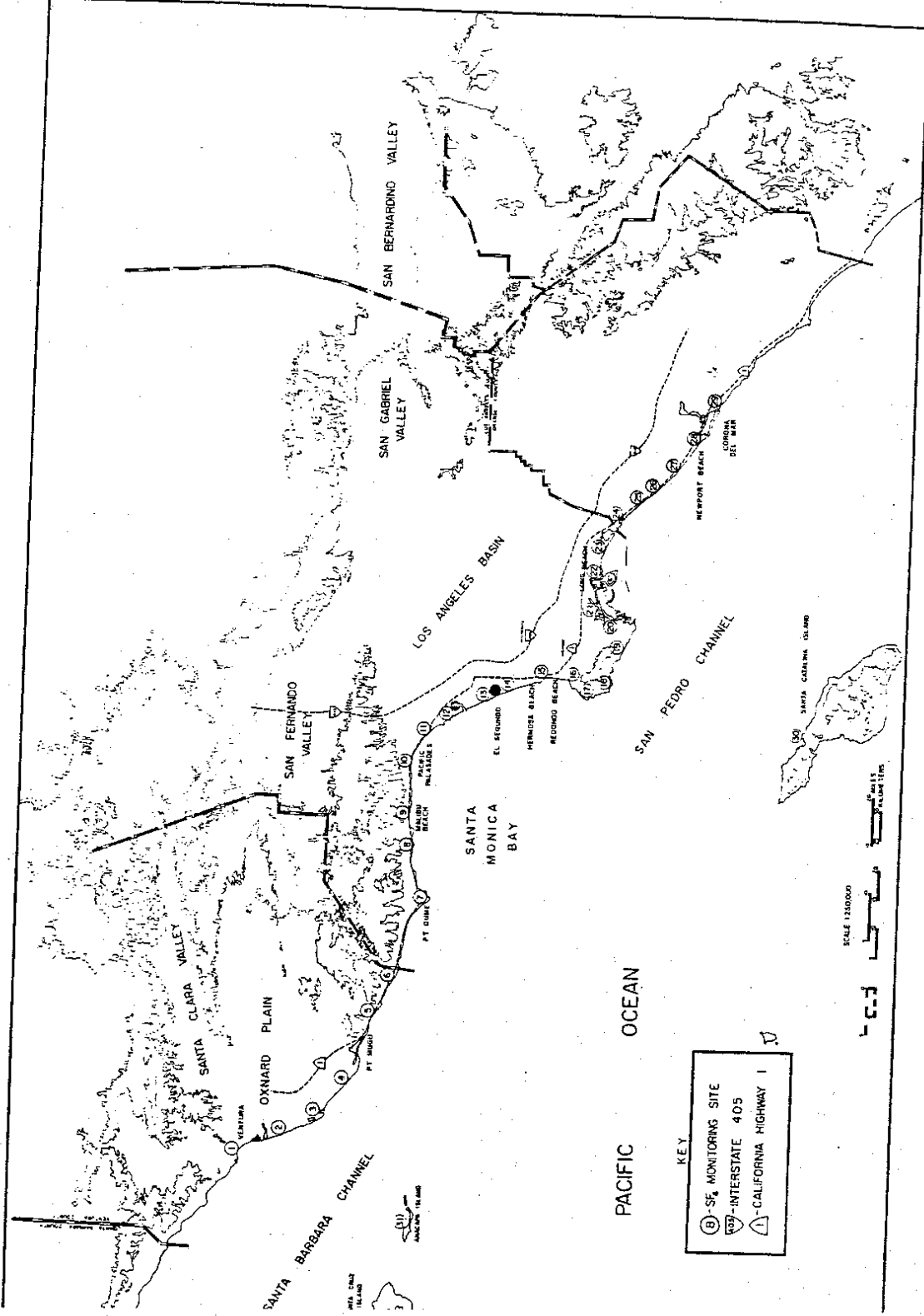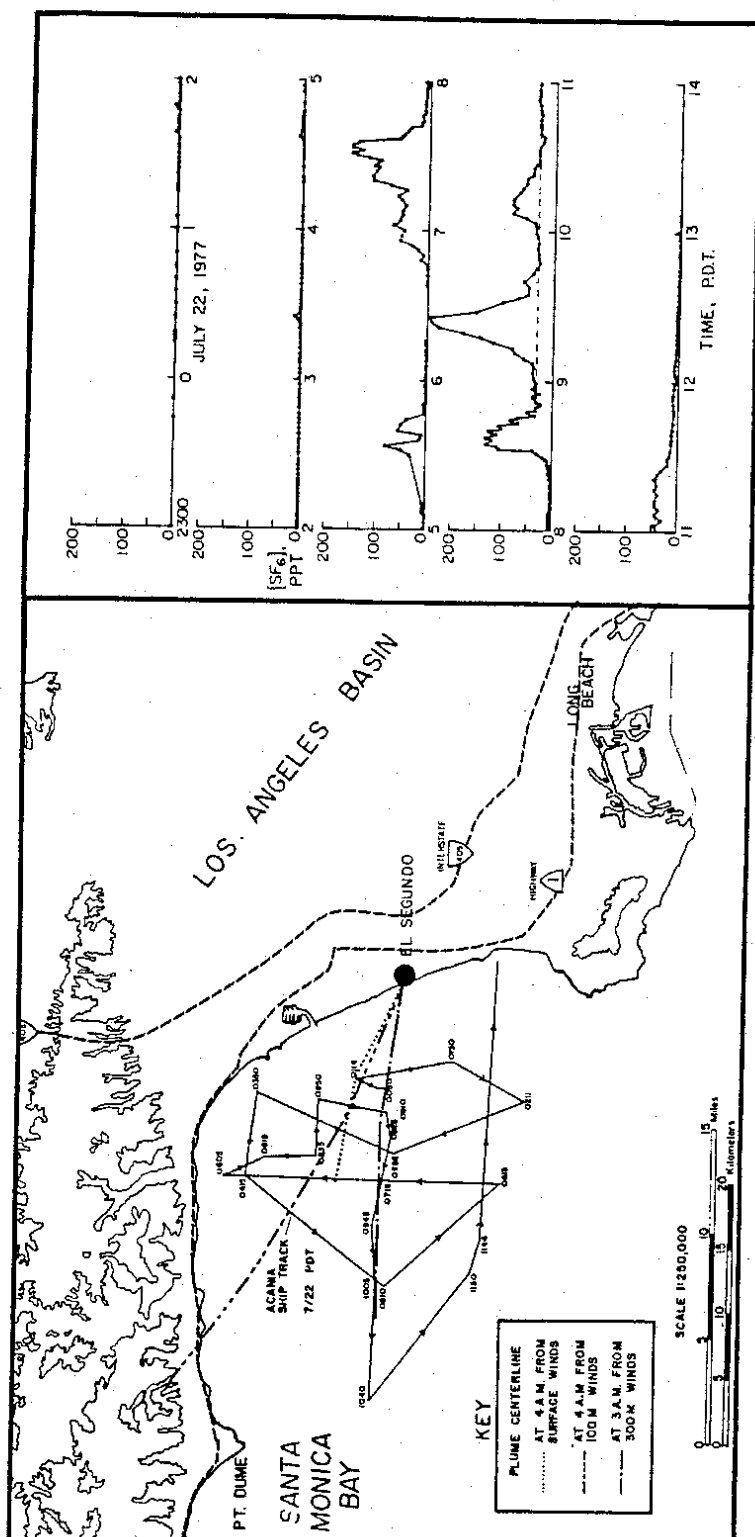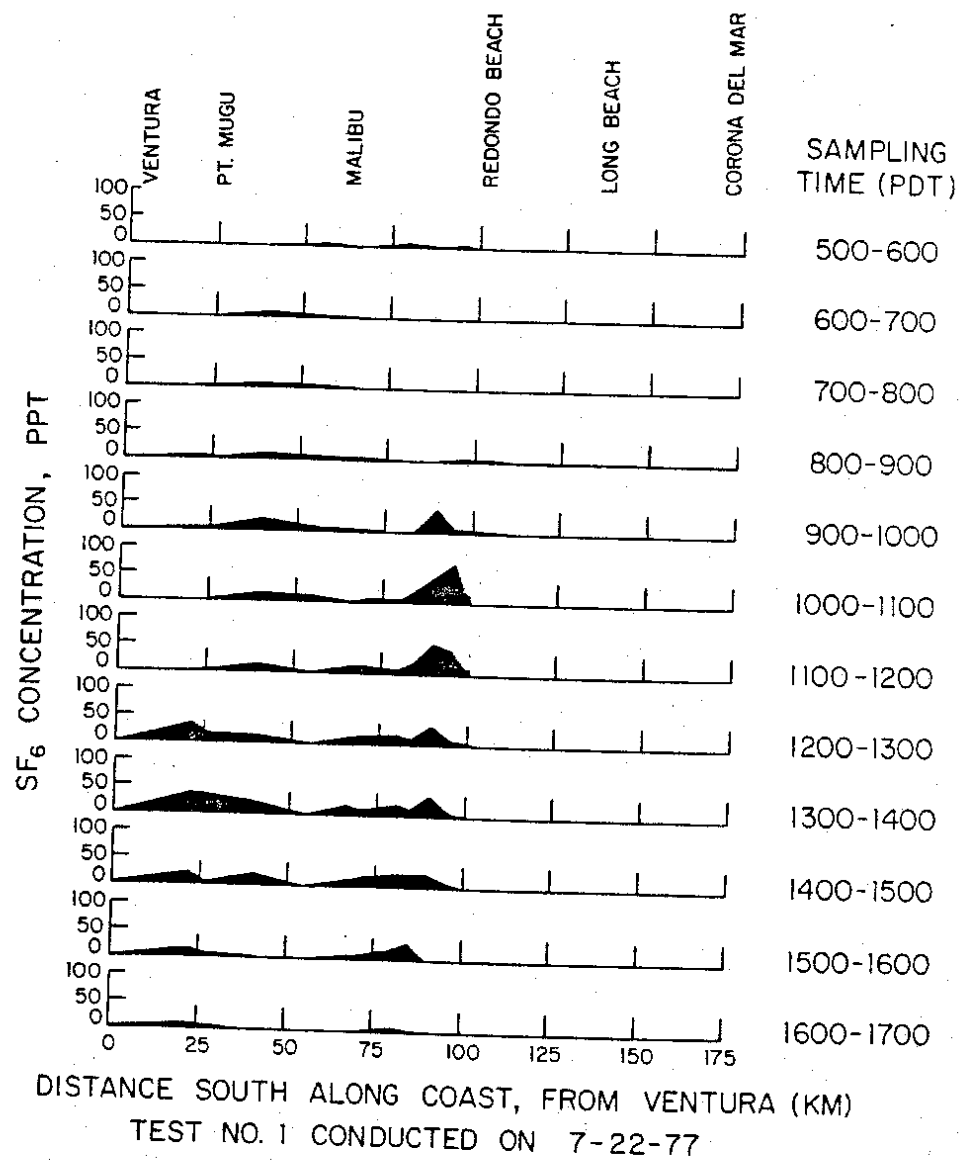   per g-mole of SF_6 released during Tests 1 and 2.
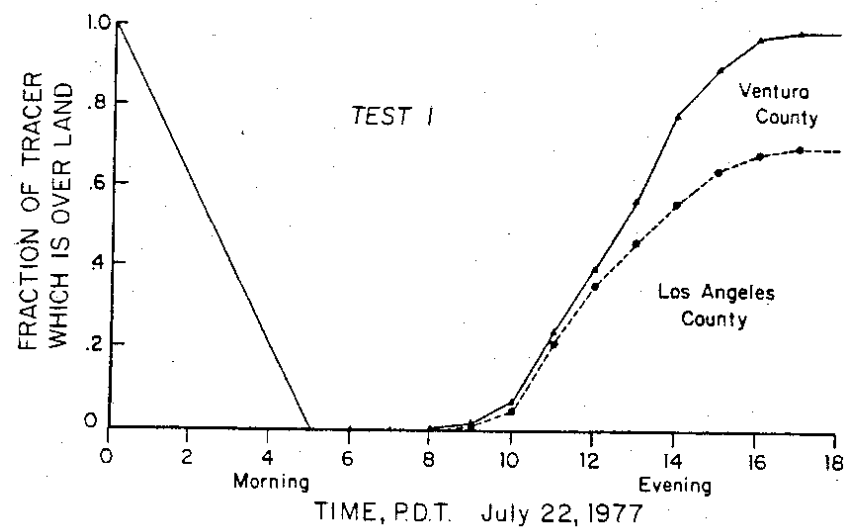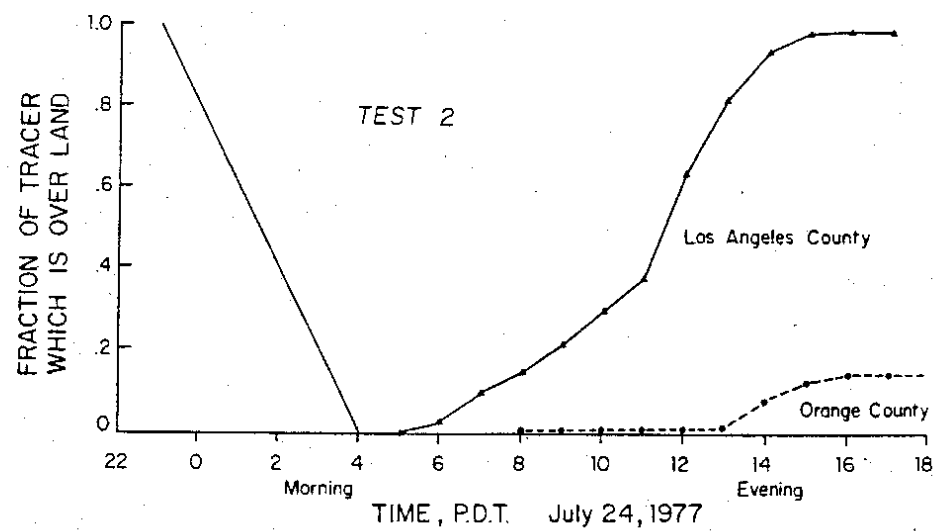
FIGURE 1

FIGURE 2

FIGURE 3

FIGURE 4a

FIGURE 4b

FIGURE 5
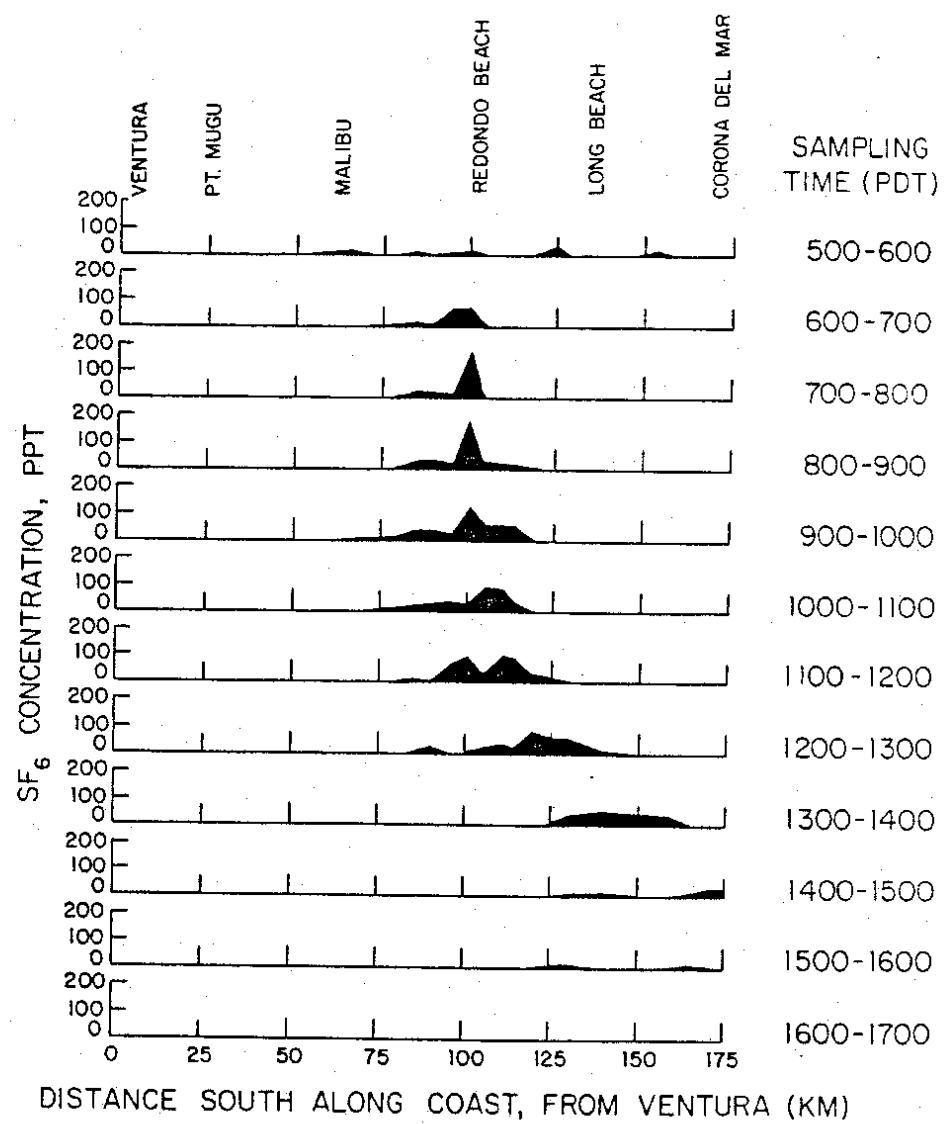
DISTANCE SOUTH ALONG COAST, FROM VENTURA (KM)

TEST NO. 2 CONDUCTED ON 7-24-77
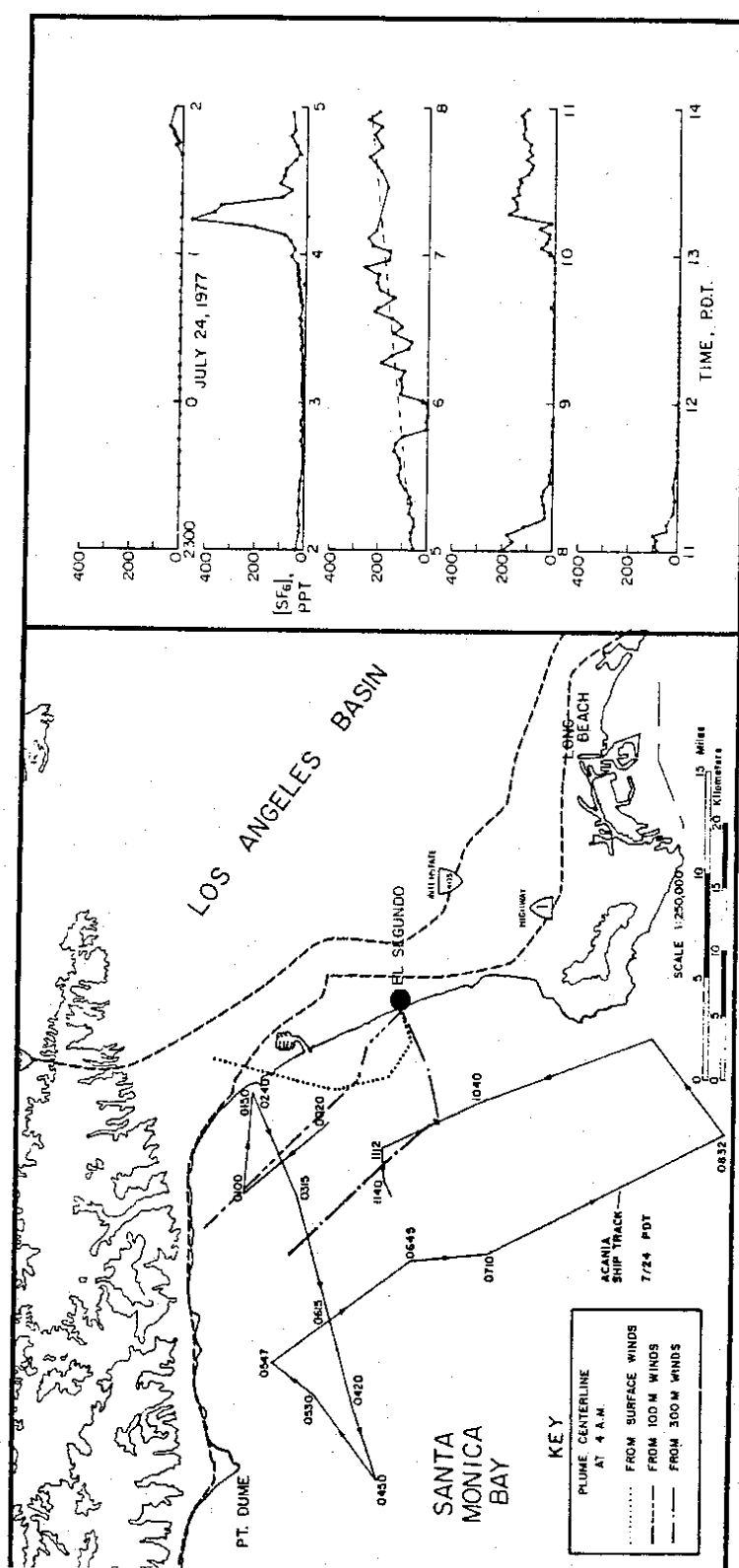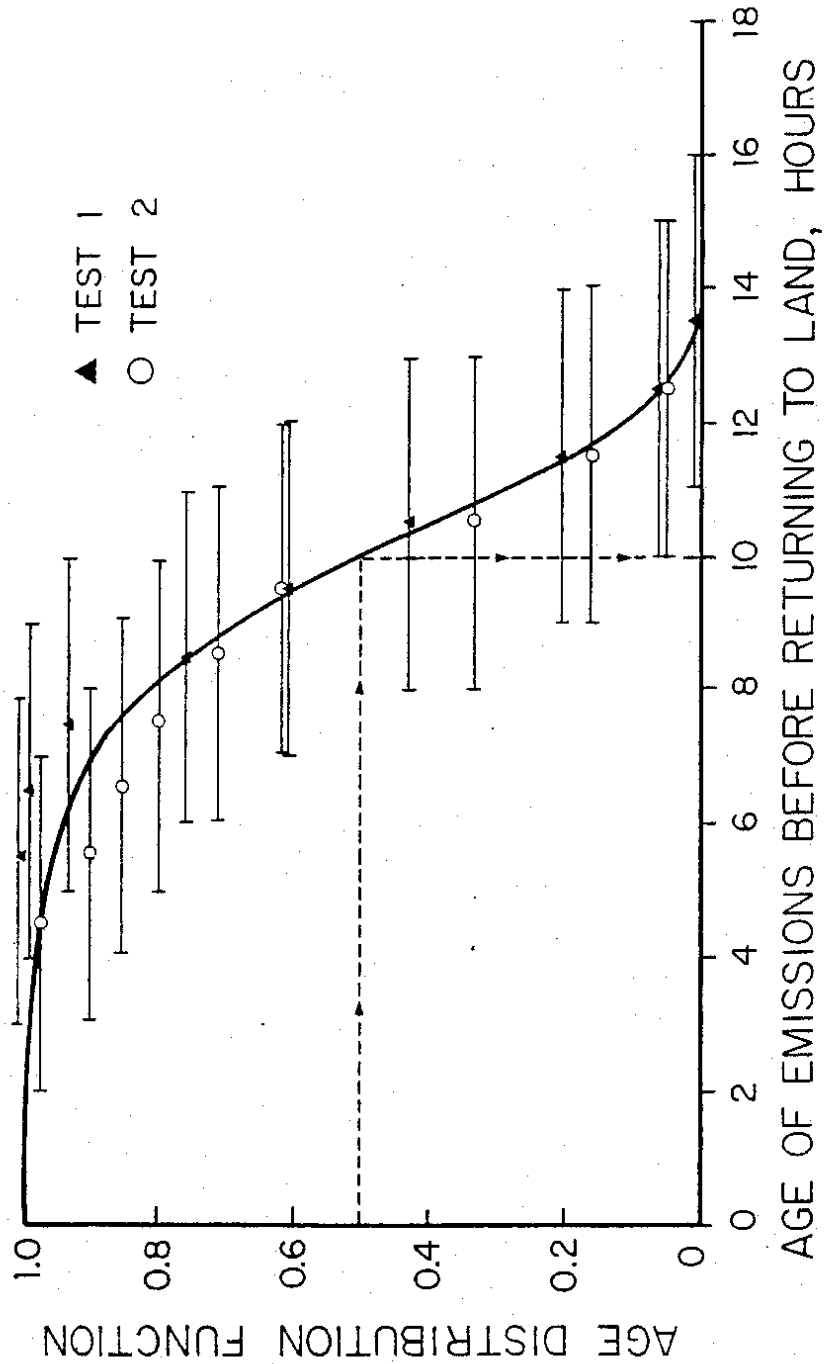
FIGURE 6
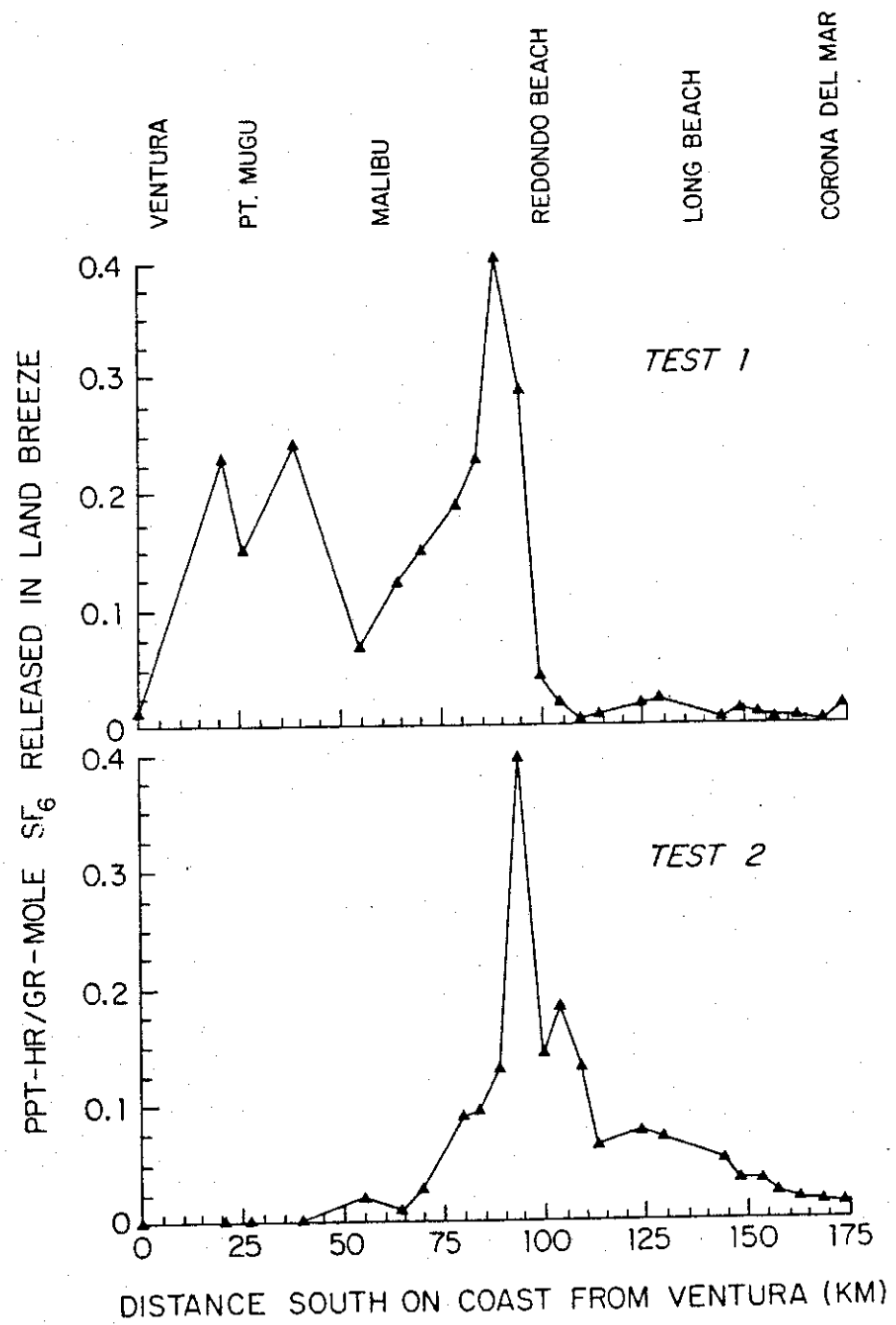
FIGURE 7

FIGURE 8

A6-202-31

APPLICATION OF ATMOSPHERIC TRACER TECHNIQUES TO DETERMINE
THE TRANSPORT AND DISPERSION ASSOCIATED WITH THE LAND-BREEZE
MOVEMENT OF AIR OVER THE LOS ANGELES COASTAL ZONE

VOLUME 1 - EXECUTIVE SUMMARY

BY

FREDRICK H. SHAIR

CALIFORNIA INSTITUTE OF TECHNOLOGY
DIVISION OF CHEMISTRY AND CHEMICAL ENGINEERING
PREPARED FOR CALIFORNIA AIR RESOURCES BOARD

DECEMBER 2, 1982

ABSTRACT

This report presents the results of seven atmospheric tracer tests in which sulfur hexaflouride was used to determine the transport and dispersion of pollutants associated with the Land and Sea Breezes of the Southern California Coastal region. Two elevated releases were made from the stack of a coastal power plant into off-shore flow. A dual tracer release was made from a ship moving north along the shipping lane between Long Beach and Ventura. Four additional releases were made from the surface during both Land and Sea Breezes. A significant portion of the tracer material released returned ashore during each test. Tracer released under off-shore flow conditions returned over a large section of the coast line whereas tracer released into a sea breeze maintained a narrower plume with higher concentrations found at greater downwind distances. The variation in plume characteristics from hour to hour and test to test reflected the complexities of the wind patterns of this region. Converging and diverging wind patterns along with flow reversals contributed to the large variations observed.

The statements and conclusions in this report are those of the Contractors and not necessarily those of the State Air Resources Board. The mention of commercial products, their source of their use in connection with material reported herein is not to be construed as either an actual or implied endorsement of such products.

INTRODUCTION

Seven large scale atmospheric tracer studies were conducted during 1977 and
1978 to probe the transport and dispersion associated with the land-breeze and
sea-breeze circulation systems along the Southern California Coast. The
primary tracer gas, sulfur hexaflouride (SF_6) was released during both
on-shore and off-shore flow conditions. Four releases were made from land and
three releases were made offshore from a boat. During one shipboard release a
second tracer, bromotriflourmethane ($CBrF_3$), was also released to provide
more detailed resolution in the samples collected. Twenty-nine samplers were
deployed along a section of the Coast extending from Corona Del Mar in Orange
County to Ventura. In addition to these hourly-average samples, a large
number of grab samples were collected by teams in automobiles, boats and
airplanes. All tracer samples collected were analyzed and the results are
presented in Volume 3 of this report.

A brief summary of each test will be presented in this volume. A summary of
tracer releases and the maximum normalized concentration measured during each
test is presented in Table 1. An extended summary of select tests and
analyses of special topics are presented in Volume 2.

Tests 1 and 2 involved releasing SF_6 for a 5-hour period during each of two
nights from stack #4 of the power plant operated by the Southern California
Edison Company. Even though a portion of the plume was apparently injected
above the base of the nighttime inversion, essentially all of the tracer was
observed to return across a control surface (from sea level to the base of the
inversion) along the coast throughout the sea breeze regime during the
following day.

The residence time distribution functions of tracer material over the sea were
almost identical in both experiments. The average residence time for tracer
material over the ocean was 10 hours in both cases; however, some of the
tracer spent as much as 16 hours out over the sea. The horizontal dispersion
of tracer was also greater than had been expected, with between 75 and 100 km
of coastline impacted by the return of SF_6 from a single elevated point
source. Data from both shipborne and coastal monitoring stations indicate

1

that the path followed by the tracer over the ocean could not have been
tracked accurately using trajectories constructed from conventionally
available meteorological data. The results of tests 1 and 2, including a
discussion of the physics of the mixing processes, are contained in Volume 2.

Test 3

The objective of test 3 was to determine the role of emission released from
ship traffic operating in the prescribed shipping lane. A dual tracer release
was made from the Naval Postgraduate School Research Vessel "Acania" for this
study. Sulfur hexaflouride (SF_6) was released from 0530-1730 PDT as the
ship moved along the shipping lane from Long Beach to a point in the Santa
Barbara Channel about 25 km north of Santa Rosa Island (see fig. 1). A second
tracer, Bromotriflouromethane, was also released at 50 lbs/hr along two
segments of the route (0530-0830 PDT, 1230-1730 PDT) in an attempt to provide
more detailed resolution concerning the segment of the route that a given
SF_6 sample came from. SF_6 was detected during the course of the test at
all twenty-nine sampling sites shown on figure 1. The highest concentrations
were recorded at the southern sites during the on-set of the sea breeze.

Test 4

Sulfur hexafluoride was released from the Acania in the middle of the Santa
Barbara Channel between 0502-0714 PDT from a location about 25 KM North of
Santa Rosa Island. Grab samples collected in Santa Barbara and Ventura
Counties indicated that the tracer concentrations were highest in Santa
Barbara County, with some lower concentrations recorded in the Ventura area.
This pattern suggests that the heaviest impact was beyond the hourly-average
sampler network. The maximum normalized concentration reported was 9616
PPT/lb-mole hr^{-1} and came from a grab sample collected near Santa Barbara.

Test 5

A shore line release of SF_6 was made from the surface at El Segundo between
0200-0430 PDT on September 8, 1977. Off-shore flow prevailed during the
release and the plume initially moved seaward and returned back onshore after
the onset of the sea breeze. The converging wind pattern at the interface
between the land-breeze and sea-breeze regimes together with flow reversals
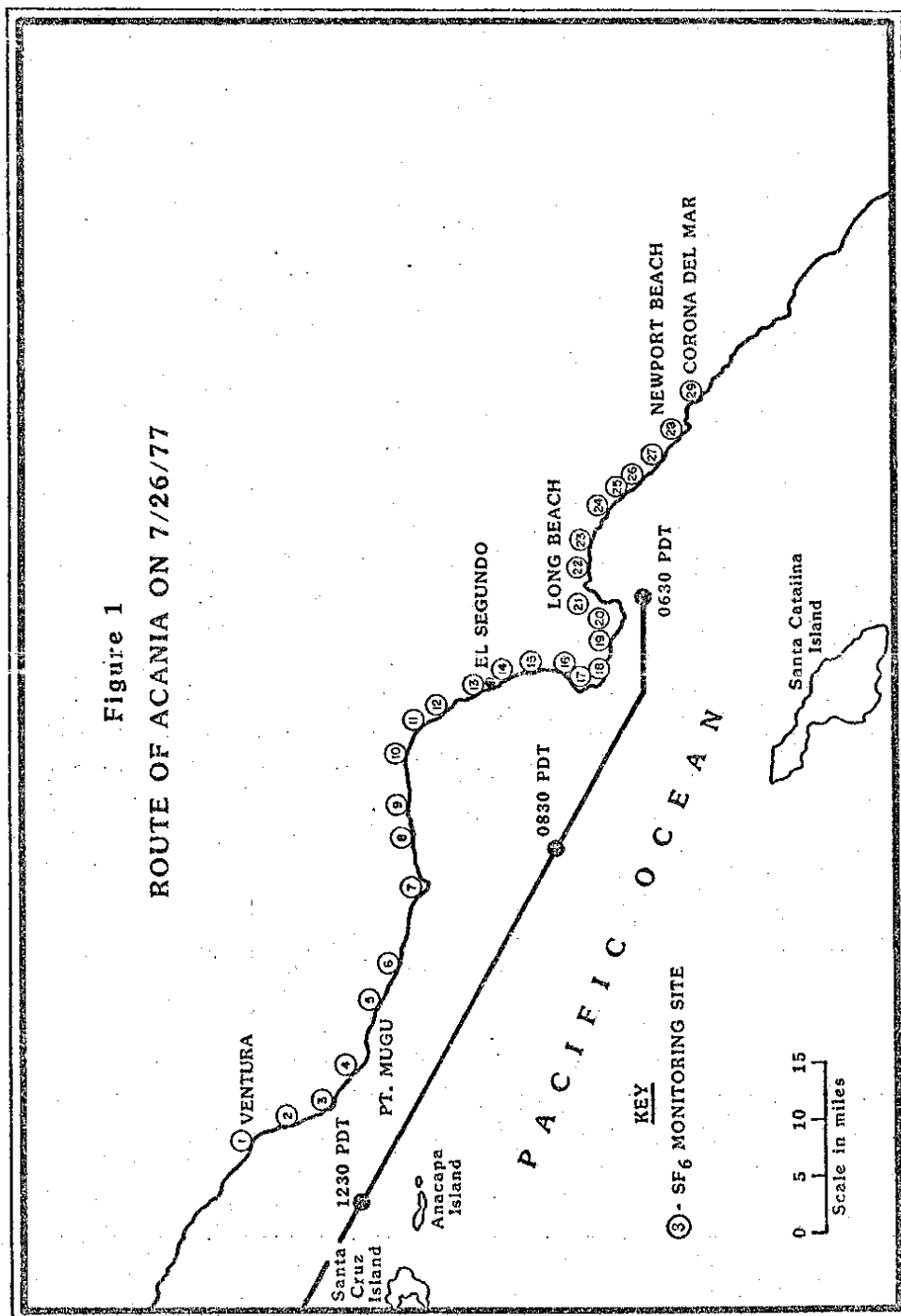
Figure 1

ROUTE OF ACANIA ON 7/26/77

VENTURA

EL SEGUNDO

LONG BEACH

NEWPORT BEACH

CORONA DEL MAR

PT. MUGU

1230 PDT

0830 PDT

0630 PDT

P A C I F I C   O C E A N

Santa Cruz Island

Anacapa Island

Santa Catalina Island

KEY

③ - SF₆ MONITORING SITE

Scale in miles

0   5   10   15

3

T A B L E 1

SF$_6$ TRACER DATA

TEST NO.	DATE	RELEASE LOCATION	RELEASE TIME (PDT)	MAXIMUM SF$_6$** CONCENTRATION	LOCATION OF MEASURED MAXIMUM CONCENTRATION
1	7/22/77	SCEPP* (elevated)	0005-0500	277	Playa Del Rey
2	7/23-24/77	SCEPP* (elevated)	2303-0400	244	Manhattan Beach
3	7/26/77	Shipping Lane (Fig.2)	0530-1730	2577	Sunset Beach
4	7/28/77	Middle of Santa Barbara Channel	0502-1714	9615	Santa Barbara
5	9/8/77	SCEPP* (surface)	0200-0430	566	Malibu
6	9/13/77	Twenty-Two Miles West of SCEPP*	0900-1400	796	Manhattan Beach
7	7/13/78	SCEPP* (Surface)	0900-1500	6562 (Grab Sample)	Eight Miles Down Wind of Release Site

*SCEPP - Southern California Edison Power Plant at El Segundo (Unit 4)

** Concentration Normalized to PPT/LB-MOLE SF^6 HR^{-1}

4

during the transition period appear to have mixed the plume and spread it over a large area. The tracer was detected at samplers located over a twenty mile wide zone and concentrations were relatively dilute. The major part of the plume returned on-shore north of the release site and a maximum normalized hourly average concentration of 339 PPT/lb-mole hr^{-1} was recorded in the Malibu area.

Test 6

An off-shore release of SF_6 was made between 0900-1400 PDT on September 13, 1977. The release was made from a boat about twenty-two miles due west of El Segundo at the on-set of the sea breeze. The plume moved directly onshore near El Segundo and covered a ten mile wide section of the Coast line. The highest normalized hourly average tracer concentration measured during this test was 796 PPT/lb-mole hr^{-1} collected at Manhattan Beach.

Test 7

SF_6 was released from the surface at El Segundo during the period 0900-1500 PDT. The tracer moved eastward across the Los Angeles basin and passed thru Banning Pass at 2000 PDT and concentrations in the pass remained above 10 PPT until 0445 PDT the following day. A traverse on the afternoon after the tracer release along highway 534 near the Colorado River measured SF_6 concentration along a segment over 85 miles long with numerous SF_6 concentrations over 10 PPT.

South Coast
Air Quality Management District
21865 Copley Drive, Diamond Bar, CA 91765-4182
(909) 396-2000 • www.aqmd.gov

Air Quality Significance Thresholds

Mass Daily Thresholds[a]		
Pollutant	**Construction[b]**	**Operation[c]**
NOx	100 lbs/day	55 lbs/day
VOC	75 lbs/day	55 lbs/day
PM10	150 lbs/day	150 lbs/day
SOx	150 lbs/day	150 lbs/day
CO	550 lbs/day	550 lbs/day
Lead	3 lbs/day	3 lbs/day
Toxic Air Contaminants (TACs) and Odor Thresholds		
TACs (including carcinogens and non-carcinogens)	Maximum Incremental Cancer Risk ≥10 in 1 million Hazard Index ≥1.0 (project increment) Hazard Index ≥3.0 (facility-wide)	
Odor	Project creates an odor nuisance pursuant to SCAQMD Rule 402	
Ambient Air Quality for Criteria Pollutants[d]		
NO2 1-hour average annual average	SCAQMD is in attainment; project is significant if it causes or contributes to an exceedance of the following attainment standards: 0.25 ppm (state) 0.053 ppm (federal)	
PM10 24-hour average annual geometric average annual arithmetic mean	10.4 µg/m³ (recommended for construction)[e] 2.5 µg/m³ (operation) 1.0 µg/m³ 20 µg/m³	
Sulfate 24-hour average	25 µg/m³	
CO 1-hour average 8-hour average	SCAQMD is in attainment; project is significant if it causes or contributes to an exceedance of the following attainment standards: 20 ppm (state) 9.0 ppm (state/federal)	

[a] Source: SCAQMD CEQA Handbook (SCAQMD, 1993)
[b] Construction thresholds apply to both the South Coast Air Basin and Coachella Valley (Salton Sea and Mojave Desert Air Basins).
[c] For Coachella Valley, the mass daily thresholds for operation are the same as the construction thresholds.
[d] Ambient air quality thresholds for criteria pollutants based on SCAQMD Rule 1303, Table A-2 unless otherwise stated.
[e] Ambient air quality threshold based on SCAQMD Rule 403.

KEY: lbs/day = pounds per day   ppm = parts per million   µg/m³ = microgram per cubic meter   ≥greater than or equal to

(Rev. January 2006)

Photochemical Modeling of Two 1984 SCCCAMP Ozone Episodes

T. W. TESCHE

Alpine Geophysics, Crested Butte, Colorado

DENNIS E. McNALLY

Numerical Solutions, Golden, Colorado

ABSTRACT

Data collected during the 1984 SCCCAMP Exploratory Study were used to develop two multiple-day ozone modeling episodes for the Urban Airshed Model (UAM). An operational model performance evaluation was performed for the 5–7 and 16–17 September 1984 episodes. Peak 1-h average ozone concentrations were reproduced on the five simulation days with accuracies (paired in time and space) ranging from 0% to −30%. The mean bias in hourly averaged ozone concentrations ranged from −6% to +11%, and the mean gross errors varied between 23% and 38%. UAM performance for ozone concentrations with the two September episodes is comparable with other recent photochemical model evaluations. Lack of sufficient measurements for model performance testing of other important photochemical species (e.g., NO, NO$_2$, volatile organic compounds) and for carrying out compensatory error analysis and related diagnostic and mechanistic investigations precluded a more rigorous scientific evaluation of UAM performance with the 1984 SCCCAMP database.

1. Introduction

Decision makers face several complex planning issues related to urban- and regional-scale ozone air pollution. For example, will nitrogen oxides (NO$_x$) control accelerate or impede progress toward ozone attainment? Can photochemical models be relied upon to estimate the future impacts of emission control programs implemented now? Can models simulate adequately the effects of individual sources or source categories of air pollution? Can effective reactive organic gas (ROG) and NO$_x$ emission reduction strategies be derived from models, weighing the desires for ozone attainment, reduction of public health impacts, and other policy goals? Can models attribute specific portions of a local ozone exceedence to near versus upwind source regions?

During the 1980s, photochemical grid models emerged as practical regulatory tools for estimating ozone air pollution impacts in urban and regional settings. Eulerian models such as the Urban Airshed Model (UAM) provide a quantitative link between source emissions and receptor concentrations at a level of detail unavailable through simpler modeling methods. Given high-resolution emissions and aerometric databases, photochemical grid models are generally able to reproduce hourly averaged ozone concentra-

tions, paired in space, to within 30%–35%. The maximum 1-h value during a 2–3 day episode can often be simulated to within 5%–10% (Tesche 1988). Given the enormous economic costs associated with ozone control programs in the United States, the use of photochemical grid models represents a technically viable, cost-effective method for air quality planning, provided adequate databases are available for model performance testing.

This paper reports the development of two multiple-day ozone modeling episodes and subsequent model performance evaluation activities carried out in support of the 1989 Air Quality Attainment Plan (AQAP) for Santa Barbara County and EPA's Federal Implementation Plan (FIP) for Ventura County. Both counties are portions of the south-central coast air basin (SCCAB), shown in Fig. 1. The two episodes were selected from the 1984 South-Central Coast Cooperative Aerometric Monitoring Program (SCCCAMP), described in detail by Dabberdt and Viezee (1987). Databases for 5–7 September 1984 and 16–17 September 1984 were constructed for the UAM to facilitate an operational performance evaluation, consisting of a series of graphical and statistical comparisons and extensive sensitivity analyses. Details of the photochemical modeling work are contained in the two project reports (Tesche et al. 1988a; Tesche and McNally 1989).

Several photochemical modeling studies have been carried out in the Santa Barbara–Ventura region. The first was the Joint Interagency Modeling Study (JIMS)

Corresponding author address: Dr. Thomas Tesche, Alpine Geophysics, P.O. Box 2059, Crested Butte, Co 81224.
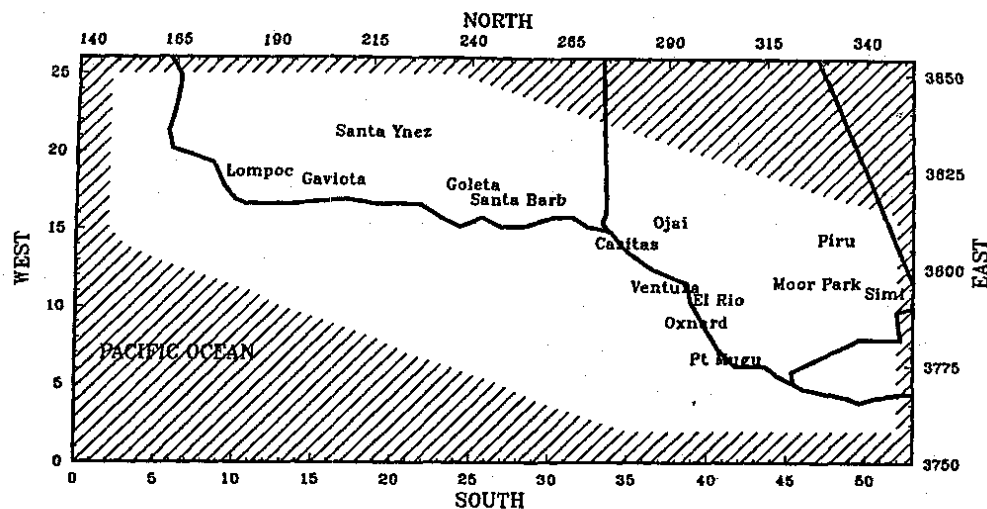
FIG. 1. The south-central coast air basin modeling and analysis region.

(Haney et al. 1986) in which the UAM was evaluated for three, 2-day episodes from the 1980 Santa Barbara Channel Oxidant Study. The California State Lands Commission sponsored a model evaluation effort with the 27–28 September 1984 SCCCAMP ozone episode (SLC 1986), and the California Air Resources Board (ARB) developed modeling databases for three ozone episodes from the 1895 SCCCAMP field program (Wagner 1989). Each of these studies included model performance testing and limited sensitivity analysis.

Section 2 summarizes the aerometric features of the two 1984 SCCCAMP ozone episodes used in this study. The photochemical and meteorological models selected and the input preparation procedures employed are described in sections 3 and 4, respectively. In section 5, we suggest an approach to rigorous model performance evaluation that should accompany every photochemical modeling study where sufficient data are available. Section 6 summarizes the operational evaluation results for both episodes. The principal limitations of the present evaluation, related primarily to database constraints, are discussed in section 7. Our conclusions are presented in section 8.

2. The 1984 SCCCAMP Exploratory Field Study

The 1984 SCCCAMP Exploratory Field Study consisted of continuous aerometric monitoring and intensive measurements specifically designed to test sampling techniques and to provide the basis for more refined experiments the following year (Dabberdt 1984). These experiments included enhanced measurements

of surface and upper-level winds, NO_x and ROG speciation, aircraft soundings, and chemical species sampling. Following the field work, SCCCAMP sponsored an analysis of the 1984 data (Tesche et al. 1985) to strengthen the design of the 1985 measurement program and to assess the suitability of the 1984 database for photochemical modeling. The first activity aided in formulating the 1985 SCCCAMP monitoring program study design and experimental protocol (Reynolds et al. 1985; Dabberdt and Viezee 1987), while the second activity led to a conceptual model of the meteorology and air quality during the sampling period.

The September 1984 data indicated that surface winds in the SCCAB follow a diurnal pattern composed of two major regimes: an afternoon–evening sea-breeze flow; and a nighttime–morning drainage flow. The sea-breeze influence is strongest over the Oxnard plain, which is directly exposed to the westerly wind flow across the Santa Barbara Channel. Some of this westerly flow is deflected south of the Santa Monica Mountains toward Los Angeles. Although onshore winds influence the flow regimes in mountain areas, an upper-level southeasterly flow was dominant during this study period above 750 m MSL. Drainage winds were an order of magnitude weaker than their onshore counterparts, and were most pronounced in channeling situations, such as in the Santa Clara River valley. Lack of data from the Santa Barbara Channel area limited characterization of the nocturnal counterclockwise eddy over the northern half of the channel. Similarly, data are needed in the vicinity of Gaviota Pass to reveal more clearly the formation of eddies by winds rounding Point

Conception. Still, there is evidence in the 1984 data of a nocturnal counterclockwise eddy over the northern portion of the Santa Monica Bay.

Upper-level air flow at six stations during September 1984 is dominated by easterly to southeasterly winds above 750–1000 m. Below 500–750 m, winds at all stations are affected by diurnal offshore–onshore flows. Strong onshore flows appear to push the lower level of the southeasterlies upward, creating a sharply defined shear zone within the boundary layer.

The timing of sea-breeze episodes varies daily but, typically, the sea breeze peaks over the Oxnard plain at about 1500 PST. This timing does not appear to be a function of distance from the coast. During the 5–7 September episode, winds were generally light and there was considerable airmass stagnation over the Santa Barbara Channel area and coastal regions. The 16–17 September ozone episode was preceded by two days of strong offshore (easterly-to-southeasterly) winds aloft; sea-breeze episodes were weak. A subsidence inversion kept vertical mixing to a minimum. On the afternoon of the 17th, the sea breeze strengthened slightly and the inversion weakened, allowing previously stagnant air to move inland and a limited amount of mixing with the upper air to occur.

Hourly averaged ozone measurements were performed during September 1984 at 16 monitoring stations. For the two episodes modeled here, the six highest stations and their respective ozone maxima are listed in Table 1. Both episodes exhibit widespread ozone levels above the federal 1-h standard (12 pphm). The 5–7 September episode not only has the higher ozone maximum (18 pphm at Casitas on the 7th), but the overall ozone concentrations for this period are greater than for 16–17 September. Both episodes coincide with peaks in the morning 850-mb temperature, a strong indicator of high ozone formation potential in southern California. During the 5–7 September period, the region of maximum afternoon ozone was shifted westward from the eastern basin on the 6th (near Simi) to a midbasin location (Casitas) on the 7th. High ozone levels are reported in Santa Barbara County on this day. A similar westerly shift does not appear on the 16–17 September.

3. Description of the models

The models used in this study included the Urban Airshed Model (UAM-II) (Ames et al. 1985), an objective analysis wind model (Goodin et al. 1980), and a modified version of the Steyn–Oke mixing-height model (Steyn and Oke 1982). Brief descriptions of each model are given here since full details are reported elsewhere.

a. The Urban Airshed Model

The UAM is an Eulerian photochemical model that simulates the emission, transport, dispersion, chemical transformation, and removal of inert and chemically reactive species in the atmospheric boundary layer (Ames et al. 1985; Morris et al. 1990). The UAM is EPA's current guideline model for refined analysis of urban ozone air pollution (EPA, 1986). Time evolution of chemically reactive pollutants are simulated through numerical solution of the species mass conservation equation, given by

$$\frac{\partial \tilde{C}_i}{\partial t} + \frac{\partial}{\partial x}(u\tilde{C}_i) + \frac{\partial}{\partial y}(v\tilde{C}_i) + \frac{\partial}{\partial z}(w\tilde{C}_i)$$

$$= \frac{\partial}{\partial x} K_H \frac{\partial \tilde{C}_i}{\partial x} + \frac{\partial}{\partial y} K_H \frac{\partial \tilde{C}_i}{\partial y}$$

$$+ \frac{\partial}{\partial z} K_V \frac{\partial \tilde{C}_i}{\partial z} + R_i(\tilde{C}_1, \cdots, \tilde{C}_N, t)$$

$$+ S_i(x, y, z, t) + R_{ni}(x, y, z, t) \quad (1)$$

where the symbol ~ represents a spatial averaging operation; C_i = the estimated value of the instantaneous concentration of pollutant i; u, v, and w = the mean wind velocity components; K_h and K_V = the horizontal and vertical eddy diffusivity components; S_i = the rate of emission of pollutant i from surface and elevated sources; R_i = the contribution of the mean concentration to the net reaction rate of pollutant i; and R_{ni} = the dry deposition rate of species i. The governing equations are coupled, nonlinear, multidimensional, and time dependent. They are ensemble-averaged and integrated using an explicit finite-difference solution

TABLE 1. Peak ozone concentrations (pphm) during the two 1984 SCCCAMP episodes.

| 5 September | | 6 September | | 7 September | | 16 September | | 17 September | |
Maxima	Station	Maxima	Station	Maxima	Station	Maxima	Station	Maxima	Station
10	Casitas Pass	17	Simi	18	Casitas Pass	11	Simi	14	Casitas Pass
9	Simi	16	Piru	15	Goleta	9	Thousand Oaks	13	Simi
8	Gaviota	16	Thousand Oaks	15	Santa Barbara	6	Piru	12	Thousand Oaks
7	Thousand Oaks	13	Ojai	13	Simi	8	Ojai	12	Santa Barbara
7	Ojai	13	Casitas Pass	13	Ojai	8	Casitas Pass	12	Ojai
		10	El Capitan	11	El Capitan, Thousand Oaks	7	Ventura	11	Goleta

technique. Advective and diffusive transport are treated sequentially using the method of fractional steps. The Smolarkiewicz (1983) method is employed to solve the advective part of the problem. The UAM is based on a terrain-following coordinate system.

For more than a decade, EPA distributed the UAM with the carbon bond II (CBM-II) kinetic mechanism (Whitten et al. 1980). This version simulates the chemical reactions of NO, NO_2, ozone, HNO_2, H_2O_2, paraffins, olefins, aromatics, aldehydes, carbonyls, PAN, SO_2, CO, sulfate aerosol, and total aerosol mass concentration. EPA released an updated version of the UAM with carbon bond IV chemistry (UAM-IV) (Gery et al. 1988) in September 1990. Details of the UAM-IV are given in Morris et al. (1990).

The UAM requires meteorological inputs that include a three-dimensional wind field, the vertical thermal structure, and estimates of the mixing height above each grid cell within the modeling domain as a function of time. Surface temperature fields and solar radiation intensity data are also needed for each simulation hour. Wind field inputs to the UAM historically have been developed through the use of simple interpolation models. Based on surface and upper-air meteorological data, these interpolation, extrapolation, and divergence-reduction routines are employed to develop three-dimensional flow fields. More recently, diagnostic and prognostic wind field models have become preferred means of constructing the transport fields (Tesche 1991).

An area and elevated source-emissions description is needed giving the temporal and spatial distribution of the pollutants emitted from all sources within the modeling region. These emission estimates have historically been developed by state and local regulatory agencies and their computation involves the use of a wide variety of calculational procedures. Dry removal processes are treated as surface boundary conditions.

The UAM estimates ozone, precursor species, and product species (e.g., nitric acid and PAN) for each hour of the simulation in all grid cells in the computational domain. Typically, the model is operated for episodes of 2–3 days duration so that the effects of uncertainties in initial conditions are minimized by the second or third simulation day. Model output is displayed in time series plots for various monitoring stations, affording comparisons between hourly average model estimates and observations. Ground-level-concentration isopleths may be plotted for various hours of each simulation day to reveal the spatial distribution of ozone concentrations and other species of interest.

b. The meteorological model

Transport fields were developed in this study using the interpolation model of Goodin et al. (1980). This wind model is a three-dimensional, objective analysis scheme that invokes mass consistency constraints. The model uses a two-step procedure. First, ground-level wind measurements are interpolated to give a surface flow field. Then, the upper-level winds (i.e., above the surface layer) are objectively analyzed to render the resultant three-dimensional flow field mass conserving. This is achieved by strongly constraining the vertical velocity. In most cases, an adjustment is made to the vertical velocity field so that the net mass transport through the model top is zero. The model uses terrain-following coordinates and a variable vertical grid mesh. Vertical velocities are determined from successive iterations of the mass conservation equation, reducing field divergence to a prescribed level. The method is computationally efficient and has been widely applied as a meteorological preprocessor in photochemical modeling studies. However, its performance is difficult to assess since it uses all available, valid wind information to construct the flow fields.

c. The mixing-height model

Several modeling procedures are available for estimating mixing heights in coastal-complex terrain. The model developed by Steyn and Oke (1982) was selected for daytime mixing-height estimation because it is formulated for coastal convective boundary layers and it directly utilizes the surface and upper-air meteorological measurements collected during SCCCAMP. The Steyn–Oke model is an extension of the Tennekes (1973) zero-order jump model, a generalized thermodynamic treatment of convective boundary-layer development. Steyn and Oke included the effects of advection and inversion subsidence, two physical processes of significance in coastal settings. The model consists of a coupled, nonlinear system of ordinary differential equations that are solved numerically given prescribed initial and boundary conditions. The Steyn–Oke model was refined in this study to include algorithms for computing the turbulent sensible heat flux as a function of surface meteorological variables and distance from the irregular SCCAB coastline.

4. Preparation of Urban Airshed Model inputs

The UAM modeling region consists of a 53 × 26 grid domain with 4-km horizontal resolution. Use of finer grid resolution, potentially helpful in resolving transport processes occurring near the coastline and mountain slopes, was impractical since the emissions grid, previously developed by state and local agencies, was fixed at 4 km. The vertical grid structure was based upon analysis of the windfields, mixing heights, aircraft measurements, and emissions source heights in the basin. The vertical grid definition consists of four vertical levels with two above the inversion and two below. A modeling domain height was set at 1000 m.

a. 1984 SCCCAMP database

The 1984 SCCCAMP Exploratory Field Study provided a database that was significantly richer than that

TABLE 2. Total precursor emissions (kg day^{-1}) for 1984 in the south-central coast air basin.

	6 September	7 September	16 September	17 September
Point sources:				
NO	20 725	22 169	19 489	18 908
NO$_2$	1671	1788	1572	1525
ROG	1651	2188	1614	1460
Area sources:				
NO	51 313	51 370	44 272	51 301
NO$_2$	4138	4143	3570	4137
ROG	113 434	112 579	94 548	112 462

afforded by the routine monitoring activities in the basin. Surface wind data, collected hourly, were available from 17 onshore sites and from 3 offshore oil production platforms. Upper-level wind monitoring was performed at five sites, supplementing the routine data collection at Point Mugu and Vandenberg Air Force Base. Twelve surface temperature stations were in operation and vertical temperature profiles were available twice daily at Vandenberg and three times a day at Point Mugu. In addition, during the 16–17 September episode, 25 vertical aircraft soundings were performed over land and water for upper air characterization. During the period 10–22 September, a total of 15 aircraft flights were performed over strategic portions of the basin, documenting the vertical and horizontal extent of temperature, humidity, turbulence, NO$_x$, ozone, and b-scat fields. This intensive measurement set combined with the information from the routine surface aerometric database represented the available database with which UAM inputs for the September episodes were prepared.

b. The emissions estimates

The UAM requires emissions estimates for all relevant anthropogenic and natural sources in the modeling region. The emissions used in this study were resolved on a 4-km grid, temporally allocated (i.e.,

hourly emissions estimates), and disaggregated according to NO$_x$ and reactive organic gas (ROG) chemical species. Emissions rates for all sources in the region were constructed from baseline estimates for total organic gas (TOG), NO$_x$, PM, SO$_2$, and CO.

The emissions estimation process was carried out by the California Air Resources Board and the two local air pollution control districts. It involved the following steps: (a) source identification; (b) source and process characterization; (c) source activity level determination; (d) emission factor estimation; (e) emission rate calculation; and (f) emission gridding, temporal splitting, and species allocation. Emissions estimates were distributed temporally and spatially, including in the vertical plane, consistent with the UAM grid mesh. Point sources were located with specific coordinates identifying their position in the grid region. Since the UAM uses stack data to compute plume rise for all point source emissions based on hourly meteorological conditions, this information was compiled as well. Area source emissions were allocated to grid cells using surrogate information such as population or industrial employment distributions for each source category. Operating schedules for typical point and area sources were used for resolving temporary emissions data to specific time periods. Day-specific emissions information, typically gathered for large point sources, was not compiled for 1984.

TABLE 3. Estimated maximum mixed-layer heights (m) at 12 monitoring stations for the September 1984 episodes.

| Monitoring station	5 September	6 September	7 September	16 September	17 September
Point Mugu	152	200	253	179	152
Santa Ynez	401	425	469	608	357
Santa Barbara	271	226	286	384	246
Ojai	282	227	427	421	319
Piru	404	329	466	626	369
Simi	374	282	529	509	359
Moorpark	362	279	503	501	356
Thousand Oaks	335	238	488	482	353
Oxnard	187	200	448	259	213
Vandenberg	203	162	255	349	292
Lompoc	315	400	394	501	357
Santa Paula	363	283	439	514	377
Average	304	271	413	444	313
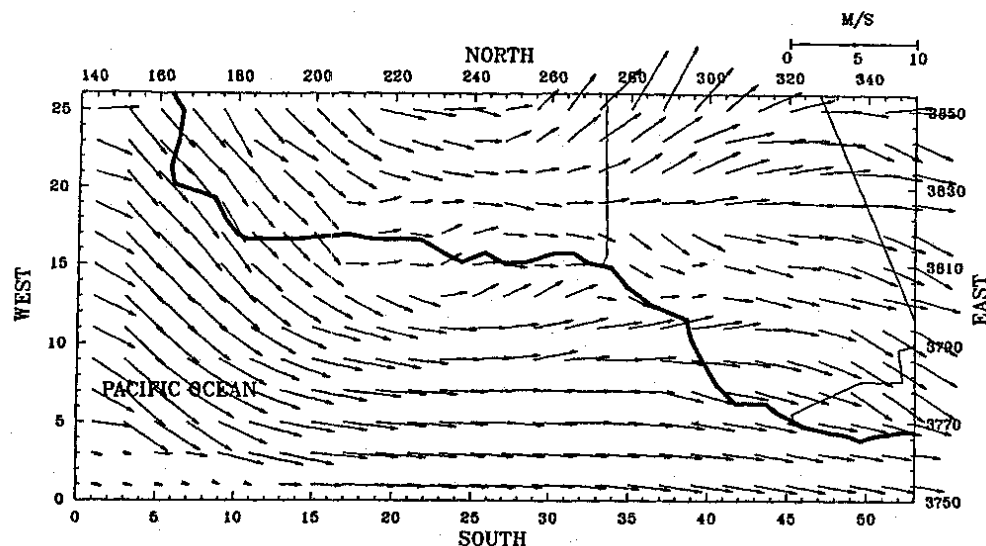
FIG. 2. Hourly surface flow field at 1600 PST 5 September 1984.

Table 2 gives emissions totals (kg day^{-1}) for NO, NO_2, and ROG for each simulation day for both point and area source files. (Emissions on the 5th were assumed to be identical to those on the 6th.) Total daily point source NO_x emissions vary slightly from the 4-day average, from −7% to +9%. For point source ROG emissions, the variation from day to day is larger on a percentage basis, from −16% to +27%. For the area sources, the variation in NO_x and ROG emissions is −11% to +4% and −13% to +5%, respectively.

c. Scalar inputs

The UAM requires a number of scalar quantities to calculate atmospheric stabilities, turbulent diffusivities, surface deposition rates, plume rise, and so on. Available meteorological observations were used with boundary-layer parameterization schemes (Holtslag and van Ulden 1983; van Ulden and Holtslag 1985; Wilczak and Phillips 1986) to calculate the surface turbulent heat flux, friction velocity, Monin–Obukhov length scale, turbulence intensity, convective velocity scale, and the temperature scale for turbulent heat transfer. These parameters were calculated hourly based on gridded terrain elevations, surface roughness, and vegetation factors, and estimates of local surface wind speed and direction, early morning temperature soundings, surface albedo, and soil moisture content.

d. Mixing heights

The UAM uses the mixing-height concept to divide the modeling domain into two regions that differ sig-

nificantly in their turbulent structures. For convective and neutral boundary layers under a strong subsidence inversion, this division into two regions is generally adequate. For the nocturnal stable boundary layer, however, finer discritization of the vertical grid mesh is desirable, particularly under stable nighttime conditions. As a compromise, a vertical grid mesh of four levels, with two cells below the nominal daytime mixing height and two cells above, was used.

The 1984 SCCCAMP study did not provide sufficient data for quantitative evaluation of the mixing-height estimates for the two September episodes. One motivation for using the Steyn–Oke model was that it incorporates greater physical realism and utilizes more of the meteorological data than other readily available

TABLE 4. Nominal inflow boundary conditions for September 1984 simulations (except as noted in text).

Species	Concentration (ppm)
NO	0.001
NO_2	0.001
O_3	0.040
CO	0.200
ETH	0.0010
OLE	0.00057
PAR	0.0215
CARB	0.00073
ARO	0.0039
PAN	0.0005
BZA	0.00001

methods. As noted, the original model formulation was modified in this study to incorporate local topographic features of the SCCAB and to compute the turbulent sensible heat flux from routine NWS observations. The modified model was then exercised with hourly data to compute daytime convective mixing heights at 12 onshore locations in the basin. Table 3 lists the maximum daytime mixing heights derived in this manner. For nighttime periods when the Steyn–Oke model is not applicable (e.g., 2000–0600 PST), we assumed a constant mixed-layer height of 75 m over the entire modeling domain, consistent with previous UAM studies in the region.

e. Wind fields

The three-dimensional wind field is one of the most important inputs to the UAM. A preferred approach to wind-field construction, particularly in coastal settings, is the use of a prognostic meteorological model (Kessler and Douglas 1989; Stauffer and Seaman 1990; Tesche 1991). Resource constraints in this study precluded this approach so we used the simple interpolation model of Goodin et al. (1980). Thirty surface and six upper-air wind stations were used as inputs to the wind interpolation model. Initial results from the wind model using only the reported data gave surface flow fields that were inadequate for photochemical modeling, primarily because most of the observational data are either along the very narrow Santa Barbara County coastal margin, or distributed throughout the Oxnard plain and the inland coastal valleys. With the exception of a few offshore platform wind stations adjacent to the coast and the two buoys near Point Conception, there is very little wind information over the ocean. Moreover, wind data over elevated, complex terrain was absent in SCCCAMP 1984. These two regions, overwater and the mountains, represent large portions of the UAM computational domain.

Lack of wind data in key areas required that we supplement the observational data in regions where data were missing or in short supply. Key subareas were identified where the local flow patterns were found, through initial interpolation, to be inadequately characterized. Supplemental speed and direction values were developed for different portions of the day based on the original interpolated wind field, observed surface and upper-air winds, the conceptual model of the episode, and previous modeling experience in the SCCAB. The conceptual model of diurnal surface flow fields (Tesche et al. 1985) guided the assignment of these supplemental wind inputs. Figure 2 is an example of the estimated surface winds at 1600 PST on 5 September. Details of the hourly flow fields for each episode are contained in the project reports.

f. Initial and boundary conditions

Initial conditions for NO, NO₂, ozone, and ROG were derived from the interpolation and extrapolation of observed concentration values at the beginning of the two simulation periods (0200 PST, 5 and 16 September). Initial conditions were based on the vertical grid structure, boundary concentrations aloft, and ambient pollutant measurements. The available aircraft measurements on the 16th and 17th did not indicate the presence of elevated ozone or precursor layers aloft, so absent data for the 5–7 September period, clean air conditions aloft were prescribed for both modeling episodes.

Boundary conditions were developed from analysis of the routine air quality monitoring data, the hydrocarbon sampling results, and the range of boundary conditions used in previous UAM modeling studies in coastal California settings. The values chosen, presented in Table 4, are a midrange estimate of background tropospheric concentrations.

Wind observations in the eastern basin (Piru and Simi) on the 6th and 7th indicated precursor transport into the SCCAB from the adjacent San Fernando Valley and the south coast air basin. Hourly air quality data from the 5–7 September for the Burbank and Re-

TABLE 6. Hydrocarbon splits used to apportion VOC measurements into carbon bond II species groups.

Carbon bond II component	5-7 September		16-17 September	
	Fraction (as carbon)	Fraction	Fraction (as carbon)	Fraction
PAR	0.778	0.778	0.770	0.770
ARO	0.152	0.025	0.153	0.026
CARB	0.021	0.021	0.027	0.027
OLE	0.020	0.010	0.018	0.009
ETH	0.031	0.016	0.030	0.015

TABLE 5. Inflow boundary conditions along the southeastern portion of the modeling region.

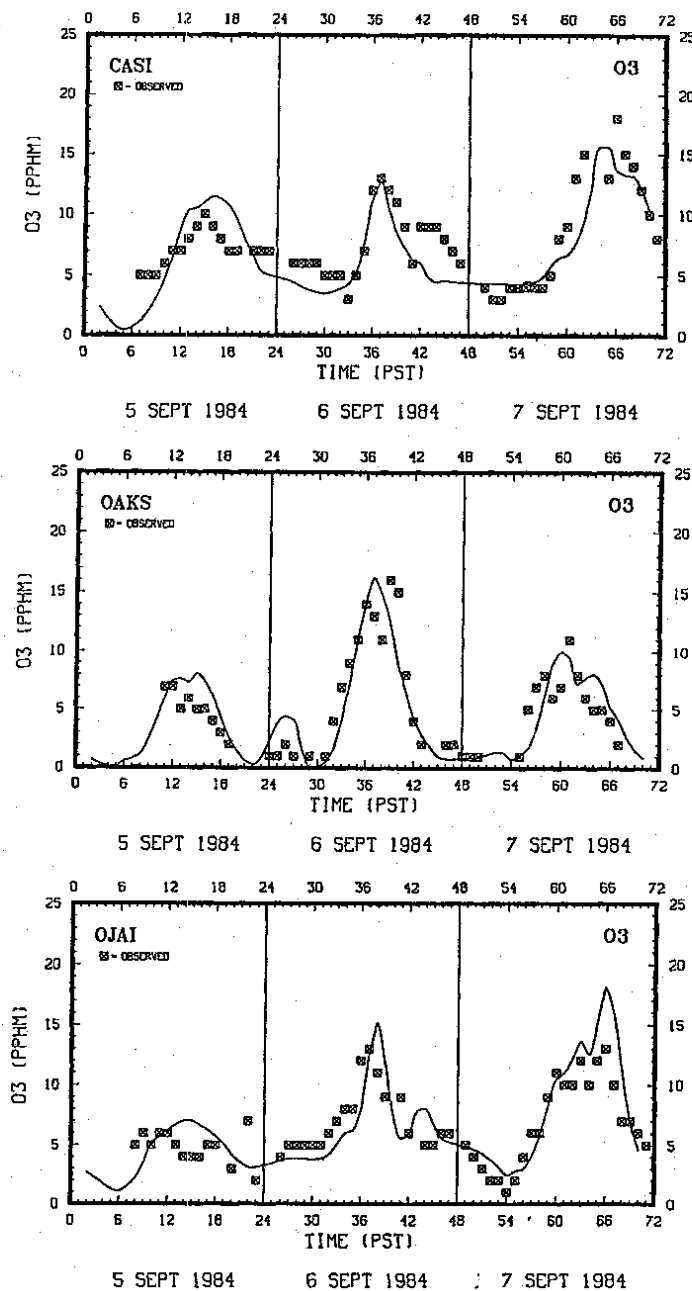| Hour (PST)	5-7 September 1948				16-17 September 1984			
	NO	NO₂	O₃	RHC	NO	NO₂	O₃	RHC
0-1	0.001	0.001	0.04	0.100	0.001	0.001	0.04	0.100
1-2	0.031	0.033	0.00	0.761	0.007	0.025	0.00	0.388
2-3	0.031	0.034	0.00	0.781	0.010	0.027	0.00	0.450
3-4	0.025	0.035	0.00	0.782	0.009	0.029	0.00	0.500
4-5	0.017	0.032	0.00	0.729	0.008	0.030	0.00	0.538
5-6	0.011	0.026	0.01	0.637	0.013	0.029	0.00	0.554
6-7	0.010	0.036	0.04	0.689	0.013	0.032	0.02	0.588
7-8	0.010	0.036	0.04	0.689	0.008	0.034	0.05	0.607
8-9	0.003	0.022	0.09	0.533	0.004	0.024	0.10	0.559
9-10	0.001	0.006	0.11	0.308	0.001	0.008	0.12	0.387
10-11	0.001	0.002	0.10	0.206	0.001	0.003	0.09	0.238
11-12	0.001	0.002	0.09	0.172	0.001	0.003	0.05	0.156
20-21	0.001	0.005	0.05	0.174	0.001	0.006	0.04	0.176
21-22	0.001	0.007	0.04	0.200	0.001	0.009	0.04	0.200
22-23	0.001	0.012	0.04	0.233	0.001	0.009	0.04	0.200
23-24	0.001	0.012	0.04	0.233	0.001	0.009	0.04	0.200

FIG. 3. Estimated and observed hourly averaged ozone concentrations for 5–7 September 1984 at: (a) Casitas, (b) Thousand Oaks, (c) Ojai, (d) Piru, (e) Santa Barbara, (f) Simi.
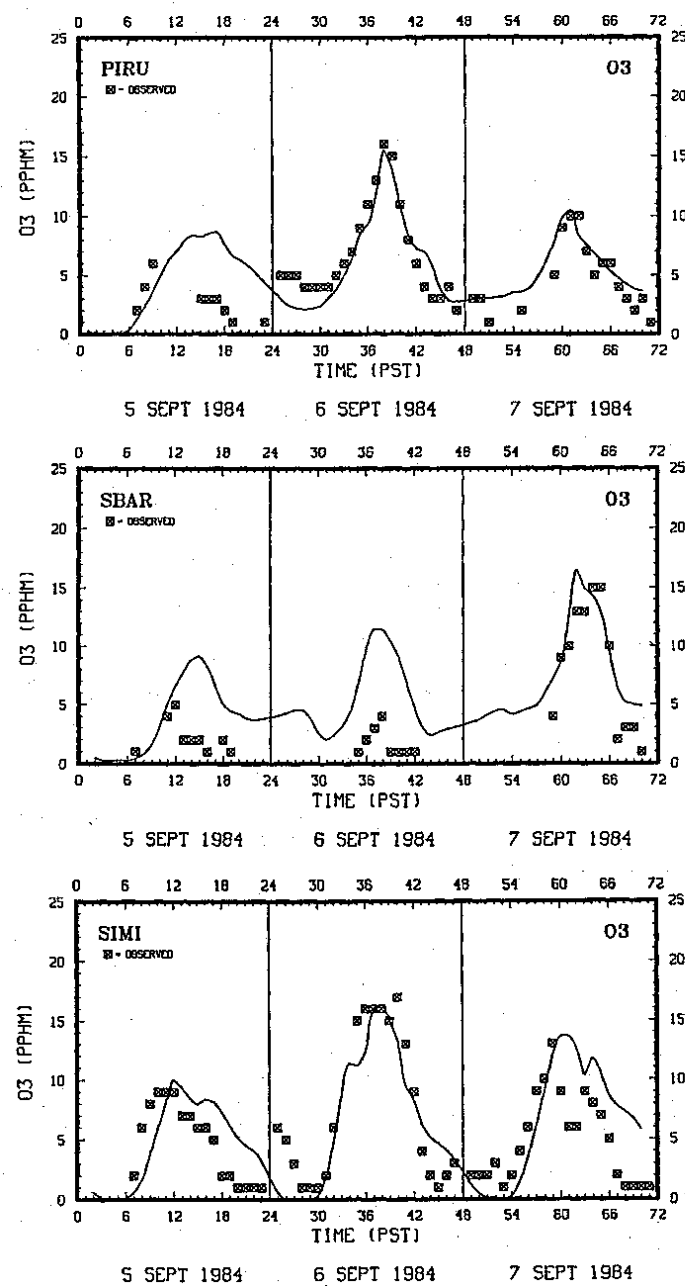
FIG. 3. (Continued)

seda stations in San Fernando Valley were obtained to prescribe boundary conditions in this region. We also examined the hourly concentrations near the eastern and southeastern portions of the present grid that were estimated in previous UAM modeling studies for the south coast air basin (Tesche et al. 1984). The resultant boundary conditions summarized in Table 5 only affect model calculations when the wind is directed into the computational domain, usually during the nighttime and morning hours.

Ambient hydrocarbon data were collected in evacuated canisters at numerous locations during the 1984 field program. This information was used in setting boundary conditions for hydrocarbons as well as for determining the splitting factors needed to apportion the reactive organic gas concentrations into the five CBM-II species categories. Because no speciated hydrocarbon sampling was performed for 5–7 September, we used the average splits from the 12 measurement days as an estimate for the 5–7 September episode. Day-specific splits were used for 16–17 September. The splitting factors are listed in Table 6. These values were used to distribute the estimated boundary ROG value (0.029 ppmC) into the five categories.

5. Photochemical model performance evaluation

One of the primary reasons for conducting a performance evaluation is to determine whether the model performs well enough to be used for regulatory purposes. As yet, no definitive guidelines for model performance evaluations exist despite nearly 20 years of

research in this field (Tesche et al. 1991). In section 6 we discuss the SCCCAMP 1984 model evaluation results using commonly employed evaluation procedures. However, to stimulate development of a consistent process for model performance evaluation in the future, we offer a few suggestions here on the approach to model performance evaluation that should be considered in subsequent studies.

Model performance evaluation is the process of testing a model's ability to estimate accurately observed measures of air quality over a range of meteorological, emissions, and air quality conditions. It focuses and directs the continuing cycle of model development, data collection, model testing, diagnostic analysis, refinement, and retesting. While a single evaluation cannot "validate" a model, it can raise serious doubts about a model's adequacy.

Performance evaluation has several components. The *operational evaluation* is an assessment of a model's ability to estimate the correct answer whether or not the process descriptions in the model are accurate. It is an examination of how well a model reproduces observed concentration fields in time and space consistent with the needs of policy analysis or regulatory decision making. Current statistical tests and methods used in operational evaluations of urban- and regional-scale models are described by Barchet (1987), Daly et al. (1988), Dennis et al. (1989), and Tesche et al. (1991). These studies suggest specific statistical and graphical techniques for operational performance evaluation, emphasizing the use of concentration residuals to estimate model accuracy and precision. Op-
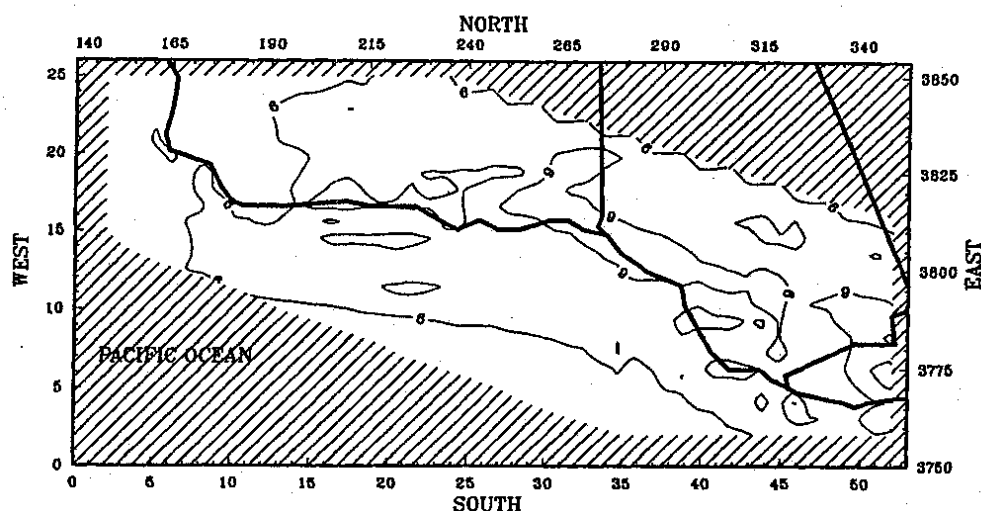

FIG. 4. Ground-level ozone estimates (pphm) between the hours of 1400 and 1500 PST 5 September 1984.

erational testing of the entire modeling system gives little, if any information about whether the results are correct from a scientific perspective or whether they are simply the fortuitous product of compensatory errors. Therefore, a "successful" operational evaluation is a necessary but insufficient condition for achieving a sound modeling exercise.

The *scientific evaluation* seeks to determine whether the model's behavior, in the aggregate and in its component modules, is consistent with prevailing theory, knowledge of physical and chemical processes, and observations. The scientific evaluation consists of several diagnostic and mechanistic tests and procedures, some of which can be prescribed in advance while others must be defined through the investigative process. These procedures have a common set of objectives, namely to: (a) identify the presence and severity of hidden or compensatory errors, (b) determine the causes of failure of a flawed model, (c) "stress" a model to ensure failure if indeed the model is flawed, and (d) provide additional insight into model performance beyond that supplied through the routine, operational evaluation procedures. "Stressing a model" is designing and carrying out performance tests that cause a model to reveal its flaw and weaknesses if it is indeed inadequate. Stressful testing is intended to reduce (or avoid) the risks associated with "weak" or otherwise inadequate tests, wherein a model is not challenged sufficiently to reveal its flaws and weaknesses or appears to be performing acceptably despite significant inadequacies in formulation or inputs.

The scientific evaluation should be carried out in three stages—diagnostic, mechanistic, and compara-

tive. *Diagnostic evaluation* consists of an assessment of a model's ability, when functioning as a whole, to simulate processes or characteristics of the system occurring during a photochemical episode (e.g., emissions, dispersion patterns, deposition rates). The tests are chosen to challenge the science in the model. Specific focus is on detailed examination of how well individual components of the model (or modules) simulate actual atmospheric processes. *Mechanistic evaluation* is an assessment of an individual modules' ability to reproduce the observed salient features of the processes it is intended to describe. When applied to all process modules that constitute the full model, mechanistic evaluation represents a test of the correctness of the underlying science. Finally, *comparative evaluation* refers to the intercomparison between different simulation models or modules (e.g., wind field generators, mixing-height algorithms, travel demand models, motor vehicle emissions factor modules, chemical kinetic mechanisms) using observed, valid data as the standard against which the intercomparisons are judged.

For the most part, our evaluation of the 1984 SCCCAMP episodes is operational. Insufficient data were collected to support detailed diagnostic, mechanistic, or comparative evaluations. Measurement data for species other than ozone were too sparse to support detailed multispecies evaluations. Only limited data were collected that might be used to test meteorological models for wind or mixing-height estimation and no data were gathered for emissions, deposition, or chemical mechanism testing. Notwithstanding these limitations, the 1984 SCCCAMP database does offer an
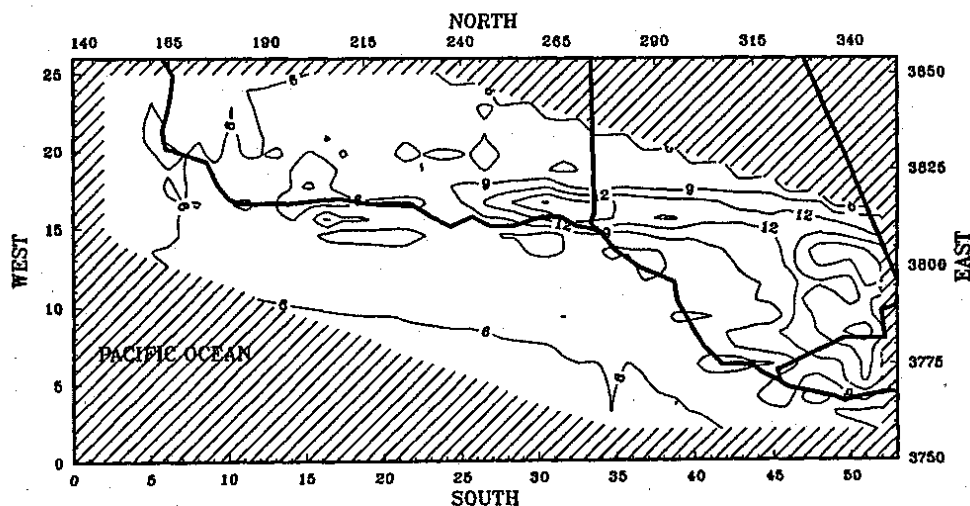

FIG. 5. Ground-level ozone estimates (pphm) between the hours of 1400 and 1500 PST 6 September 1984.

opportunity to carry out a reasonably detailed operational evaluation. The principal results of this analysis are discussed next; full details are presented in the project reports.

6. Results of the performance evaluations

a. 5–7 September 1984

A 66-h simulation of the 5–7 September 1984 ozone episode was carried out beginning at 0200 PST on the 5th. Ozone time series plots at six monitoring stations representative of high ozone locations during the 3-day period are shown in Fig. 3. The solid line represents the modeled hourly averaged ozone concentrations (pphm) in the grid cell containing the monitoring station. The boxes correspond to the hourly averaged ozone observations. As indicated in Table 1, the maximum observed ozone concentration on the 5th was 10 pphm at Casitas while the peak values on the following two days were significantly higher, with ozone maxima of 17 pphm (Simi) and 18 pphm (Casitas) on the 6th and 7th, respectively. As shown in Fig. 3a, the UAM estimated a peak of 12 pphm at Casitas on the 5th, one hour after the time of maximum reported ozone. With the exception of the Santa Barbara monitoring station, the peak concentrations on the 6th are fairly well reproduced. On the 7th, the diurnal profiles reproduce the main features of the observations. There are obvious underestimation problems at some of the stations, particularly during the nighttime and early morning hours.

Figures 4–6 present hourly averaged ground-level ozone isopleths (in pphm) at 1400 PST on the 5–7

September. The shaded region represents those portions of the UAM grid excluded from model calculations to reduce CPU time. On the 5th, an elongated, narrow region of moderate (9 pphm) ozone concentrations is simulated along a northwest–southeast axis from Santa Barbara to Moorpark. On the 6th, a localized region of high ozone (16 pphm) is simulated in the elevated terrain of the Santa Ynez Mountains northeast of the city of Santa Barbara. Based on backward (in time) trajectory analyses, this ozone "cloud" appears to have had its origin earlier in the episode from aged air parcels located over the Santa Barbara Channel and from urban emissions in the Santa Barbara–Goleta region. Farther inland, another area of elevated ozone is simulated on the 6th in the subregion surrounding Piru and Simi. Backward trajectory analyses indicate that this ozone cloud likely has had its origin over the urbanized region along the Ventura County coast. On the 6th and 7th, the modeled ozone cloud in Santa Barbara County appears to be displaced slightly to the north compared with the surface measurements. Figure 6 indicates that on the 7th, distinct subregions of high ozone are also simulated, again in the eastern portions of each county. However, the locations of the maximum ozone impacts on the 7th are shifted westward somewhat compared with the 6th.

The maximum observed ozone concentration the 7th is 18 pphm at Casitas, yet the maximum estimated value is 12.6 pphm. Examination of the ground-level concentration fields indicates that higher ozone concentrations are estimated a few grid cells to the north of the Casitas monitor. A similar, though less pronounced, shift in estimated and observed ozone fields
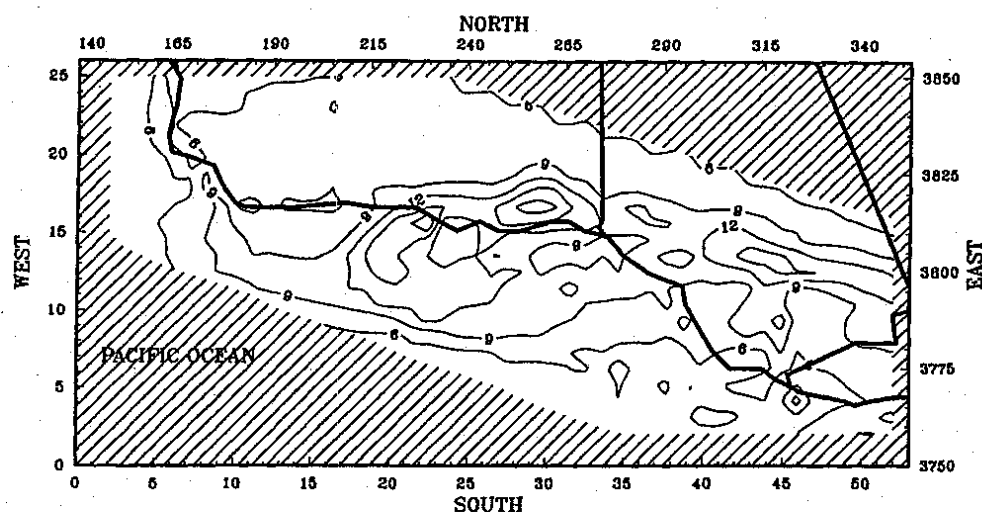

FIG. 6. Ground-level ozone estimates (pphm) between the hours of 1400 and 1500 PST 7 September 1984.

TABLE 7. Model performance in simulating maximum 1-h ozone concentrations
for the 5–7 September 1984 episode (concentrations in pphm).

Monitoring station	5 September			6 September			7 September		
	Observed concentration	Predicted concentration	Percentage difference	Observed concentration	Predicted concentration	Percentage difference	Observed concentration	Predicted concentration	Percentage difference
ELRO	4.0	7.3	82	6.0	8.2	36	7.0	8.2	18
SIMI	9.0	10.0	11	17.0	16.3	−4	13.0	13.7	5
SBAR	5.0	9.2	84	4.0	11.5	187	15.0	16.5	10
CASI	10.0	12.0	20	13.0	9.9	−24	18.0	12.6	−30
PIRU	6.0	8.7	45	16.0	15.5	−3	10.0	10.5	5
OJAI	7.0	7.0	0	13.0	15.2	17	13.0	18.1	39
OAKS	7.0	8.2	17	16.0	16.3	2	11.0	10.0	−9
ELCP	5.0	6.5	31	10.0	6.2	−38	11.0	13.4	22
GOLA	7.0	6.7	−4	8.0	9.0	12	15.0	14.2	−5
VBGW	4.0	3.8	−5	4.0	4.8	19	6.0	6.0	−1
VBGH	3.0	4.1	37	3.0	4.9	64	6.0	5.7	−6
SYNZ	6.0	8.3	38	4.0	7.1	78	8.0	7.7	−4
LOMH	3.0	5.6	87	3.0	6.8	125	6.0	7.1	19
GAVI	8.0	6.3	−22	6.0	6.5	9	13.0	10.3	−21
Avg	6.0	7.4		8.8	9.9		10.9	11.0	

is apparent in the vicinity of the Ojai monitor. Here, the model estimates a peak value of 18.1 pphm (compared to an observed peak of 13 pphm) while a few grid cells away the model estimates values equal to or greater than the observations. Thus, near these monitoring stations, UAM estimates are comparable to the maximum values observed, but the spatial offset of the modeled ozone cloud produces a 5 pphm underestimation at one site (Casitas) and a 5 pphm overestimation at the other (Ojai) when the estimates and observations are matched in time and space.

Maximum observed and estimated hourly averaged ozone concentrations at each monitoring station for the three simulation days are listed in Table 7. For 5 September, the average observed ozone maximum is 6.0 pphm, compared with a peak average value of 7.4 pphm. On the 6th, the ozone peaks at Simi and Piru were underestimated by −4% and −3%. At Thousand Oaks, the peak was overestimated by 2% on the 6th. The peak estimation performance on the 7th is somewhat poorer. The maximum observed value of 18 pphm at Casitas was underestimated by 30%. However, the average peak model estimate over all 14 monitoring stations was nearly identical to the average measured value (10.9 pphm vs 11.0 pphm).

The accuracy of peak ozone concentrations may be described in several ways. The 6 September ozone results shown in Table 7 may be used to exemplify three methods. A stringent method is to compute the spatially paired accuracy of the peak model estimate. This is based on the maximum observed ozone value in the basin on the 6th (17 pphm at Simi) and the maximum estimated value at the same location (16.3 pphm), but not necessarily at the same hour. This measure of accuracy is −4%. Another method gives the "unpaired accuracy of the peak estimate." This is computed with

TABLE 8. Airshed model ozone performance statistics for the two September 1984 simulations
(concentrations greater than or equal to 4 pphm).

| Performance measure	5 September	6 September	7 September	16 September	17 September
Maximum estimated station ozone concentration (pphm)	12.0 (Casi)	16.3 (Simi)	18.1 (Ojai)	11.0 (Piru)	12.5 (Ojai)
Maximum observed ozone concentration (pphm)	10.0 (Casi)	17.0 (Simi)	18.0 (Casi)	11.0 (Simi)	14.0 (Casi)
Ratio of estimated to observed maxima	1.201	0.961	1.004	1.000	0.891
Accuracy (paired) of peak estimation (percent)	+20%	−4%	−30%	0%	18%
Accuracy (unpaired) of peak estimate (percent)	+20%	−4%	−30%	0%	11%
Mean normalized deviation (bias)	+0.108	−0.056	0.036	0.093	−0.046
Mean absolute normalized deviation (error)	0.377	0.324	0.234	0.264	0.262
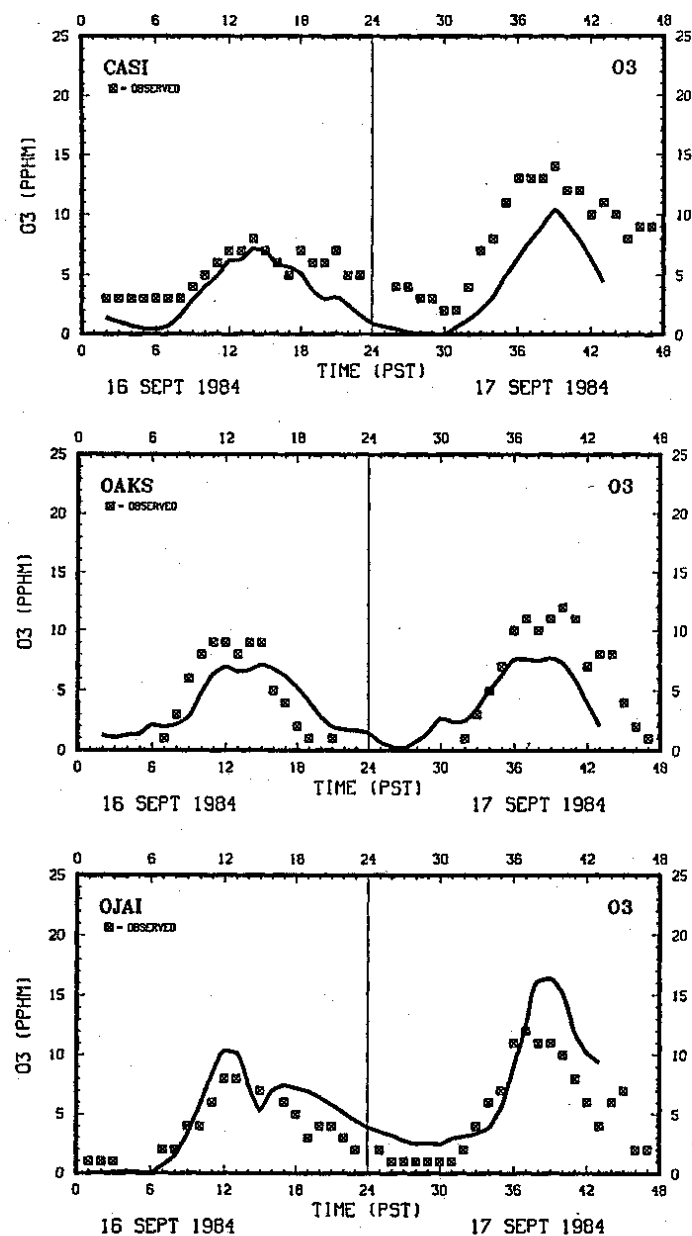
FIG. 7. Estimated and observed hourly averaged ozone concentrations for 16–17 September 1984 at: (a) Casitas, (b) Thousand Oaks, (c) Ojai, (d) Piru, (e) Santa Barbara, (f) Simi.
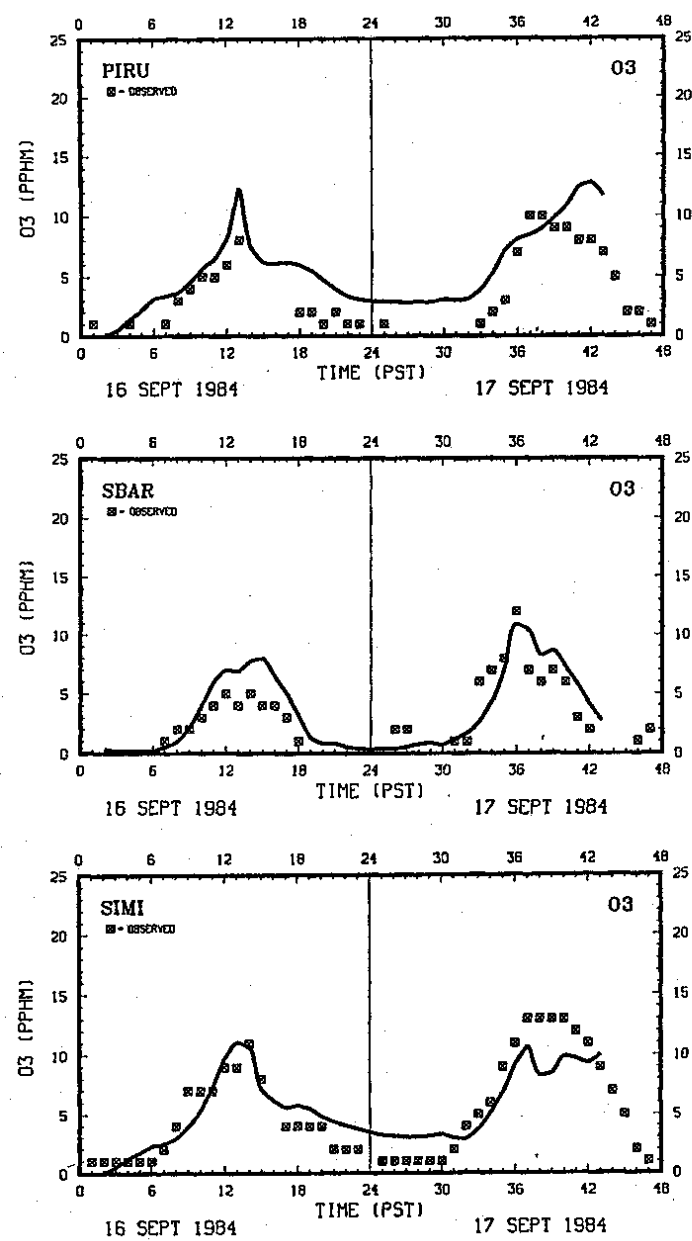
T. W. TESCHE AND DENNIS E. McNALLY
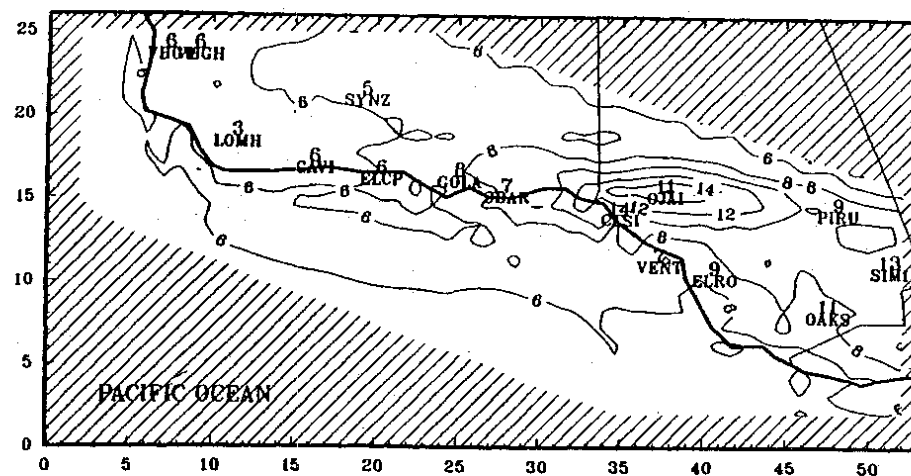

Fig. 7. (Continued)

FIG. 8. Ground-level ozone estimates (pphm) between the hours of 1500 and 1600 PST 17 September 1984.

the basin maximum of 17 pphm at Simi and the highest ozone estimate of *any* of the monitoring stations in the basin. In this case, the highest estimated value is 16.3 pphm at Thousand Oaks and Simi, which leads to the same numerical value as before, −4%. The third method involves computing the spatially paired accuracies of peak estimation at each monitoring station (above 4 pphm) and then averaging the results to yield the "average of the station peak estimation accuracies." For the three simulation days, these averages are 27%, 16%, and 14%, respectively. Each of these measures of

accuracy provide some insight into the modeling results but they need to be considered in the broader context of two other important residual measures—bias and error.

Table 8 presents the bias and error statistics for the 5–7 September episode. Bias is computed as the average of the signed residuals of the model estimate–observation pairs normalized by the observed concentration. This quantity is calculated using all residual pairs (all hours and all monitors) for which the observed ozone values equal or exceed 4 pphm. The gross error is com-

TABLE 9. Model performance in simulating maximum 1-h ozone concentrations for the 16–17 September 1984 episode (concentrations in pphm).

	16 September			17 September		
Monitoring station	Observed maximum concentration	Predicted maximum concentration	Percentage difference	Observed maximum concentration	Predicted maximum concentration	Percentage difference
ELRO	6.0	7.5	24	10.0	8.4	−16
SIMI	11.0	10.9	−1	13.0	10.7	−18
VENT	7.0	7.9	12	10.0	8.0	−21
SBAR	5.0	6.8	35	12.0	11.1	−8
CASI	8.0	7.6	−5	14.0	11.5	−18
PIRU	8.0	11.6	37	10.0	12.3	23
OJAI	8.0	10.2	27	12.0	12.5	4
OAKS	9.0	7.5	−17	12.0	9.3	−23
ELCP	6.0	6.1	1	6.0	6.8	14
GOLA	6.0	6.5	9	11.0	8.6	−22
VBGW	5.0	5.0	0	6.0	5.1	−14
VBGH	6.0	5.3	−11	6.0	5.3	−12
SYNZ	5.0	6.8	36	6.0	6.5	8
LOMH	5.0	5.9	17	4.0	5.5	37
GAVI	4.0	4.8	19	7.0	5.5	−22
Avg	6.6	7.3		9.3	8.5	

puted from the mean absolute normalized residual. The UAM overestimates ozone levels by 10.8% on the 5th and the overall gross error is 37.7%. This error is relatively high, in part because the concentrations on the 5th are generally low; thus, the denominators in the error calculation are typically smaller numbers compared with the 6th and 7th. On the 6th, there is a small bias toward underestimation, −5.6%. On the 7th, the bias is +3.6%. The gross errors on the 6th and 7th are 32.4% and 23.4%, respectively.

b. 16–17 September 1984

Time-series plots of estimated and observed ozone concentrations at the six monitoring stations for the 16–17 September 1984 simulation are given in Fig. 7. The model does better in reproducing the 16th's ozone levels compared with the 5th. On the 17th, the model overestimates at some stations and underestimates at others. Figure 8 is the ground-level ozone isopleth at 1500 PST on 17 September. As with the previous episode, a region of high ozone concentrations (16 pphm) is simulated north of Ojai in the elevated terrain of the Santa Ynez Mountains.

Table 9 lists the peak hourly ozone estimates and observations for this episode. On the 16th, the highest observed value is 11 pphm at Simi. The model estimates a concentration of 10.9 pphm at Simi, giving an error of −1%. The maximum estimated value, 11.6 pphm at Piru, gives an unpaired accuracy of peak estimation of +5%. The average peak estimation error over all monitoring stations on the 16th is 11%. On the 17th, the maximum observed ozone concentration is 14 pphm at Casitas. The peak estimate at the same location is 11.5 pphm, giving a peak estimation accuracy of −18%. The unpaired accuracy of peak estimation for the 17th is −11%. Considering the peak accuracy over all stations, the model shows a very slight tendency to underestimate on the 17th with value of −9%.

Table 8, introduced earlier, gives ozone bias and error estimates for the 16–17th episode also. The model overestimates hourly concentrations by 9.3% on the 16th and underestimates them by −4.6% on the 17th. Gross errors for ozone are 26.4% and 26.2%, respectively, for the two days.

7. Discussion

The evaluation statistics we have calculated for the two 1984 SCCCAMP ozone episodes are typical of the accuracy, bias, and error results reported in similar urban-scale photochemical modeling studies (Tesche 1988). It is tempting to claim that these results confirm that the model is operating properly but there are at least three reasons why we believe that just the opposite should be suspected, pending further investigation.

First, simply because the model produces results comparable to a host of previous evaluations does not demonstrate reliable performance. The definition, calculation, and reporting of performance measures has varied widely among modeling groups; no consistent evaluation methodology has been employed. Few, if any, of the previous studies, carried out a sufficiently robust set of diagnostic and mechanistic analyses to confirm that the accuracy, bias, and error statistics reported truly meant that the models were operating properly. Absent important diagnostic tests (e.g., multispecies comparisons) and mechanistic evaluations, it may be that previous photochemical model evaluations were inadvertently "tuned" to the observed ozone values.

Second, it is quite likely that hidden, or compensatory errors exist within the present model simulations that have not been revealed through the operational evaluation. For example, we previously noted the absence of detailed upper-air information with which to evaluate the performance of the mixing-height algorithms. It is conceivable that the mixing heights could be systematically underestimated. If so, this bias would produce higher ozone concentrations for both episodes based on our detailed mixing-height sensitivity experiments (Tesche et al. 1988b). Conversely, the on-hydrocarbon emission inventories are generally thought to be biased low (Seinfeld 1988), which will cause the model to underestimate ozone. Thus, the effects of mixing heights that are too low could compensate for the underestimation in hydrocarbon emissions to produce ozone concentrations that appear to be correct but for the wrong reason. A major objective of the scientific performance evaluation is to locate and quantify the magnitude of compensatory errors through a series of successively more stressful tests. Performance of these mechanistic and diagnostic tests requires sets of measurements that were not intended to be part of the 1984 SCCCAMP Exploratory Field Study.

Third, while there is a rich history of photochemical model performance evaluation using past ozone episodes, there has been very little work done to evaluate the reasonableness of ozone estimates when models are used to simulate the effects of control strategies in future years. Ideally, the adequacy of a photochemical model in correctly estimating the effects of emission changes on ambient air quality should be evaluated directly by examining model performance for applications involving significantly altered emission strengths and spatial patterns. Such an evaluation should be performed with emission estimates for the same region that correspond to years sufficiently separate in time. Since such a procedure is most likely impractical, as an alternative, one should evaluate the model for two or more different regions, using input data of comparable quality.

These limitations do not preclude the use of the 1984 episodes in designing and testing emissions control strategies. Rather, they should be carefully considered when devising control strategies and interpreting sim-

ulation results since the risks raised by compensating errors are increased.

One concern we were not able to address adequately in this study involves the use of three different models to apply wind, temperature, and mixing-height fields. The use of separate model input preprocessor programs to generate components of the meteorological fields raises the potential for dynamic and thermodynamic inconsistencies in the transport and thermal fields. Since this approach is commonly used today in urban- and regional-scale photochemical modeling, the potential significance of these inconsistencies should be investigated.

8. Conclusions

The 1984 SCCCAMP Exploratory Field Study provides useful photochemical modeling episodes in the south-central coast air basin. Two periods, 5–7 September and 16–17 September 1984, have been simulated, providing a technical basis for Santa Barbara County's Air Quality Attainment Plan and the EPA's Federal Implementation Plan for Ventura County. An operational ozone model performance evaluation was performed for the 5–7 and 16–17 September 1984 episodes. The UAM reproduced the peak 1-h ozone concentrations (paired in time and space) on the five simulation days with accuracies ranging from 0% to −30%. The average bias, the tendency to over- or underestimate hourly averaged ozone concentrations, ranged between −6% and +11%. The average gross errors in hourly estimates varied between 23% and 38%. UAM performance in simulating hourly averaged ozone concentrations for both episodes is found to compare well with other recent photochemical model evaluations in the United States.

The major limitation of the present evaluation study involves the absence of detailed diagnostic and mechanistic analyses. The 1984 SCCCAMP database was not designed to support a scientific model performance exercise so data essential for multispecies evaluations, testing of individual model components such as windfields, emissions, deposition, or chemistry, and for performing compensatory error analyses are not collected. Consequently, decision-makers must exercise caution in the interpretation of emission control scenarios derived from the 5–7 September and 16–17 September 1984 databases since these important evaluative tests were not carried out.

A pressing challenge in photochemical model evaluation today is the need to devise and implement more rigorous techniques for revealing the presence and effects of compensatory errors in model simulations. Meeting this challenge will require thoughtful construction of a set of stress tests that may be applied to the entire modeling system as well as to its component parts. Unfortunately, even the most intensive databases currently available have important limitations. De-

tailed stress testing and compensatory error analysis will necessitate the collection of new, highly specialized databases. Ultimately, public policy makers will have to decide: (a) just how important the answers to the questions raised in section 1 are to them, in terms of supporting their decision-making needs, (b) and just how much money is appropriate to spend for data collection and modeling analyses to obtain these answers.

REFERENCES

Ames, J., T. C. Meyers, L. E. Reid, D. C. Whitney, S. H. Golding, S. R. Hayes and S. D. Reynolds, 1985: SAI airshed model operations manuals: Volume I—user's manual. Rep. by Systems Applications, Inc., San Rafael, CA., EPA-68-02-2429, 265 pp.

Barchet, W. R., 1987: Evaluation of regional-scale air quality-models: Chairman reps. from four workshops. Electric Power Research Institute, Research Project 1630–40, 153 pp. [Available from Battelle Pacific Northwest Laboratories, Richland, WA.]

Dabberdt, W. F., 1984: Preliminary summary of the 1984 South-Central Coast Cooperative Aerometric Monitoring Program (SCCCAMP) exploratory study. 71 pp. [Available from SRI, Altadena, CA.]

——, and W. Viezee, 1987: South Central Coast Cooperative Aerometric Monitoring Program (SCCCAMP). *Bull. Amer. Meteor. Soc.*, 68, 1098–1110.

Daly, C., M. A. Yocke, R. L. Dennis, S. Seilkop and P. M. Roth, 1988: Protocol for evaluating the predictive performance of the regional acidic Deposition Models RADM and ADOM. Environmental Protection Agency 68-02-4129, Atmospheric Sciences Research Laboratory, Research Triangle Park, NC, 127 pp.

Dennis, R. L., W. R. Barchet, T. L. Clark, S. K. Seilkop and P. M. Roth, 1989: Evaluation of regional acid deposition models. State-of-Science Tech. Rep. No. 5, National Acid Precipitation Assessment Program, Washington, D.C., 187 pp.

Environmental Protection Agency, 1986: Guideline on air quality models (Revised). EPA-450/2-78-027R, United States Environmental Protection Agency, Office of Air Quality Planning and Standards, Research Triangle Park, NC, 137 pp.

Gery, M. W., G. Z. Whitten and J. P. Killus 1988: Development and testing of the CBM-IV for urban and regional modeling. EPA/600/3-88/012, United States Environmental Protection Agency, Research Triangle Park, NC, 137 pp.

Goodin, W. R., G. J. McRae and J. H. Seinfeld, 1980: An objective analysis technique for constructing three-dimensional urban-scale wind fields. *J. Appl. Meteor.*, 19, 96–106.

Haney, J. L., D. R. Souten, T. W. Tesche, L. R. Chinkin, H. Hogo and M. C. Dudik, 1986: Evaluation and Application of the PARIS photochemical model in the South Central Coast Air Basin, SYSAPP-86/065 Rep. by Systems Applications, 383 pp. [Available from United States Environmental Protection Agency.]

Holtslag, A. A. M., and A. P. van Ulden, 1983: A simple scheme for daytime estimates of the surface fluxes from routine weather data. *J. Climate Appl. Meteor.*, **22**, 517–529.

Kessler, R. C., and S. G. Douglas, 1989: Numerical simulation of mesoscale airflow in the South Central Coast Air Basin. SYSAPP-89/077, Final Rep., 252 pp. [Available from Systems Applications, Inc., San Rafael, CA.]

Morris, R. E., T. C. Myers and J. L. Haney, 1990: User's guide for the urban airshed model: Volume I. User's manual for UAM (CB-IV). Report by Systems Applications, Inc., No. SYSAPP-90/018a, 259 pp. [Available from U.S. Environmental Protection Agency, Office of Air Quality Planning and Standards, Research Triangle Park, NC.]

Reynolds, S. D., T. W. Tesche and D. R. Souten, 1985: Overall study protocol for the South Central Coast Cooperative Aerometric Monitoring Program. Final Rep. to the Western Oil and Gas Association, 287 pp. [Available from Systems Applications, Inc., San Rafael, CA.

Seinfeld, J. H., 1988: Ozone air quality models: a critical review. *J. Air Pollut. Control Assoc.*, **38**, 616–645.

SLC, 1986: Environmental impact rep, environmental impact statement for proposed ARCO coal oil point project: Appendix 4—air quality—meteorology: Volume II. [Available from California State Lands Commission, Sacramento, CA.]

Smolarkiewicz, P. K., 1983: A simple positive definite advection scheme with small implicit diffusion. *Mon. Wea. Rev.*, **111**, 479–486.

Stauffer, D. R., and N. L. Seaman, 1990: Use of four-dimensional data assimilation in a limited-area mesoscale model. *Mon. Wea. Rev.*, **118**, 1250–1277.

Steyn, D. G., and T. R. Oke, 1982: The depth of the daytime mixed layer at two coastal sites: A model and its validation. *Bound. Layer Meteor.*, **24**, 161–180.

Tennekes, H., 1973: A model for the dynamics of the inversion above the convective boundary layer, *J. Atmos. Sci.*, **30**, 558–567.

Tesche, T. W., 1988: Accuracy of ozone air quality models. *J. Environ. Eng.*, **114**, 739–752.

——, 1991: Evaluating procedures for using numerical meteorological models as input to photochemical models. *7th Joint Conference on Applications of Air Pollution Meteorology*, New Orleans, Amer. Meteor. Soc., 6 pp.

——, and D. E. McNally, 1989: Urban airshed modeling in support of the ventura ozone federal implementation plan. Rep. to the United States Environmental Protection Agency, Region IX, EPA Contract No. 68-02-4392, Work Assignment No. 37, 97 pp.

——, C. Seigneur, B. Oliver and J. L. Haney, 1984: Modeling ozone control strategies in Los Angeles. *J. Environ. Eng.*, **110**, 208–225.

——, C. Daly, B. D. Miller and S. D. Reynolds, 1985: Analysis of the data collected in the 1984 SCCCAMP field program. SYS-APP-85/029, Final Program Rep. to the South-Central Coast Cooperative Aerometric Monitoring Program, 208 pp. [Available from Systems Applications, Inc., San Rafael, CA.]

——, J. G. Wilkinson, D. E. McNally, R. Kapahi and B. Oliver, 1988a: Photochemical modeling of two SCCCAMP 1984 oxidant episodes: Volume II: Modeling procedures and evaluation results, Final Program Rep. to the United States Environmental Protection Agency, Region IX, San Francisco, CA, 352 pp.

——, D. E. McNally and J. G. Wilkinson, 1988b: Importance of boundary layer measurements for urban airshed modeling. *81st Modeling of the Air Pollution Control Association*, Dallas, 18 pp.

——, P. Georgopoulos, J. H. Seinfeld, P. M. Roth, F. W. Lurmann and G. Cass, 1990: Improvement of procedures for evaluating photochemical models. Final Rep. to the California Air Resources Board, Contract No. A832-103, Sacramento, CA, 352 pp.

van Ulden, A. P., and A. A. M. Holtslag, 1985: Estimation of atmospheric boundary layer parameters for diffusion applications. *J. Climate Appl. Meteor.*, **24**, 1196–1207.

Wagner, K. K., 1989: Evaluation of NO$_x$ and reactive hydrocarbon emission controls for ozone in the South Central Coast Air Basin of California. *82nd Annual Meeting of the Air and Waste Management Association*, Anaheim, CA, 9 pp.

Whitten, G. Z., H. Hogo and J. P. Killus, 1980: The carbon-bond mechanism: A condensed kinetic mechanism for photochemical smog. *Environ. Sci. Technol.*, **14**, 657–682.

Wilczak, J. M., and M. S. Phillips, 1986: An indirect estimation of convective boundary layer structure for use in pollution dispersion models. *J. Climate Appl. Meteor.*, **25**, 1069–1624.

3.2 Natural Gas-fired Reciprocating Engines

3.2.1 General[1-3]

Most natural gas-fired reciprocating engines are used in the natural gas industry at pipeline compressor and storage stations and at gas processing plants. These engines are used to provide mechanical shaft power for compressors and pumps. At pipeline compressor stations, engines are used to help move natural gas from station to station. At storage facilities, they are used to help inject the natural gas into high pressure natural gas storage fields. At processing plants, these engines are used to transmit fuel within a facility and for process compression needs (e.g., refrigeration cycles). The size of these engines ranges from 50 brake horsepower (bhp) to 11,000 bhp. In addition, some engines in service are 50 - 60 years old and consequently have significant differences in design compared to newer engines, resulting in differences in emissions and the ability to be retrofitted with new parts or controls.

At pipeline compressor stations, reciprocating engines are used to power reciprocating compressors that move compressed natural gas (500 - 2000 psig) in a pipeline. These stations are spaced approximately 50 to 100 miles apart along a pipeline that stretches from a gas supply area to the market area. The reciprocating compressors raise the discharge pressure of the gas in the pipeline to overcome the effect of frictional losses in the pipeline upstream of the station, in order to maintain the required suction pressure at the next station downstream or at various downstream delivery points. The volume of gas flowing and the amount of subsequent frictional losses in a pipeline are heavily dependent on the market conditions that vary with weather and industrial activity, causing wide pressure variations. The number of engines operating at a station, the speed of an individual engine, and the amount of individual engine horsepower (load) needed to compress the natural gas is dependent on the pressure of the compressed gas received by the station, the desired discharge pressure of the gas, and the amount of gas flowing in the pipeline. Reciprocating compressors have a wider operating bandwidth than centrifugal compressors, providing increased flexibility in varying flow conditions. Centrifugal compressors powered by natural gas turbines are also used in some stations and are discussed in another section of this document.

A compressor in storage service pumps gas from a low-pressure storage field (500 - 800 psig) to a higher pressure transmission pipeline (700 - 1000 psig) and/or pumps gas from a low-pressure transmission line (500 - 800 psig) to a higher pressure storage field (800 - 2000 psig).

Storage reciprocating compressors must be flexible enough to allow operation across a wide band of suction and discharge pressures and volume variations. The compressor must be able to compress at high compression ratios with low volumes and compress at low compression ratios with high volumes. These conditions require varying speeds and load (horsepower) conditions for the reciprocating engine powering the reciprocating compressor.

Reciprocating compressors are used at processing plants for process compression needs (e.g. refrigeration cycles). The volume of gas compressed varies, but the pressure needed for the process is more constant than the other two cases mentioned above.

3.2.2 Process Description[1-3]

Natural gas-fired reciprocating engines are separated into three design classes: 2-cycle (stroke) lean-burn, 4-stroke lean-burn, and 4-stroke rich-burn. Two-stroke engines complete the power cycle in a

single crankshaft revolution as compared to the two crankshaft revolutions required for 4-stroke engines. All engines in these categories are spark-ignited.

In a 2-stroke engine, the air-to-fuel charge is injected with the piston near the bottom of the power stroke. The intake ports are then covered or closed, and the piston moves to the top of the cylinder, compressing the charge. Following ignition and combustion, the power stroke starts with the downward movement of the piston. As the piston reaches the bottom of the power stroke, exhaust ports or valves are opened to exhaust, or scavenge, the combustion products, and a new air-to-fuel charge is injected. Two-stroke engines may be turbocharged using an exhaust-powered turbine to pressurize the charge for injection into the cylinder and to increase cylinder scavenging. Non-turbocharged engines may be either blower scavenged or piston scavenged to improve removal of combustion products. Historically, 2-stroke designs have been widely used in pipeline applications. However, current industry practices reflect a decline in the usage of new 2-stroke engines for stationary applications.

Four-stroke engines use a separate engine revolution for the intake/compression cycle and the power/exhaust cycle. These engines may be either naturally aspirated, using the suction from the piston to entrain the air charge, or turbocharged, using an exhaust-driven turbine to pressurize the charge. Turbocharged units produce a higher power output for a given engine displacement, whereas naturally aspirated units have lower initial costs and require less maintenance.

Rich-burn engines operate near the stoichiometric air-to-fuel ratio (16:1) with exhaust excess oxygen levels less than 4 percent (typically closer to 1 percent). Additionally, it is likely that the emissions profile will be considerably different for a rich-burn engine at 4 percent oxygen than when operated closer to stoichiometric conditions. Considerations such as these can impact the quantitative value of the emission factor presented. It is also important to note that while rich-burn engines may operate, by definition, with exhaust oxygen levels as high as 4 percent, in reality, most will operate within plus or minus 1 air-to-fuel ratio of stoichiometry. Even across this narrow range, emissions will vary considerably, sometimes by more than an order of magnitude. Air-to-fuel ratios were not provided in the gathered emissions data used to develop the presented factors.

Lean-burn engines may operate up to the lean flame extinction limit, with exhaust oxygen levels of 12 percent or greater. The air to fuel ratios of lean-burn engines range from 20:1 to 50:1 and are typically higher than 24:1. The exhaust excess oxygen levels of lean-burn engines are typically around 8 percent, ranging from 4 to 17 percent. Some lean-burn engines are characterized as clean-burn engines. The term "clean-burn" technology is a registered trademark of Cooper Energy Systems and refers to engines designed to reduce NO_x by operating at high air-to-fuel ratios. Engines operating at high air-to-fuel ratios (greater than 30:1) may require combustion modification to promote stable combustion with the high excess air. These modifications may include a turbo charger or a precombustion chamber (PCC). A turbo charger is used to force more air into the combustion chamber, and a PCC is used to ignite a fuel-rich mixture that propagates into the main cylinder and ignites the very lean combustion charge. Lean-burn engines typically have lower oxides of nitrogen (NO_x) emissions than rich-burn engines.

3.2.3 Emissions

The primary criteria pollutants from natural gas-fired reciprocating engines are oxides of nitrogen (NO_x), carbon monoxide (CO), and volatile organic compounds (VOC). The formation of nitrogen oxides is exponentially related to combustion temperature in the engine cylinder. The other pollutants, CO and VOC species, are primarily the result of incomplete combustion. Particulate matter (PM) emissions include trace amounts of metals, non-combustible inorganic material, and condensible,

semi-volatile organics which result from volatized lubricating oil, engine wear, or from products of incomplete combustion. Sulfur oxides are very low since sulfur compounds are removed from natural gas at processing plants. However, trace amounts of sulfur containing odorant are added to natural gas at city gates prior to distribution for the purpose of leak detection.

It should be emphasized that the actual emissions may vary considerably from the published emission factors due to variations in the engine operating conditions. This variation is due to engines operating at different conditions, including air-to-fuel ratio, ignition timing, torque, speed, ambient temperature, humidity, and other factors. It is not unusual to test emissions from two identical engines in the same plant, operated by the same personnel, using the same fuel, and have the test results show significantly different emissions. This variability in the test data is evidenced in the high relative standard deviation reported in the data set.

3.2.3.1 Nitrogen Oxides -
Nitrogen oxides are formed through three fundamentally different mechanisms. The principal mechanism of NO_x formation with gas-fired engines is thermal NO_x. The thermal NO_x mechanism occurs through the thermal dissociation and subsequent reaction of nitrogen (N_2) and oxygen (O_2) molecules in the combustion air. Most NO_x formed through the thermal NO_x mechanism occurs in high-temperature regions in the cylinder where combustion air has mixed sufficiently with the fuel to produce the peak temperature fuel/air interface. The second mechanism, called prompt NO_x, occurs through early reactions of nitrogen molecules in the combustion air and hydrocarbon radicals from the fuel. Prompt NO_x reactions occur within the flame and are usually negligible compared to the level of NO_x formed through the thermal NO_x mechanism. The third mechanism, fuel NO_x, stems from the evolution and reaction of fuel-bound nitrogen compounds with oxygen. Natural gas has negligible chemically bound fuel nitrogen (although some molecular nitrogen is present).

Essentially all NO_x formed in natural gas-fired reciprocating engines occurs through the thermal NO_x mechanism. The formation of NO_x through the prompt NO_x mechanism may be significant only under highly controlled situations in rich-burn engines when the thermal NO_x mechanism is suppressed. The rate of NO_x formation through the thermal NO_x mechanism is highly dependent upon the stoichiometric ratio, combustion temperature, and residence time at the combustion temperature. Maximum NO_x formation occurs through the thermal NO_x mechanism near the stoichiometric air-to-fuel mixture ratio since combustion temperatures are greatest at this air-to-fuel ratio.

3.2.3.2 Carbon Monoxide and Volatile Organic Compounds -
CO and VOC emissions are both products of incomplete combustion. CO results when there is insufficient residence time at high temperature to complete the final step in hydrocarbon oxidation. In reciprocating engines, CO emissions may indicate early quenching of combustion gases on cylinder walls or valve surfaces. The oxidation of CO to carbon dioxide (CO_2) is a slow reaction compared to most hydrocarbon oxidation reactions.

The pollutants commonly classified as VOC can encompass a wide spectrum of volatile organic compounds that are photoreactive in the atmosphere. VOC occur when some of the gas remains unburned or is only partially burned during the combustion process. With natural gas, some organics are carryover, unreacted, trace constituents of the gas, while others may be pyrolysis products of the heavier hydrocarbon constituents. Partially burned hydrocarbons result from poor air-to-fuel mixing prior to, or during, combustion, or incorrect air-to-fuel ratios in the cylinder during combustion due to maladjustment of the engine fuel system. Also, low cylinder temperature may yield partially burned hydrocarbons due to excessive cooling through the walls, or early cooling of the gases by expansion of the combustion volume caused by piston motion before combustion is completed.

3.2.3.3 Particulate Matter[4] -

PM emissions result from carryover of noncombustible trace constituents in the fuel and lubricating oil and from products of incomplete combustion. Emission of PM from natural gas-fired reciprocating engines are generally minimal and comprise fine filterable and condensible PM. Increased PM emissions may result from poor air-to-fuel mixing or maintenance problems.

3.2.3.4 Carbon Dioxide, Methane, and Nitrous Oxide[5] -

Carbon dioxide (CO_2), methane (CH_4), and nitrous oxide (N_2O) are referred to as greenhouse gases. Such gases are largely transparent to incoming solar radiation; however, they absorb infrared radiation re-emitted by the Earth. Where available, emission factors for these pollutants are presented in the emission factors tables of this section.

3.2.4 Control Technologies

Three generic control techniques have been developed for reciprocating engines: parametric controls (timing and operating at a leaner air-to-fuel ratio); combustion modifications such as advanced engine design for new sources or major modification to existing sources (clean-burn cylinder head designs and prestratified charge combustion for rich-burn engines); and postcombustion catalytic controls installed on the engine exhaust system. Post-combustion catalytic technologies include selective catalytic reduction (SCR) for lean-burn engines, nonselective catalytic reduction (NSCR) for rich-burn engines, and CO oxidation catalysts for lean-burn engines.

3.2.4.1 Control Techniques for 4-Cycle Rich-burn Engines[4,6] -

Nonselective Catalytic Reduction (NSCR) -

This technique uses the residual hydrocarbons and CO in the rich-burn engine exhaust as a reducing agent for NO_x. In an NSCR, hydrocarbons and CO are oxidized by O_2 and NO_x. The excess hydrocarbons, CO, and NO_x pass over a catalyst (usually a noble metal such as platinum, rhodium, or palladium) that oxidizes the excess hydrocarbons and CO to H_2O and CO_2, while reducing NO_x to N_2. NO_x reduction efficiencies are usually greater than 90 percent, while CO reduction efficiencies are approximately 90 percent.

The NSCR technique is effectively limited to engines with normal exhaust oxygen levels of 4 percent or less. This includes 4-stroke rich-burn naturally aspirated engines and some 4-stroke rich-burn turbocharged engines. Engines operating with NSCR require tight air-to-fuel control to maintain high reduction effectiveness without high hydrocarbon emissions. To achieve effective NO_x reduction performance, the engine may need to be run with a richer fuel adjustment than normal. This exhaust excess oxygen level would probably be closer to 1 percent. Lean-burn engines could not be retrofitted with NSCR control because of the reduced exhaust temperatures.

Prestratified Charge -

Prestratified charge combustion is a retrofit system that is limited to 4-stroke carbureted natural gas engines. In this system, controlled amounts of air are introduced into the intake manifold in a specified sequence and quantity to create a fuel-rich and fuel-lean zone. This stratification provides both a fuel-rich ignition zone and rapid flame cooling in the fuel-lean zone, resulting in reduced formation of NO_x. A prestratified charge kit generally contains new intake manifolds, air hoses, filters, control valves, and a control system.

3.2.4.2 Control Techniques for Lean-burn Reciprocating Engines[4,6] -

Selective Catalytic Reduction[4,6] -

Selective catalytic reduction is a postcombustion technology that has been shown to be effective in reducing NO_x in exhaust from lean-burn engines. An SCR system consists of an ammonia storage, feed, and injection system, and a catalyst and catalyst housing. Selective catalytic reduction systems selectively reduce NO_x emissions by injecting ammonia (either in the form of liquid anhydrous ammonia or aqueous ammonium hydroxide) into the exhaust gas stream upstream of the catalyst. Nitrogen oxides, NH_3, and O_2 react on the surface of the catalyst to form N_2 and H_2O. For the SCR system to operate properly, the exhaust gas must be within a particular temperature range (typically between 450 and 850°F). The temperature range is dictated by the catalyst (typically made from noble metals, base metal oxides such as vanadium and titanium, and zeolite-based material). Exhaust gas temperatures greater than the upper limit (850°F) will pass the NO_x and ammonia unreacted through the catalyst. Ammonia emissions, called NH_3 slip, are a key consideration when specifying a SCR system. SCR is most suitable for lean-burn engines operated at constant loads, and can achieve efficiencies as high as 90 percent. For engines which typically operate at variable loads, such as engines on gas transmission pipelines, an SCR system may not function effectively, causing either periods of ammonia slip or insufficient ammonia to gain the reductions needed.

Catalytic Oxidation -

Catalytic oxidation is a postcombustion technology that has been applied, in limited cases, to oxidize CO in engine exhaust, typically from lean-burn engines. As previously mentioned, lean-burn technologies may cause increased CO emissions. The application of catalytic oxidation has been shown to be effective in reducing CO emissions from lean-burn engines. In a catalytic oxidation system, CO passes over a catalyst, usually a noble metal, which oxidizes the CO to CO_2 at efficiencies of approximately 70 percent for 2SLB engines and 90 percent for 4SLB engines.

3.2.5 Updates Since the Fifth Edition

The Fifth Edition was released in January 1995. Revisions to this section since that date are summarized below. For further detail, consult the memoranda describing each supplement or the background report for this section. These and other documents can be found on the Clearinghouse for Inventories/Emission Factors (CHIEF) electronic bulletin board (919-541-5742), or on the new Emission Factor and Inventory Group (EFIG) home page (http://www.epa.gov/ttn/chief).

Supplement A, February 1996

- In the table for uncontrolled natural gas prime movers, the Source Classification Code (SCC) for 4-cycle lean-burn was changed from 2-01-002-53 to 2-02-002-54. The SCC for 4-cycle rich-burn was changed from 2-02-002-54 to 2-02-02-002-53.

- An SCC (2-02-002-53) was provided for 4-cycle rich-burn engines, and the "less than" symbol (<) was restored to the appropriate factors.

Supplement B, October 1996

- The introduction section was revised.

- Text was added concerning process description of turbines.

- Text concerning emissions and controls was revised.

- References in various tables were editorially corrected.

- The inconsistency between a CO_2 factor in the table and an equation in the footnote was corrected.

Supplement F, July 2000

- Turbines used for natural gas compression were removed from this section and combined with utility turbines in Section 3.1. Section 3.2 now only contains information on natural gas-fired reciprocating engines.

- All emission factors were updated based on emissions data points taken from 70 emission reports containing over 400 source tests. Many new emission factors have been incorporated in this section for speciated organic compounds, including hazardous air pollutants.

TABLE 3.2-1 UNCONTROLLED EMISSION FACTORS FOR 2-STROKE LEAN-BURN ENGINES[a]
(SCC 2-02-002-52)

Pollutant	Emission Factor (lb/MMBtu)[b] (fuel input)	Emission Factor Rating
Criteria Pollutants and Greenhouse Gases		
NO_x[c] 90 - 105% Load	3.17 E+00	A
NO_x[c] <90% Load	1.94 E+00	A
CO[c] 90 - 105% Load	3.86 E-01	A
CO[c] <90% Load	3.53 E-01	A
CO_2[d]	1.10 E+02	A
SO_2[e]	5.88 E-04	A
TOC[f]	1.64 E+00	A
Methane[g]	1.45 E+00	C
VOC[h]	1.20 E-01	C
PM10 (filterable)[i]	3.84 E-02	C
PM2.5 (filterable)[i]	3.84 E-02	C
PM Condensable[j]	9.91 E-03	E
Trace Organic Compounds		
1,1,2,2-Tetrachloroethane[k]	6.63 E-05	C
1,1,2-Trichloroethane[k]	5.27 E-05	C
1,1-Dichloroethane	3.91 E-05	C
1,2,3-Trimethylbenzene	3.54 E-05	D
1,2,4-Trimethylbenzene	1.11 E-04	C
1,2-Dichloroethane	4.22 E-05	D
1,2-Dichloropropane	4.46 E-05	C
1,3,5-Trimethylbenzene	1.80 E-05	D
1,3-Butadiene[k]	8.20 E-04	D
1,3-Dichloropropene[k]	4.38 E-05	C
2,2,4-Trimethylpentane[k]	8.46 E-04	B
2-Methylnaphthalene[k]	2.14 E-05	C
Acenaphthene[k]	1.33 E-06	C

Table 3.2-1. UNCONTROLLED EMISSION FACTORS FOR 2-STROKE LEAN-BURN
ENGINES

(Continued)

Pollutant	Emission Factor (lb/MMBtu)[b] (fuel input)	Emission Factor Rating
Acenaphthylene[k]	3.17 E-06	C
Acetaldehyde[k,l]	7.76 E-03	A
Acrolein[k,l]	7.78 E-03	A
Anthracene[k]	7.18 E-07	C
Benz(a)anthracene[k]	3.36 E-07	C
Benzene[k]	1.94 E-03	A
Benzo(a)pyrene[k]	5.68 E-09	D
Benzo(b)fluoranthene[k]	8.51 E-09	D
Benzo(e)pyrene[k]	2.34 E-08	D
Benzo(g,h,i)perylene[k]	2.48 E-08	D
Benzo(k)fluoranthene[k]	4.26 E-09	D
Biphenyl[k]	3.95 E-06	C
Butane	4.75 E-03	C
Butyr/Isobutyraldehyde	4.37 E-04	C
Carbon Tetrachloride[k]	6.07 E-05	C
Chlorobenzene[k]	4.44 E-05	C
Chloroform[k]	4.71 E-05	C
Chrysene[k]	6.72 E-07	C
Cyclohexane	3.08 E-04	C
Cyclopentane	9.47 E-05	C
Ethane	7.09 E-02	A
Ethylbenzene[k]	1.08 E-04	B
Ethylene Dibromide[k]	7.34 E-05	C
Fluoranthene[k]	3.61 E-07	C
Fluorene[k]	1.69 E-06	C
Formaldehyde[k,l]	5.52 E-02	A

Table 3.2-1. UNCONTROLLED EMISSION FACTORS FOR 2-STROKE LEAN-BURN ENGINES
(Concluded)

Pollutant	Emission Factor (lb/MMBtu)[b] (fuel input)	Emission Factor Rating
Indeno(1,2,3-c,d)pyrene[k]	9.93 E-09	D
Isobutane	3.75 E-03	C
Methanol[k]	2.48 E-03	A
Methylcyclohexane	3.38 E-04	C
Methylene Chloride[k]	1.47 E-04	C
n-Hexane[k]	4.45 E-04	C
n-Nonane	3.08 E-05	C
n-Octane	7.44 E-05	C
n-Pentane	1.53 E-03	C
Naphthalene[k]	9.63 E-05	C
PAH[k]	1.34 E-04	D
Perylene[k]	4.97 E-09	D
Phenanthrene[k]	3.53 E-06	C
Phenol[k]	4.21 E-05	C
Propane	2.87 E-02	C
Pyrene[k]	5.84 E-07	C
Styrene[k]	5.48 E-05	A
Toluene[k]	9.63 E-04	A
Vinyl Chloride[k]	2.47 E-05	C
Xylene[k]	2.68 E-04	A

[a] Reference 7. Factors represent uncontrolled levels. For NO_x, CO, and PM10, "uncontrolled" means no combustion or add-on controls; however, the factor may include turbocharged units. For all other pollutants, "uncontrolled" means no oxidation control; the data set may include units with control techniques used for NOx control, such as PCC and SCR for lean burn engines, and PSC for rich burn engines. Factors are based on large population of engines. Factors are for engines at all loads, except as indicated. SCC = Source Classification Code. TOC = Total Organic Compounds. PM10 = Particulate Matter ≤ 10 microns (μm) aerodynamic diameter. A "<" sign in front of a factor means that the corresponding emission factor is based on one-half of the method detection limit.
[b] Emission factors were calculated in units of (lb/MMBtu) based on procedures in EPA

Method 19. To convert from (lb/MMBtu) to (lb/10^6 scf), multiply by the heat content of the fuel. If the heat content is not available, use 1020 Btu/scf. To convert from (lb/MMBtu) to (lb/hp-hr) use the following equation:

$$\text{lb/hp-hr} = \text{(lb/MMBtu)} \text{(heat input, MMBtu/hr)} \text{(1/operating HP, 1/hp)}$$

[c] Emission tests with unreported load conditions were not included in the data set.

[d] Based on 99.5% conversion of the fuel carbon to CO_2. CO_2 [lb/MMBtu] = (3.67)(%CON)(C)(D)(1/h), where %CON = percent conversion of fuel carbon to CO_2, C = carbon content of fuel by weight (0.75), D = density of fuel, 4.1 E+04 lb/10^6 scf, and h = heating value of natural gas (assume 1020 Btu/scf at 60°F).

[e] Based on 100% conversion of fuel sulfur to SO_2. Assumes sulfur content in natural gas of 2,000 gr/10^6 scf.

[f] Emission factor for TOC is based on measured emission levels of 43 tests.

[g] Emission factor for methane is determined by subtracting the VOC and ethane emission factors from the TOC emission factor. Measured emission factor for methane compares well with the calculated emission factor, 1.48 lb/MMBtu vs. 1.45 lb/MMBtu, respectively.

[h] VOC emission factor is based on the sum of the emission factors for all speciated organic compounds less ethane and methane.

[i] Considered ≤ 1 μm in aerodynamic diameter. Therefore, for filterable PM emissions, PM10(filterable) = PM2.5(filterable).

[j] No data were available for condensable PM emissions. The presented emission factor reflects emissions from 4SLB engines.

[k] Hazardous Air Pollutant as defined by Section 112(b) of the Clean Air Act.

[l] For lean burn engines, aldehyde emissions quantification using CARB 430 may reflect interference with the sampling compounds due to the nitrogen concentration in the stack. The presented emission factor is based on FTIR measurements. Emissions data based on CARB 430 are available in the background report.

Table 3.2-2. UNCONTROLLED EMISSION FACTORS FOR 4-STROKE LEAN-BURN ENGINES[a]
(SCC 2-02-002-54)

Pollutant	Emission Factor (lb/MMBtu)[b] (fuel input)	Emission Factor Rating
Criteria Pollutants and Greenhouse Gases		
NO_x[c] 90 - 105% Load	4.08 E+00	B
NO_x[c] <90% Load	8.47 E-01	B
CO[c] 90 - 105% Load	3.17 E-01	C
CO[c] <90% Load	5.57 E-01	B
CO_2[d]	1.10 E+02	A
SO_2[e]	5.88 E-04	A
TOC[f]	1.47 E+00	A
Methane[g]	1.25 E+00	C
VOC[h]	1.18 E-01	C
PM10 (filterable)[i]	7.71 E-05	D
PM2.5 (filterable)[i]	7.71 E-05	D
PM Condensable[j]	9.91 E-03	D
Trace Organic Compounds		
1,1,2,2-Tetrachloroethane[k]	<4.00 E-05	E
1,1,2-Trichloroethane[k]	<3.18 E-05	E
1,1-Dichloroethane	<2.36 E-05	E
1,2,3-Trimethylbenzene	2.30 E-05	D
1,2,4-Trimethylbenzene	1.43 E-05	C
1,2-Dichloroethane	<2.36 E-05	E
1,2-Dichloropropane	<2.69 E-05	E
1,3,5-Trimethylbenzene	3.38 E-05	D
1,3-Butadiene[k]	2.67E-04	D
1,3-Dichloropropene[k]	<2.64 E-05	E
2-Methylnaphthalene[k]	3.32 E-05	C
2,2,4-Trimethylpentane[k]	2.50 E-04	C
Acenaphthene[k]	1.25 E-06	C

Table 3.2-2. UNCONTROLLED EMISSION FACTORS FOR 4-STROKE LEAN-BURN ENGINES
(Continued)

Pollutant	Emission Factor (lb/MMBtu)[b] (fuel input)	Emission Factor Rating
Acenaphthylene[k]	5.53 E-06	C
Acetaldehyde[k,l]	8.36 E-03	A
Acrolein[k,l]	5.14 E-03	A
Benzene[k]	4.40 E-04	A
Benzo(b)fluoranthene[k]	1.66 E-07	D
Benzo(e)pyrene[k]	4.15 E-07	D
Benzo(g,h,i)perylene[k]	4.14 E-07	D
Biphenyl[k]	2.12 E-04	D
Butane	5.41 E-04	D
Butyr/Isobutyraldehyde	1.01 E-04	C
Carbon Tetrachloride[k]	<3.67 E-05	E
Chlorobenzene[k]	<3.04 E-05	E
Chloroethane	1.87 E-06	D
Chloroform[k]	<2.85 E-05	E
Chrysene[k]	6.93 E-07	C
Cyclopentane	2.27 E-04	C
Ethane	1.05 E-01	C
Ethylbenzene[k]	3.97 E-05	B
Ethylene Dibromide[k]	<4.43 E-05	E
Fluoranthene[k]	1.11 E-06	C
Fluorene[k]	5.67 E-06	C
Formaldehyde[k,l]	5.28 E-02	A
Methanol[k]	2.50 E-03	B
Methylcyclohexane	1.23 E-03	C
Methylene Chloride[k]	2.00 E-05	C
n-Hexane[k]	1.11 E-03	C
n-Nonane	1.10 E-04	C

Table 3.2-2. UNCONTROLLED EMISSION FACTORS FOR 4-STROKE LEAN-BURN
ENGINES
(Continued)

Pollutant	Emission Factor (lb/MMBtu)[b] (fuel input)	Emission Factor Rating
n-Octane	3.51 E-04	C
n-Pentane	2.60 E-03	C
Naphthalene[k]	7.44 E-05	C
PAH[k]	2.69 E-05	D
Phenanthrene[k]	1.04 E-05	D
Phenol[k]	2.40 E-05	D
Propane	4.19 E-02	C
Pyrene[k]	1.36 E-06	C
Styrene[k]	<2.36 E-05	E
Tetrachloroethane[k]	2.48 E-06	D
Toluene[k]	4.08 E-04	B
Vinyl Chloride[k]	1.49 E-05	C
Xylene[k]	1.84 E-04	B

[a] Reference 7. Factors represent uncontrolled levels. For NO_x, CO, and PM10,
"uncontrolled" means no combustion or add-on controls; however, the factor may include
turbocharged units. For all other pollutants, "uncontrolled" means no oxidation control;
the data set may include units with control techniques used for NOx control, such as PCC
and SCR for lean burn engines, and PSC for rich burn engines. Factors are based on large
population of engines. Factors are for engines at all loads, except as indicated. SCC =
Source Classification Code. TOC = Total Organic Compounds. PM-10 = Particulate
Matter $\leq$ 10 microns (μm) aerodynamic diameter. A "<" sign in front of a factor means
that the corresponding emission factor is based on one-half of the method detection limit.
[b] Emission factors were calculated in units of (lb/MMBtu) based on procedures in EPA
Method 19. To convert from (lb/MMBtu) to (lb/10^6 scf), multiply by the heat content of
the fuel. If the heat content is not available, use 1020 Btu/scf. To convert from
(lb/MMBtu) to (lb/hp-hr) use the following equation:

$$lb/hp\text{-}hr = {}_{(}lb/MMBtu{)} {}_{(}heat\ input,\ MMBtu/hr{)} {}_{(}1/operating\ HP,\ 1/hp{)}$$

[c] Emission tests with unreported load conditions were not included in the data set.
[d] Based on 99.5% conversion of the fuel carbon to CO_2. CO_2 [lb/MMBtu] =
(3.67)(%CON)(C)(D)(1/h), where %CON = percent conversion of fuel carbon to CO_2,
C = carbon content of fuel by weight (0.75), D = density of fuel, 4.1 E+04 lb/10^6 scf, and

h = heating value of natural gas (assume 1020 Btu/scf at 60°F).
e Based on 100% conversion of fuel sulfur to SO_2. Assumes sulfur content in natural gas of 2,000 gr/10^6 scf.
f Emission factor for TOC is based on measured emission levels from 22 source tests.
g Emission factor for methane is determined by subtracting the VOC and ethane emission factors from the TOC emission factor. Measured emission factor for methane compares well with the calculated emission factor, 1.31 lb/MMBtu vs. 1.25 lb/MMBtu, respectively.
h VOC emission factor is based on the sum of the emission factors for all speciated organic compounds less ethane and methane.
i Considered ≤ 1 μm in aerodynamic diameter. Therefore, for filterable PM emissions, PM10(filterable) = PM2.5(filterable).
j PM Condensable = PM Condensable Inorganic + PM-Condensable Organic
k Hazardous Air Pollutant as defined by Section 112(b) of the Clean Air Act.
l For lean burn engines, aldehyde emissions quantification using CARB 430 may reflect interference with the sampling compounds due to the nitrogen concentration in the stack. The presented emission factor is based on FTIR measurements. Emissions data based on CARB 430 are available in the background report.

Table 3.2-3. UNCONTROLLED EMISSION FACTORS FOR 4-STROKE RICH-BURN
ENGINES[a]
(SCC 2-02-002-53)

Pollutant	Emission Factor (lb/MMBtu)[b] (fuel input)	Emission Factor Rating
Criteria Pollutants and Greenhouse Gases		
NO_x[c] 90 - 105% Load	2.21 E+00	A
NO_x[c] <90% Load	2.27 E+00	C
CO[c] 90 - 105% Load	3.72 E+00	A
CO[c] <90% Load	3.51 E+00	C
CO_2[d]	1.10 E+02	A
SO_2[e]	5.88 E-04	A
TOC[f]	3.58 E-01	C
Methane[g]	2.30 E-01	C
VOC[h]	2.96 E-02	C
PM10 (filterable)[i,j]	9.50 E-03	E
PM2.5 (filterable)[j]	9.50 E-03	E
PM Condensable[k]	9.91 E-03	E
Trace Organic Compounds		
1,1,2,2-Tetrachloroethane[l]	2.53 E-05	C
1,1,2-Trichloroethane[l]	<1.53 E-05	E
1,1-Dichloroethane	<1.13 E-05	E
1,2-Dichloroethane	<1.13 E-05	E
1,2-Dichloropropane	<1.30 E-05	E
1,3-Butadiene[l]	6.63 E-04	D
1,3-Dichloropropene[l]	<1.27 E-05	E
Acetaldehyde[l,m]	2.79 E-03	C
Acrolein[l,m]	2.63 E-03	C
Benzene[l]	1.58 E-03	B
Butyr/isobutyraldehyde	4.86 E-05	D
Carbon Tetrachloride[l]	<1.77 E-05	E

Table 3.2-3. UNCONTROLLED EMISSION FACTORS FOR 4-STROKE RICH-BURN ENGINES
(Concluded)

Pollutant	Emission Factor (lb/MMBtu)[b] (fuel input)	Emission Factor Rating
Chlorobenzene[l]	<1.29 E-05	E
Chloroform[l]	<1.37 E-05	E
Ethane[n]	7.04 E-02	C
Ethylbenzene[l]	<2.48 E-05	E
Ethylene Dibromide[l]	<2.13 E-05	E
Formaldehyde[l,m]	2.05 E-02	A
Methanol[l]	3.06 E-03	D
Methylene Chloride[l]	4.12 E-05	C
Naphthalene[l]	<9.71 E-05	E
PAH[l]	1.41 E-04	D
Styrene[l]	<1.19 E-05	E
Toluene[l]	5.58 E-04	A
Vinyl Chloride[l]	<7.18 E-06	E
Xylene[l]	1.95 E-04	A

[a] Reference 7. Factors represent uncontrolled levels. For NO_x, CO, and PM-10, "uncontrolled" means no combustion or add-on controls; however, the factor may include turbocharged units. For all other pollutants, "uncontrolled" means no oxidation control; the data set may include units with control techniques used for NOx control, such as PCC and SCR for lean burn engines, and PSC for rich burn engines. Factors are based on large population of engines. Factors are for engines at all loads, except as indicated. SCC = Source Classification Code. TOC = Total Organic Compounds. PM10 = Particulate Matter $\leq$ 10 microns (μm) aerodynamic diameter. A "<" sign in front of a factor means that the corresponding emission factor is based on one-half of the method detection limit.

[b] Emission factors were calculated in units of (lb/MMBtu) based on procedures in EPA Method 19. To convert from (lb/MMBtu) to (lb/10^6 scf), multiply by the heat content of the fuel. If the heat content is not available, use 1020 Btu/scf. To convert from (lb/MMBtu) to (lb/hp-hr) use the following equation:

$$lb/hp-hr = (lb/MMBtu)(heat\ input,\ MMBtu/hr)(1/operating\ HP,\ 1/hp)$$

[c] Emission tests with unreported load conditions were not included in the data set.
[d] Based on 99.5% conversion of the fuel carbon to CO_2. CO_2 [lb/MMBtu] = (3.67)(%CON)(C)(D)(1/h), where %CON = percent conversion of fuel carbon to CO_2,

C = carbon content of fuel by weight (0.75), D = density of fuel, 4.1 E+04 lb/10^6 scf, and h = heating value of natural gas (assume 1020 Btu/scf at 60°F).

e Based on 100% conversion of fuel sulfur to SO_2. Assumes sulfur content in natural gas of 2,000 gr/10^{6}scf.

f Emission factor for TOC is based on measured emission levels from 6 source tests.

g Emission factor for methane is determined by subtracting the VOC and ethane emission factors from the TOC emission factor.

h VOC emission factor is based on the sum of the emission factors for all speciated organic compounds. Methane and ethane emissions were not measured for this engine category.

i No data were available for uncontrolled engines. PM10 emissions are for engines equipped with a PCC.

j Considered ≤ 1 μm in aerodynamic diameter. Therefore, for filterable PM emissions, PM10(filterable) = PM2.5(filterable).

k No data were available for condensable emissions. The presented emission factor reflects emissions from 4SLB engines.

l Hazardous Air Pollutant as defined by Section 112(b) of the Clean Air Act.

m For rich-burn engines, no interference is suspected in quantifying aldehyde emissions. The presented emission factors are based on FTIR and CARB 430 emissions data measurements.

n Ethane emission factor is determined by subtracting the VOC emission factor from the NMHC emission factor.

References For Section 3.2

1.   *Engines, Turbines, And Compressors Directory*, American Gas Association, Catalog #XF0488.

2.   *Standards Support And Environmental Impact Statement, Volume I: Stationary Internal Combustion Engines*, EPA-450/2-78-125a, U. S. Environmental Protection Agency, Office of Air Quality Planning and Standards, Research Triangle Park, NC, July 1979.

3.   *Alternative Control Techniques Document - NO_x Emissions From Stationary Reciprocating Engines*, EPA-453/R-93-032, July 1993.

4.   *Handbook - Control Technologies For Hazardous Air Pollutants*, EPA-625/6-91-014, June 1991.

5.   *Limiting Net Greenhouse Gas Emissions In The United States, Volume II: Energy Responses*, Report for the Office of Environmental Analysis, Office of Policy, Planning and Analysis, Department of Energy (DOE), DOE/PE-0101 Volume II, September 1991.

6.   C. Castaldini, *NO_x Reduction Technologies For Natural Gas Industry Prime Movers*, GRI-90/0215, Gas Research Institute, Chicago, IL, August 1990.

7.   *Emission Factor Documentation for AP-42 Section 3.2, Natural Gas-Fired Reciprocating Engines*, EPA Contract No. 68-D2-0160, Alpha-Gamma Technologies, Inc., Raleigh, North Carolina, July 2000.